Thesis for the degree of Doctor of Philosophy
in Natural Science

Lipidic Cubic Phase Microcrystallization and its Application in Serial Crystallography

---

Rebecka Andersson

UNIVERSITY OF GOTHENBURG

Department of Chemistry and Molecular Biology

Gothenburg, Sweden, 2020

Thesis for the degree of Doctor of Philosophy in Natural Science

Lipidic Cubic Phase Microcrystallization and its Application in Serial Crystallography

Rebecka Andersson

Cover: Microcrystals of ba_3-type cytochrome *c* oxidase in lipidic cubic phase visualized in a glass well.

ISBN: 978-91-8009-114-5 (Tryck)
ISBN: 978-91-8009-115-2 (PDF)
Tillgänglig via http://hdl.handle.net/2077/66804

Department of Chemistry and Molecular Biology
Division of Biochemistry and Structural Biology
University of Gothenburg
SE-405 30 Gothenburg, Sweden

Printed by Stema Specialtryck AB
Gothenburg, Sweden, 2020

"All sorts of things can happen when you're open to new ideas and playing around with things." - Stephanie Kwolek, Chemist.

Abstract

Every living organism contain a cell membrane which is an important cell structure with a vast variety of different functions such as cell signaling, transportation and energy production. One of the most important functions is to produce energy for the cell to thrive. In humans and other organisms, oxygen is used as the final electron acceptor to drive reactions that pump protons across the membrane to create an electrochemical proton gradient. This electrochemical proton gradient is then harvested for the production of ATP, the currency of life. Even though the membrane proteins that are responsible for the electrochemical proton gradient belong to one of the most well-studied membrane protein families, there are still mechanisms to be revealed. Two of these mechanisms are proton pumping across the membrane and the route of oxygen to the active site of cytochrome *c* oxidase, the final enzyme in the respiratory chain that reduces oxygen to water. By using X-ray serial crystallography these mechanisms can be revealed.

Previous research has found that membrane protein crystallization is greatly improved if the environment of the protein mimics the native environment. Reconstituting the membrane proteins in a lipidic cubic phase, a membrane mimicking lipid bilayer, increases membrane protein stability and crystal packing. As a result, large volumes of good quality microcrystals for X-ray serial crystallography can be obtained. Our studies present a method that allows for better visualization of the crystallization process of microcrystals in lipidic cubic phase. The method was then used to produce microcrystals of a ba_3-type cytochrome *c* oxidase which resulted in the first room temperature structure at 2.3 Å resolution. This work was extended by a procedure to bind CO to the active site of the protein crystals, a first step for revealing the mechanisms of proton pumping and oxygen migration within the enzyme.

The method was also successfully used for other proteins where new crystallization hits were found and optimized. These include sensory rhodopsin II from halophilic archea and reaction centre from *Blastochloris viridis*. For reaction centre, the method was also used in combination with crystal seeding to create a new procedure for microcrystallization. The work presented in this thesis provides a foundation for further development of serial crystallography and for producing microcrystals for time resolved studies.

List of papers

Paper I

R. Andersson*, C. Safari*, P. Båth, R. Bosman, A. Shilova, P. Dahl, S. Gosh, A. Dunge, R. Kjeldsen-Jensen, J. Nan, R. L. Shoeman, M. Kloos, R. B. Doak, U. Mueller, R. Neutze & G. Brändén, "Well-based crystallization of lipidic cubic phase microcrystals for serial X-ray crystallography" *Acta Cryst. (2019) D75, 937-946, doi: 10.1107/S2059798319012695*

*Both authors contributed equally

Paper II

R. Andersson, C. Safari, R. Dods, E. Nango, R. Tanaka, A. Yamashita, T. Nakane, K. Tono, Y. Joti, P. Båth, E. Dunevall, R. Bosman, O. Nureki, S. Iwata, R. Neutze and G. Brändén. *"Serial femtosecond crystallography structure of cytochrome c oxidase at room temperature" Scientific Reports 7, 4518 (2017) doi: 10.1038/s41598-017-05817-z*

Paper III

C. Safari, R. Andersson, S. Gosh, J. Johannesson, P. Båth, R. Bosman, P. Dahl, E. Nango, R. Tanaka, E. Dunevall, P. Börjesson, O. Uwangue, D. Zoric, G. Hammarin, M. Panman, E. Svensson, G. Ortolani, T. Tanaka, T. Tosha, H. Takeda, H. Naitow, T. Arima, A. Yamashita, M. Sugahara, T. Nakane, O. Nureki, S. Iwata, R. Neutze and G. Brändén. *"Room-temperature structure of CO-bound ba_3-type cytochrome c oxidase reveals mechanistic differences between A-type and B-type enzymes" Manuscript (2020).*

Paper IV

P. Båth, P. Börjesson, R. Bosman, C. Wickstrand, R. Dods, T. B. Úlfarsdóttir, P. Dahl, M. J. García-Bonete, J. B. Linse, G. Ortolani, R. Andersson, C. Safari, E. Dunevall, S. Ghosh, E. Nango, R. Tanaka, T. Nakane, A. Yamashita, K. Tono, Y. Joti, T. Tanaka, S. Owada, T. Arima, O. Nureki, S. Iwata, G. Brändén and R. Neutze. "*Lipidic cubic phase serial femtosecond crystallography structure of a photosyntecic reaction centre" Manuscript (2020)*

Paper V

R. Bosman, G. Ortolani, S. Ghosh, T. B. Úlfarsdóttir, D. James, P. Börjesson, G. Hammarin, R. Andersson, C. Safari, T. Weinert, F. Dworkowski, T. Takashi, J. Standfuss, G. Brändén and R. Neutze, *"Structural basis for the prolonged photocycle of Sensory Rhodopsin II revealed by serial millisecond crystallography" Manuscript (2020)*

Related Papers that I have co-authored but that are not included in this thesis:

Paper VI

R. Dods, P. Båth, D Morozov, V. Ahlberg Gagnér, D. Arnlund, H. L. Luk, J. Kübel, M. Maj, A. Vallejos, C. Wickstrand, R. Bosman, K. R. Beyerlein, G. Nelson, M. Liang, D. Milathianaki, J. Robinson, R. Harimoorthy, P. Berntsen, E. Malmerberg, L. Johansson, R. Andersson, S. Carbajo, E. Claesson, C. E. Conrad, P. Dahl, G. Hammarin, M. S. Hunter, C. Li, S. Lisova, A. Royant, C. Safari, A. Sharma, G. J. Williams, O. Yefanov, S. Westenhoff, J. Davidsson, D. P. DePonte, S. Boutet, A. Barty, G. Katona, G. Groenhof, G. Brändén and R. Neutze, *"Ultrafast changes in photosynthetic reaction centres visualized using Xfel radiation" accepted 28th September 2020, Nature*

Paper VII

R. Dods, P. Båth, D. Arnlund, K. R. Beyerlein, G. Nelson, M. Liang, R. Harimoorthy, P. Berntsen, E. Malmgren, L. Johansson, R. Andersson, R. Bosman, S. Carbajo, E. Claesson, C. E. Conrad, P. Dahl, G. Hammarin, M. S Hunter, C. Li, S. Lisova, D. Milathianaki, J. Robinson, C. Safari, A. Sharma, G. Williams, C. Wickstrand, O. Yefanov, J. Davidsson, D. P DePonte, A. Barty, G. Brändén and R. Neutze, *"From makrocrystals to microcrystals: a strategy for membrane protein serial crystallography", Structure (2017) doi:10.1016/j.str.2017.07.002*

Paper VIII

E. Nango, A. Royant, M. Kubo, T. Nakane, C. Wickstrand, T. Kimura, T. Tanaka, K. Tono, C. Y. Song, R. Tanaka, T. Arima, A. Yamashita, J. Kobayashi, T. Hosaka, E. Mizohata, P. Nogly, M. Sugahara, D. Nam, T. Nomura, T. Shimamura, D. Im, T. Fujiwara, Y. Yamanaka, B. Jeon, T. Nishizawa, K. Oda, M. Fukuda, R. Andersson, P. Båth, R. Dods, J. Davidsson, S. Matsuoka, S. Kawatake, M. Murata, O. Nureki, S. Owada, T. Kameshima, T. Hatsui, Y. Joti, G. Schertler, M. Yabashi, A. N. Bondar, J. Standfuss, R. Neutze and S. Iwata. "A three-dimensional movie of structural changes in bacteriorhodopsin" *Science (2016) Vol. 354, Iss. 6319, 1552-1557, doi: 10.1126/science.aah3497*

Paper IX

W. Wahlgren, E. Dunevall, R. North, A. Paz, M. Scalise, P. Bisignano, J. Bengtsson-Palme, P. Goyal, E. Claesson, R. Caing-Carlsson, R. Andersson, K. Beis, U. Nilsson, A. Farewell, L. Pochini, C. Indiveri, M. Grabe, R. C. J. Dobson, J. Abrahamson, S. Ramaswamy and R. Friemann, *"Substrate-bound outward-open structure of a Na-coupled sialic acid symporter reveals a new Na site", Nature communications (2018) May 1; vol 9(1), pp. 1753*

Contribution list

Paper I

Developed the crystallization methods and protocols. Prepared the manuscript.

Paper II

Developed protocols for cultivating cells, protein production, purification and crystallization. Prepared all the sample for the experiment and collected data at SACLA, Japan. Processed the data and prepared the manuscript.

Paper III

Cultivated cells, crystallized the protein and prepared sample for the experiment. Led the practical work at one experiment.

Paper IV

Involved with developing the crystallization method

Paper V

Supported during crystallization for protocol development and joined an experiment

Abbreviations

C*c*O: Cytochrome *c* Oxidase
HCOs: Heme-Copper Oxidases
LCP: Lipidic cubic phase
MAG: Monoacylglycerol
MO: Monoolein
MR: Molecular replacement
PDB ID: Protein Data Bank Identification
PEG: Polyethylene glycol
RT: Room temperature
SFX: Serial femtosecond crystallography
SX: Serial crystallography
TMH: Transmembrane helix
TR: Time-resolved
XFEL: X-ray Free electron laser

Contents

Chapter 1

1. Introduction

1.1 The cell membrane

Every organism, from single cell bacteria to complex multicellular mammals, need a cell membrane for protection, organizing tasks and to compartmentalize. It's also known that most of the cellular processes are linked with the membrane either directly or indirectly in some way. Therefore, cell membranes are considered to be one of the key structures in cell biology (Yang & Hinner, 2015).

The cell membranes consist of two layers of polar head groups forming a bilayer (seen in figure 1) with a hydrophobic core in between. The hydrophobic core in biological membranes mostly consists of two fatty acid chains while the hydrophilic head group consists of phosphate group. The membranes can differ in phospholipid species – both regarding their phospholipid head group and the fatty acyl chains. To this core structure of phospholipids, other fatty acids and/or lipids can be added such as sterols which add to the complexity. In mammalian cells cholesterol can represent up to 40 % of the total lipid content (Bernardino de la Serna, Schütz, Eggeling, & Cebecauer, 2016; van Meer & de Kroon, 2011). The different phospholipid species together with the additives of other molecular structures, changes the physical properties, such as viscosity and the interleaflet coupling of the membrane (Fujimoto & Parmryd, 2017; van Meer & de Kroon, 2011).

There are several models regarding the plasma membrane and one of the best known is the "fluid mosaic model" of Singer and Nicolson (Singer & Nicolson, 1972) where the membrane is portrayed as a "fluid lipid bilayer" that is occasionally interrupted by proteins. This fluidity provides an advantage over other more rigid cellular components since it enables the molecules in the membrane to diffuse, rotate and move over long distances within the bilayer. The membrane is not as fluid as the cytosol and is regarded more as a two-dimensional fluid, held together by the structure of the phospholipid bilayer (Bernardino de la Serna et al., 2016; Luby-Phelps et al., 1993). Cells can also modify the viscosity of the hydrophobic core by altering the saturation of their lipid acyl chains. This in turn enables the membrane to adapt to environmental changes such as temperature (Fraenkel & Hopf, 1940). Another way for the cell to alter the viscosity of the membrane is to modify the lipid composition or by the addition of proteins and other molecules that can vary in space and time (Bernardino de la Serna et al., 2016).

In addition to the fluid mosaic model, there are a few other models that support the fluidity of the bilayer but give evidence that membrane components are restricted in lateral movements. This evidence gave rise to a compartmentalized view of the membrane, where proteins, lipids

and actin organize into micro-and nano-domains (Cambi & Lidke, 2012; Eggeling et al., 2009; Lillemeier, Pfeiffer, Surviladze, Wilson, & Davis, 2006; Lingwood & Simons, 2010; van Zanten, Cambi, & Garcia-Parajo, 2010). The compartmentalization can be described in a short way that different types of lipids, proteins and actins favor certain interaction partners which leads to nanoclusters of domains that can be observed as 'islands', 'rafts' and 'corrals' respectively. The membrane also has an important role when it comes to post-translational modifications of membrane proteins. Membrane associated proteins can undergo a post-translational modification when localized into the membrane. By acylation of specific amino acids with acyl groups from the lipid acyl chains, the acyl group can mediate the interaction of a protein with the hydrophobic core of the membrane (Cambi & Lidke, 2012).

1.2 Membrane proteins

Membrane proteins are located at the cell membrane and are both structurally and functionally diverse and constitute about half of the mass of the plasma membrane. Membrane proteins can be divided into two large groups; intrinsic- and peripheral proteins, depending upon how they are attached to the phospholipidic bilayer. Due to the variety of membrane protein functions, membrane proteins enable the membrane to carry out a wide set of different activities such as cell signaling, energy production and transportation of different small molecules and ions (Dupuy & Engelman, 2008; Uzman, 2001) which is also why the membrane proteins are estimated to be encoded by roughly 30 % of the human genome (Finkelstein, 2014). On account of this, over 50 % of the commercial drugs available target membrane proteins (Overington, Al-Lazikani, & Hopkins, 2006; Rask-Andersen, Almén, & Schiöth, 2011).

1.3 Cell respiration

1.3.1 Mitochondrial electron transport chain

One of the most important roles of membrane proteins is to convert energy into an electrochemical membrane proton gradient to be used in the formation of adenosine triphosphate (ATP). ATP is a molecule with high-energy chemical bonds that are cleaved in chemical reactions to make the cell thrive and reproduce. ATP is foremost formed when the intrinsic protein F-type ATPase (complex V) catalyzes the phosphorylation of adenosine diphosphate (ADP), a reaction driven by the electrochemical proton gradient across the inner mitochondrial membrane. In single cell organisms such as bacteria, the ATP synthase is located in the plasma- or the light dependent thylakoid membrane while other types of organisms contain them in energy-producing organelles (Nicholls, 2013).

To maintain the electrochemical gradient across the membrane to keep the ATP production uninterrupted, several membrane-associated proteins are involved in proton pumping. These membrane proteins convert chemical- or light energy to an electrochemical potential by passing electrons to electron carriers with higher redox potential. These redox reactions releases energy that is used for proton translocation across the membrane. In humans, four different membrane-

integrated proteins (complex I-IV) are involved in the electron transfer known as the respiratory chain or electron transport chain (ETC) (Ramsay, 2019).

Complex I and II accept electrons from the reduced states of the coenzymes nicotinamide adenine dinucleotide (NADH) and flavin adenine dinucleotide ($FADH_2$) (Figure 1) and initiates the electron transfer chain leading to the reduction of coenzyme Q_{10} (QH_2). For complex I, the shuffle of electrons from NADH to coenzyme Q_{10} result in a proton transfer from the inner negative side (N-side, matrix) to the outer positive side (P-side, intermembrane space) of the inner mitochondrial membrane. Complex II accepts electron from $FADH_2$ and reduces coenzyme Q_{10} without translocating protons across the membrane. The electrons then passes from coenzyme Q_{10} to complex III which in turn shuffles them on to cytochrome *c* while pumping protons over the membrane. Cytochrome *c* then finally transfer the electrons to complex IV where oxygen with high redox potential, acts as the final electron acceptor and is reduced to water simultaneously as the complex utilize the energy released to pump protons to the P-side of the inner mitochondrial membrane (Nicholls, 2013). The flow of the electrons through the ETC and proton pumping across the mitochondrial membrane create a mitochondrial electrochemical charge difference and potential ($\Delta\Psi m$), an intermediate form of energy storage, that results from the redox reactions. The driving force of the ECT is the Gibbs free energy state that is related to the redox potential of the components. By shuffling electrons from a molecule with low redox potential to a higher redox potential, energy is released from the system, making the reactions in ETC exergonic (Zorova et al., 2018).

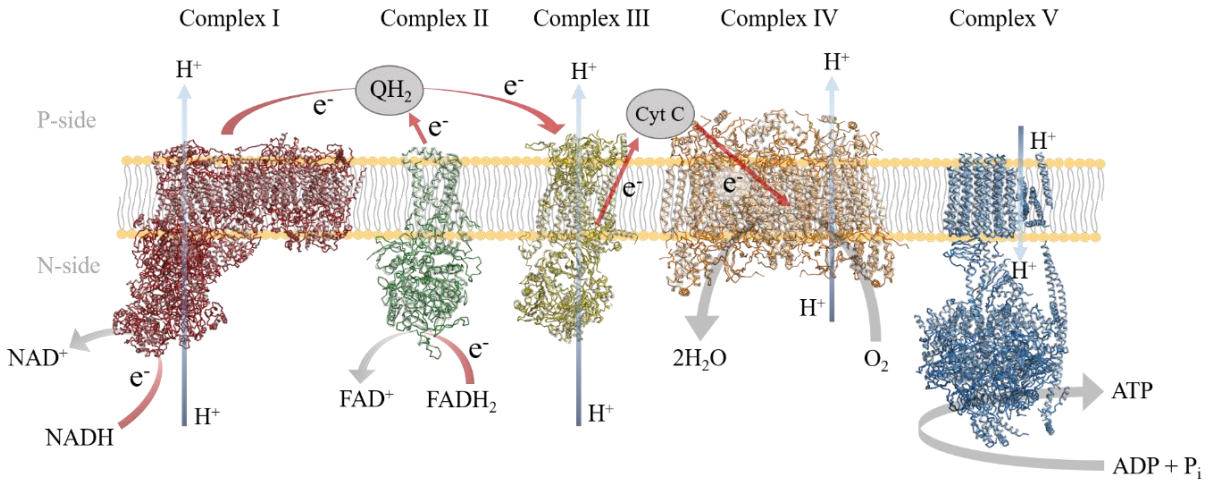

Figure 1. Model over the electron transport chain (ETC) at the inner mitochondrial membrane during aerobic respiration. Blue arrows indicate proton transfer across the membrane and red arrows illustrate electron movement along the electron transport chain. The reduced states of the coenzymes NADH and $FADH_2$ act as electron donors to the ETC and are re-reduced by electrons in the previous steps of the cellular respiration; glycolysis, link reaction and Krebs cycle (Nicholls, 2013). The grey arrow at complex IV indicates a reduction of oxygen to water while the grey arrow at complex V (F_0F_1-ATPase) represents the phosphorylation of ADP to ATP. Model of the proteins are made from the following PDB IDs (from left to right): 5LDW, 3ABV, 5KLV, 3WG7 and 5DN6.

1.3.2 Bacterial electron transport chain

The ETC of bacteria vary over species but always contain a common denominator of a number of coupled redox reactions that generate an electrochemical potential that can either be used directly or power the ATP production. Bacteria can utilize a wide set of different electron donors such as inorganic matter and organic matter as initiators of the electron transport chain. As a final acceptor, larger more complex organisms are forced to use oxygen compared to bacteria that are more diverse in using also other types of terminal electron acceptor such as nitrate, sulfate, carbon dioxide and fumarate to support their ATP synthesis (Kracke, Vassilev, & Krömer, 2015). The high redox potential of oxygen makes it a very attractive electron acceptor for any aerobic- and facultative anaerobic bacteria to use and therefore always used in first instance if present (Schmidt-Rohr, 2020).

1.4 Heme-coppar oxidases

1.4.1 The superfamily

Heme-coppar oxidases (HCOs) are a diverse superfamily of membrane proteins including the terminal cytochrome *c* oxidase of the mitochondrial ETC and ubiquinol oxidase in *Escherichia coli* (*E. coli*) (García-Horsman et. al., 1994). They catalyze the reduction of oxygen to water:

$$O_2 + 4e^- + 4H^+ \rightarrow 2H_2O \tag{1.1}$$

The redox reactions involved in shuffling electrons in the HCOs allow for protons to be pumped across the membrane against the electrochemical potential, which in turn give the more complex reaction:

$$O_2 + 4e^- + 4H^+_{N\,(s)} + 4H^+_{N\,(p)} \rightarrow 2H_2O + 4H^+_{P\,(p)} \tag{1.2}$$

Where N stands for the negative side (N-side) and P for the positive side (P-side) of the membrane, while (s) and (p) represent substrate for oxygen reduction and protons for electrochemical gradient respectively.

By definition, HCOs are enzymes with the presence of a six-coordinated low-spin heme and a catalytic site with a binuclear center containing a high-spin heme and a copper ion (Cu_B) in subunit I. There are also six histidine residues binding these prosthetic groups that are conserved in all HCOs (Pereira, Santana, & Teixeira, 2001). It is in the binuclear center that the reduction of oxygen take place and in the reaction at least four protons are involved. The site is well imbedded in the protein, approximately 13 Å from the P-side and 30 Å from the N-side of the membrane (in aa_3-type C*c*Os, further described in section 1.4.2). The HCOs must ensure

controlled proton pumping across the membrane and supply protons to the reduction of water either through a separate proton channel or the same (Pereira, Gomes, & Teixeira, 2002).

The HCOs vary in terms of subunit composition, heme groups and electron donors and can be divided into three types; A, B and C, depending on the fingerprint of their proton-pumping cores (Pereira et al., 2001). Type A HCOs is the largest group of HCOs and is also the most studied group since it contains the mitochondrial cytochrome *c* oxidase. Type A HCOs are characterized by two proton pumping channels (D- and K-channel) and a catalytic tyrosine residue bound to one of the histidine residues in helix VI of subunit I. In contrast, type B and C HCOs only have one proton conducting channel (K-channel analogue). Type B HCOs share the catalytic tyrosine location in helix VI with the type A HCOs while type C HCOs locate their catalytic tyrosine residue in helix VII of subunit II (Buse et al., 1999; Pereira et al., 2001).

1.4.2 *Aa*$_3$-type cytochrome *c* oxidase

Of the type A HCOs, bacterial *aa*$_3$-type C*c*O from *Rhodobacter sphaeroides* (*R.* sphaeroides) (Figure 2) and *Paracoccus denitrificans* (*P. denitrificans*) are often used as model proteins due to their similar kinetics of proton pumping to eukaryotes. Together with C*c*O from bovine heart, which is commonly used due to the amount of pure protein that can be extracted, these model proteins are one of the most studied among the HCOs (Brändén, Gennis, & Brzezinski, 2006; J P Hosler et al., 1992; Yoshikawa et al., 2006). The first crystal structure to be completely solved was the *aa*$_3$-type C*c*O from *P. denitrificans* at 2.8 Å resolution (Iwata, Ostermeier, Ludwig, & Michel, 1995), followed by the bovine heart C*c*O in 1996 (Tsukihara et al., 1996). Six years later the first structure of *R. sphaeroides* HCO was determined (Svensson-Ek et al., 2002).

The *aa*$_3$-type C*c*Os contain several structural characteristics that have been visualized by X-ray crystallography. Subunit I consists of at least 12 transmembrane helices (TMHs) that provide the protein scaffold for the redox centers and forming three pores for proton transfer; A, B and C. Three amino acids, beside the histidine ligands to the prosthetic groups, are strictly conserved within the *aa*$_3$-type C*c*Os: a tryptophan-, a valine- and an arginine residue. The tryptophan residue located in helix VI is critical for the proton pumping mechanism for *aa*$_3$-type *Cco* (but not for *ba*$_3$-type C*c*O*)* while the valine residue is highly conserved in all of the *aa*$_3$-type *CcO*s. The arginine residue located in the loop of helices XI and XII is linked to the low-spin heme group and is essential for the exit of protons (Buse et al., 1999; Pereira et al., 2001; Yu et al., 2011). Subunit II contains a large cluster of ten beta sheets on the P-side of the membrane that holds a copper site with two electron accepting copper ions termed Cu_A (Figure 2). The subunit also contains two alpha helices that are associated with subunit I (Soulimane, Buse, et al., 2000). The third subunit, subunit III, is unique for the *aa*$_3$-type C*c*Os and has a life-extension role to the complex by increasing the proton uptake that shortens the life-span of reactive oxygen species which can cause loss of Cu_B from the active site and turnover-induced inactivation (Hosler, 2004).

1.4.3 The proton channels

Of the proposed proton transfer pathways in the HCOs, the D-channel of A-type C*c*Os is the best characterized. The D-proton channel consists of mostly polar residues and a highly conserved aspartate residue (D), facing the N-side, that has given the channel its name (Figure 2). Already before crystal structures were available, this aspartate residue was known to be important for proton pumping and it is now considered as the proton uptake site of the D-channel. The protons then continue through a hydrophilic pathway to two highly conserved asparagine residues, proposed to have a gating mechanism but their role are still being actively discussed. In addition, a glutamate residue is located about half way in the middle of the channel which is suggested to be highly important for the proton pumping mechanism in bacterial aa_3-type C*c*Os. The other part of the channel is a hydrophobic cavity that continues from the glutamate residue to the binuclear site. How the protons are being transferred in this cavity is still unclear but there are suggestions about functional water molecules transiently present above the glutamate residue (Iwata et al., 1995; Tsukihara et al., 1996; Wikström, Krab, & Sharma, 2018). The D-channel is located in the upper part of pore B and lower part of pore A and it is suggested that bacterial aa_3-type C*c*Os use the D-channel to transfer both protons needed for water formation and protons for the electrochemically proton gradient (Wikström et al., 2018). In contrast, there are arguments that the D-channel of mitochondrial aa_3-type *CcO*s only transfer substrate protons to the BNC while another channel, H-channel, is responsible for the translocation of protons across the membrane (Yoshikawa & Shimada, 2015). However, these theories concerning the H-channel are still not accepted within the field of CcOs.

The K-channel, named after a highly conserved lysine (K) terminates at the binuclear site. It is highly conserved in location in all three types of C*cO*s, suggesting that this channel has been used as a proton transfer route even in the earliest forms of HCOs. It contains the important key residue tyrosine that is covalently bound to one of the histidine ligands of Cu_B and is believed to supply the active site with two substrate protons (Buse et al., 1999; Pereira et al., 2001; Wikström et al., 2018). It has also been proposed that the proton uptake of the K-channel is regulated due to the bindning of a wide set of ligands to the region next to it (Qin, Hiser, Mulichak, Garavito, & Ferguson-Miller, 2006). Yet, how the K-channel operates together with the D-channel is still unclear.

For B-type C*c*Os and C-type C*c*Os, there is an analogue to the K-channel. This channel is proposed to be responsible for both the substrate and the pumped protons but the mechanism is still unclear, especially the route from the BNC to the P-side of the membrane (Wikström et al., 2018). Altough, it it proposed that the lower number of protons being pumped over the membrane is linked to the usage of only one proton translocation route in B- and C-type CcOs instead of two as is common for A-type CcOs (Kannt et al., 1998).

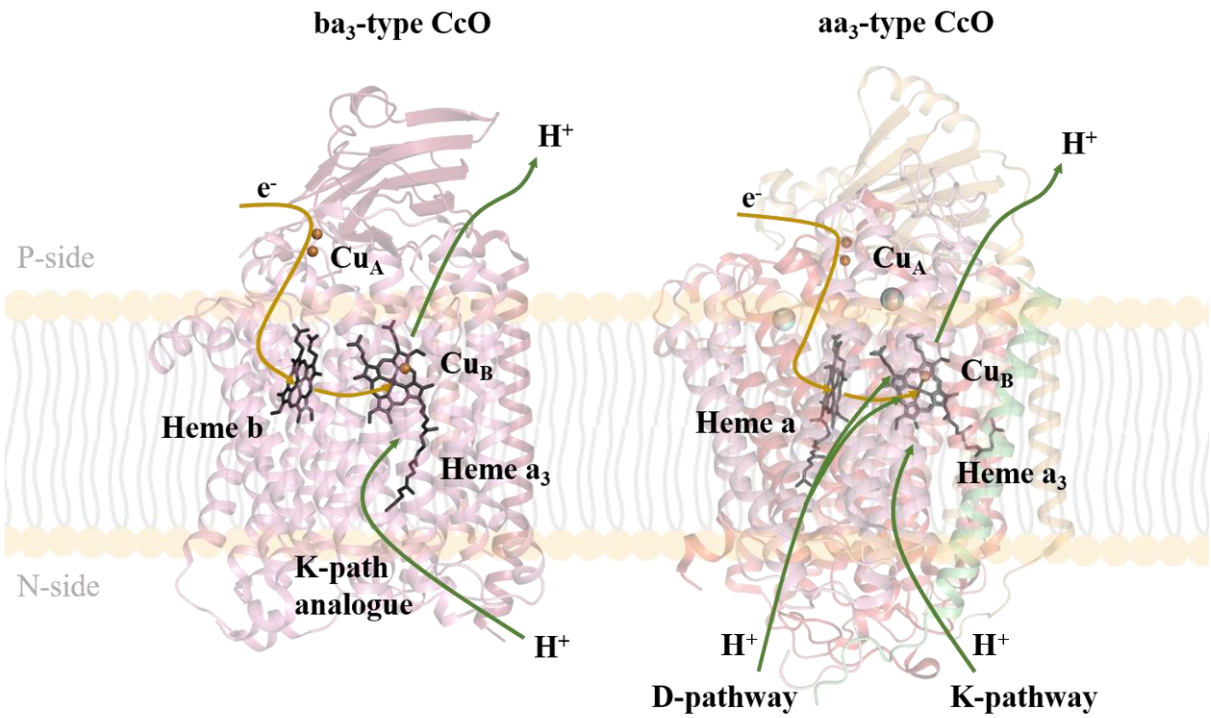

Figure 2. Model of a *ba*$_3$-type (*T. thermophilus*) and *aa*$_3$-type C*c*O (*R. sphaeroides*) with heme groups shown in the transmembrane part of the protein. The orange arrows indicate the electron pathway, moving from the Cu_A-site to the heme a_3 via heme *a* (*aa*$_3$) and *b* (*ba*$_3$). The green arrows show the proton pathway from the N-side through the D-pathway and K-pathway (*aa*$_3$) and K-path analogue (*ba*$_3$) to the heme a_3 for substrate protons for oxygen reduction and for P-side designated protons. PDB ID for the structures are: 3S8F (*ba*$_3$) and 1M56 (*aa*$_3$) (Svensson-Ek et al., 2002; Tiefenbrunn et al., 2011).

1.4.4 *Ba3*-type cytochrome *c* oxidase

The heat tolerant bacteria *Thermus thermophilus* (*T. thermophilus)* strain HB8 has two different terminal oxidases that reduce oxygen to water; *ba*$_3$ and *caa*$_3$. *Ba*$_3$-type C*c*O was the first crystal structure of a B-type HCO to be determined to a resolution at 2.4 Å (Soulimane, Buse, et al., 2000). The *ba*$_3$-type C*c*O accepts electron from the thermostable cytochrome c_{552} (Soulimane et al., 1997) and show a remarkable reactivity towards ligands such as CN^-, CO, NO and H_2O_2. These ligands bind to the heme a_3 of the *ba*$_3$-type C*c*O with the aberrant binding of CN^- to the ferrous state of the iron in the heme group in contrast to the ferric group that is more common in ligation in other oxidases. Furthermore, carbon monoxide binds 50-100 times stronger to the binuclear site of the reduced *ba*$_3$-type C*c*O compared to the *aa*$_3$-type enzyme in bovine heart (Giuffrè et al., 1999; Kim et al., 1998; Surerus et al., 1992). However, even though the A-type C*c*Os are a very well-studied group of proteins, little is still known about the ligand transfer channel in them which is essential for understanding of the mechanism of the protein. There are several suggestions on oxygen routes to the BNC in *aa*$_3$-type C*c*Os, where consensus seems

to be that they start in the membrane hydrophobic region of subunit I and terminates close to the redox active tyrosine. There are also suggestions that these oxygen transfer routes are regulated in some way by the lining residues of the cavity forming the channel (Oliveira, Damas, Baptista, & Soares, 2014). For *ba*$_3$-type C*c*O, the ligand channel differentiate from the *aa*$_3$-type C*c*O channel. While *aa*$_3$-type C*c*O contain a constriction site, a site with suggested regulation of ligand transfer, with a Trp and a Phe in it, *ba*$_3$-type C*c*O has a tyrosine (Tyr133) and a threonine (Thr231) located there instead, two smaller residues compared to the ones in *aa*$_3$-type C*c*O. This is thought to be linked to the ten times faster binding of ligands to heme *a*$_3$ in *ba*$_3$ compared to *aa*$_3$. Furthermore, *ba*$_3$-type C*c*O also contains a highly conserved valine residue that is proposed to be important for oxygen to access the BNC (Funatogawa et al., 2017).

The three subunits of *ba*$_3$-type C*c*O (Figure 3) are all encoded by three separate structural genes (Keightley et al., 1995). The 61.7 kDa subunit I consists of 13 TMH which differentiate the protein from other HCOs that commonly contains 12 TMH (Radzi Noor & Soulimane, 2012). The structure also shows shortened loops which might increase the termostability of the protein by decreasing the entropy of unfolding (Razvi & Scholtz, 2006; Thompson & Eisenberg, 1999). All but one of the redox centers within the proteins are located in the subunit I; the low spin heme *b*, the high spin heme *a*$_3$ and Cu_B where the copper ion together with the iron in heme *a*$_3$ make up the binuclear center (Soulimane, Buse, et al., 2000). Heme *b* is axially ligated by two histidine ligands (His72 and His386) while four other histidine residues and one tyrosine residue coordinate the binuclear center (His233, His282-284 and Tyr237). The heme *a*$_3$ in *ba*$_3$-type C*c*O have a hydrophobic hydroxyethylgeranylgeranyl (HEGG) side chain bound as opposed to the hydroxyethylfarnesyl (HEF) found in other HCOs. There is evidence that the HEGG moiety increase the stability at high temperature with its straight structure that reaches to the cytoplasmic side (Lubben & Morand, 1994). There are also studies showing that the long hydrocarbon chain is important for the function of high spin hemes (Saiki, Mogi, & Anraku, 1992).

Subunit II (18.5 kDa), a polar domain on the P-side of the membrane, consists of several β-sheets and one single TMH. It contains the binuclear copper redox center Cu_A, accepting electrons from the heat stable protein Cytochrome *c*$_{552}$ (Radzi Noor & Soulimane, 2012).

The third subunit, IIa, was first discovered and identified during determination of the first X-ray crystal structure. It consists of 34 residues forming a single TMH of 3.8 kDa (Soulimane, Buse, et al., 2000; Soulimane, Than, Dewor, Huber, & Buse, 2000). Overexpression experiments show that subunit IIa is vital for stabilizing the protein (Chen et al., 2005).

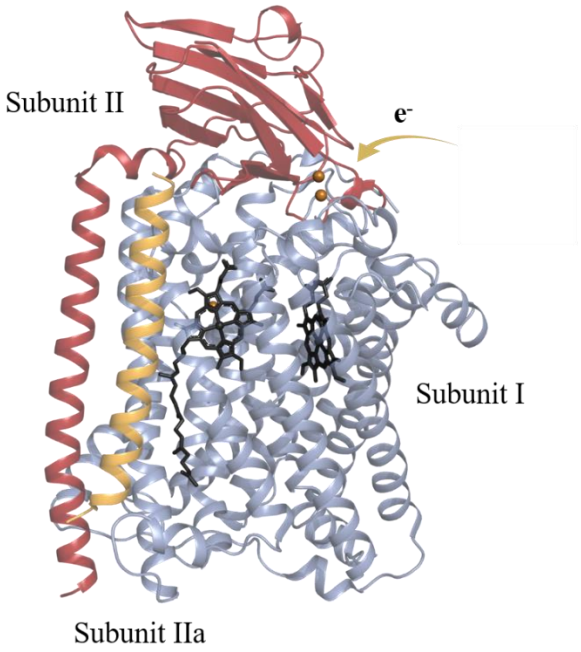

Figure 3. Structure of *ba*$_3$-type C*c*O to view the three different subunits in the protein and how the redox centers are localized in them. Cu_A, situated on the upper right in the picture, consists of wo copper ions and is where the electrons first is donated from Cyt c_{552} and is the only redox center located in subunit II whereas the others are located in subunit I (heme *b*, heme *a*$_3$ and Cu_B. Subunit I consists of 13 TMHs which is seen in blue while subunit II is made up by a polar domain of β-sheets and one TMH (red). Subunit IIa only consists of a single TMH seen in yellow. PDB ID: 3S8F

1.4.5 Redox reactions and intermediate states in C*c*Os

Since the *aa*$_3$-type C*c*O is the most studied model protein of the HCOs, its catalytic cycle will be described more in detail (Figure 4). The first step that initiate redox cycle within the enzyme, is a two-electron donation to the Cu_A-site located in subunit II. The electrons are then transferred to the high-spin catalytic site of heme *a*$_3$/*Cu*$_B$ in subunit I via the low spin heme *a*. The heme *a*$_3$/Cu_B (BNC) center needs to be reduced by two electrons before an oxygen molecule can bind. Further, two additional electrons are needed to break the O-O bond to a total of four electrons and four protons to produce two water molecules. Of these four electrons, two are provided by the reduced heme *a*$_3$-domain and one from the Cu_B-ion, which in turn oxidize the ferrous iron in heme *a*$_3$ into a heme $a_3^{(+4)}$ and $Cu_B^{(+)}$ to $Cu_B^{(2+)}$. The last electron needed for the reduction of oxygen to be complete depend on the reduction-state of heme *a*-domain (Brändén et al., 2006). If it is reduced externally, e.g. with dithionite, the domain can donate an electron to the complex. On the other hand, if heme *a* is oxidized, the electron will be donated by a hydroxyl-group from the highly conserved redox active tyrosine in the catalytic site (Gennis, 1998; Macmillan, Kannt, Behr, Prisner, & Michel, 1999). The shuffling of electrons between the redox centers in the protein are coupled to proton pumping to a total of four $protons_{(p)}$ from the N-side of the membrane to the P-side and the turnover activity of the *aa*$_3$-C*c*O is measured to 1600 electrons per second at pH 6.5 in *R. Sphaeroides* (J P Hosler et al., 1992).

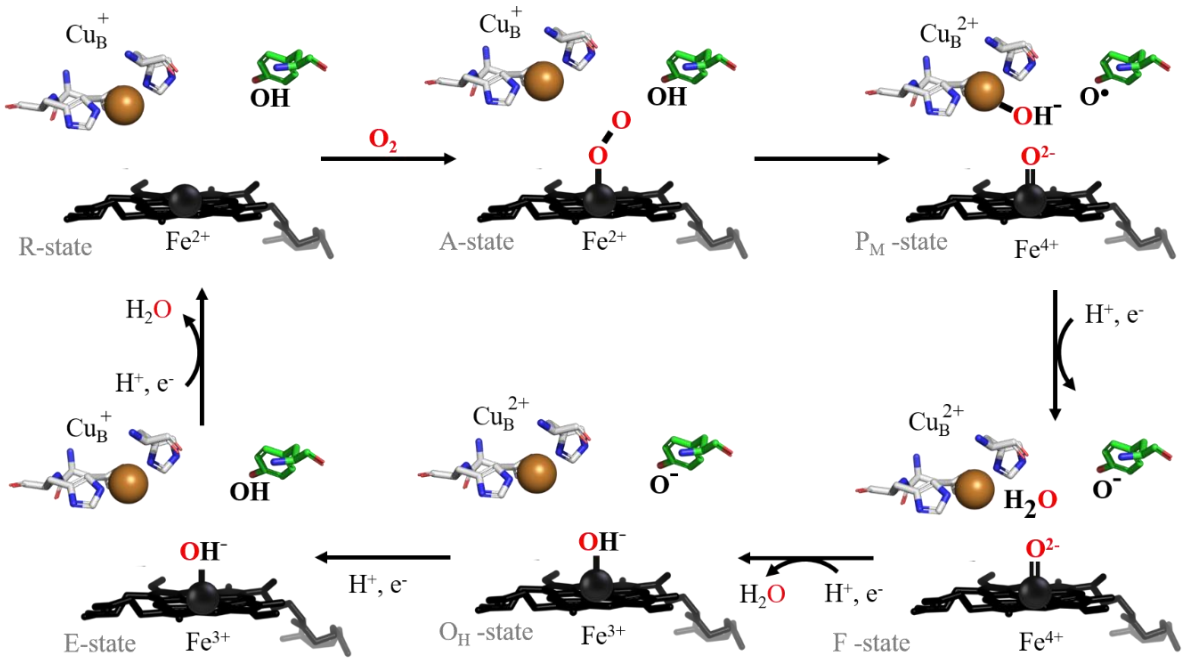

Figure 4. A representation of the electron shuffling within the active site of C*c*Os. The iron atom in heme a_3 oxidates from Fe^{2+} to Fe^{4+} and $Cu_B^{(1+)}$ to $Cu_B^{(2+)}$ while reducing oxygen. The redox active tyrosine donates both an electron and a proton to the reaction. The reaction cycle starts with reduction of the BNC with two electron, denoted R-state. When an oxygen molecule binds, the A-state is formed. In the next step, P_M, one electron is donated by a conserved tyrosine residue which creates a radical and cleavage of the oxygen molecule. By addition of a proton and an electron in the F- and O_H-state, a water molecule in each step can be formed. Each transfer of electrons in step P_M to F, F to O_H, O_H to E and E to R result in one proton being pumped across the membrane to a total of four protons. Figure is remade from Brändén et al. 2006.

1.5 Energy transduction and sensory signaling

1.5.1 Reaction centre

Plants, algae and cyanobacteria produce carbohydrates by harvesting the energy of sunlight. They thereby power virtually all of the biological activity on the planet with only a few exceptions. In plants this is achieved by photon absorption by two photosystems: Photosystem I and II (PSI and PSII). PSI and PSII transfer electrons from water to ferredoxin by a series of redox reactions driven by differences in redox potentials. A similar protein to PSI and PSII is reaction centre (RC) that found in the purple photosynthetic bacteria *Blastochloris viridi* (*Bl. viridi*). Compared to PSII, RCs absorb photons but are missing an oxygen evolving site. Therefore, purple photosynthetic bacteria either use sulphur as an electron donor or re-use their electrons in a cyclic electron transfer system. *Bl. viridi* use the latter system of cycling electrons

which allow them to thrive in anaerobic environments without the need of an electron donor (Imhoff, 2007).

RC from *Bl. viridis* was the first membrane protein to be structurally determined by X-ray crystallography and consists of two subunits containing five TMH each, a cytochrome subunit on the cytoplasmic side and a hydrophilic domain of a single alpha helix on the periplasmic side. Apart from the protein itself, RC is surrounded by 17 light harvesting proteins that function as an antenna. This ring of light harvesting proteins capture photons and direct them to RC to initiate an electron transfer chain. Since it was first membrane protein to be structurally determined, RC has commonly been used as a model protein for all photosynthetic reactions (Barber, 2017; Nowicka & Kruk, 2016).

1.5.2 Rhodopsins

Sensory rhodopsin II (SRII) from *Natronomonas pharaonis* (*N. pharaonis*) is a microbial photosensitive protein with seven TMH and a retinal molecule (Figure 5). It is part of a large family of at least 1000 members with broad diversity such as ion pumping, ion gating and sensory perception. SRII is responsible for the movement of archaea to find optimal light conditions using a flagella (Sharma, Spudich, & Doolittle, 2006). It binds to a signal tranducing protein (HtrII) and has been a model system for bacterial signal transduction across the plasma bilayer. Bacteriorhodopsin (bR) from *Halobacterium salinarium* (*H. salinarium*) is another protein from the same retinal-containing family and is very well studied due to its proton pumping mechanism. As with SRII, bR has a retinal molecule buried in the protein and a conserved lysine that is covalently bound to helix G through a Schiff base, which is a conserved part of the active site. Upon light triggering, the retinal molecule isomerizes which in bR causes a deprotonation of the Schiff base and a protonation of an aspartic acid residue. This is the starting point of various structural changes that in the end sums up to a proton transfer to the cytoplasmic side from the extracellular side (Pebay-Peyroula, Rummel, Rosenbusch, & Landau, 1997; A Royant et al., 2001). In SRII similar mechanistic events occur with the deprotonation of the Schiff base and protonation of an aspartic acid residue, but with no net proton pumping. For SRII the complete photocycle takes about two seconds while it lasts about ten milliseconds for bR. A theory is that the prolonged photocycle for SRII is needed to amplify and transfer the signal (Klare et al., 2006; Lozier, Bogomolni, & Stoeckenius, 1975).

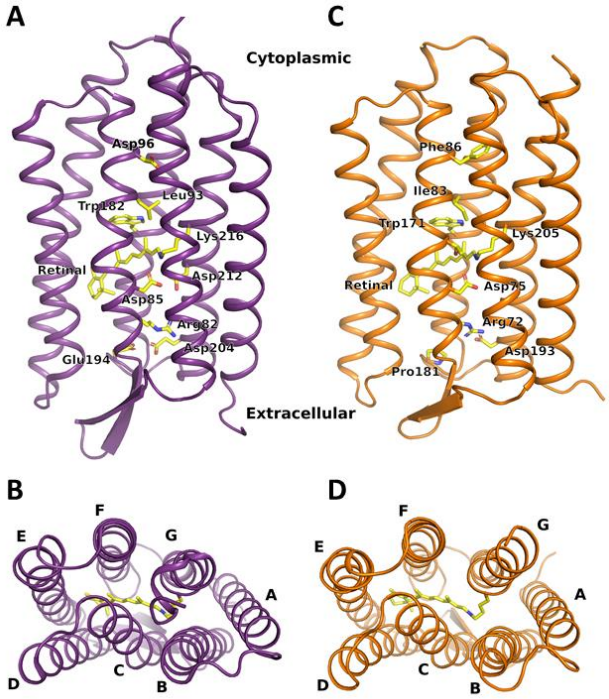

Figure 5. The figure display bR (A and B) and SRII (C and D) in side views (A and C) and from a cytoplasmic view (B and D) to showcase the similarities of the two proteins. Even though they have similar chemical 3D structures, their biological function is widely different suggesting a common ancestor. Figure from paper V

1.6 Scope of the thesis

Structure determination using X-ray crystallography is an important part in understanding mechanistic features of membrane proteins. For the C*c*Os, the mechanism of proton pumping is still under elucidation. By triggering structural changes with carbon monoxide and preparing for future binding with oxygen as a ligand, mechanistic features regarding proton pumping can be revealed by trapping intermediates using pump-probe X-ray serial crystallography.

Determining membrane protein structures with serial X-ray crystallography demand large volumes of crystals each of which should be smaller than 20 micrometer in size. Therefore, a crystallization method that can meet the demand of screening and producing large volumes of functional protein crystals in a membrane-mimicking system, such as *in meso* methods, is of importance.

Hence the aim of this thesis is divided into two parts:

Firstly, developing a method of producing membrane protein crystals in lipidic cubic phase in a system that can be monitored over time with high magnifications using a stereomicroscope, to aid screening, optimization and production of microcrystals for serial crystallography.

Secondly, evaluating the methods applicability in serial crystallography studies at synchrotron and XFEL sources by using widely different membrane protein targets to gain biological insights.

2. Chapter 2

2. Methodology

2.1 Cell cultivation (paper I-III)

2.1.1 *Thermus thermophilus*

The Gram-negative bacteria *Thermus thermophilus* (*T. thermophilus*) used to produce ba_3- type C*c*O, is an extremely thermophilic organism that inhabits high temperature conditions in hot springs where they thrive in temperatures around 65-72 ºC. About 69 mole percent of the DNA consists of G-C pairings and by heating bulk samples of protein extracted from the bacteria, only 10% of the protein was denatured when exposed at 110 ºC for 5 min (Oshima & Imahori, 1974). The HB8 strain of *T. thermophilus* is a facultative anaerobe which means it can thrive under both aerobic and anaerobic conditions. Under anaerobic conditions, the bacteria can utilize nitrate as an electron acceptor since it has a nitrate reductase gene cluster (Ramírez-Arcos, Fernández-Herrero, & Berenguer, 1998).

T. thermophilus encodes for two terminal oxidases in the presence of oxygen, caa_3-type cytochrome *c* oxidase (caa_3-type C*c*O) and ba_3-type C*c*O (Radzi Noor & Soulimane, 2012). In contrast to caa_3 that is produced constitutively, ba_3 is only produced when oxygen levels are low. At 70 ºC, the solubility of oxygen has decreased to ~60 % compared to at 25 ºC (Wilhelm, Battino, & Wilcock, 1977) which increase the production of the high oxygen-affinity ba_3-C*c*O. When oxygen levels are high, the low oxygen-affinity caa_3-C*c*O will dominate as the terminal oxidase. This is because the ba_3-C*c*O has much higher affinity for ligands such as O_2 and CO compared to the caa_3-enzyme. However, ba_3-C*c*O only translocate two protons across the membrane instead of four protons like caa_3-C*c*O does (Kannt et al., 1998; Radzi Noor & Soulimane, 2012).

2.1.2 Gene expression

Gene expression of membrane proteins often differ from soluble protein gene expression in a few aspects. As an example, the yield of membrane proteins in their natural host is not very abundant and membrane proteins often have to be overexpressed recombinantly. Also, the stability of membrane proteins are much lower in aqueous solutions when compared to soluble proteins. This is due to their hydrophobic regions, folding mechanism and interactions with surrounding lipids such as sterols and proteins. Loss of stability can cause aggregation and decrease of function. To obtain ba_3-C*c*O, the protein is expressed recombinantly in its native host, *T. thermophilus* strain HB8, with a 6-polyhistidine-tag (His-tag) in the N-terminal of subunit I (Chen et al., 2005).

2.1 Membrane protein purification (paper I-III)

2.2.1 Solubilization

When cells are harvested and the membranes resulting from cell lysis of sonication are collected, the target protein must be extracted from its native environment into solution by solubilization. Solubilization can be carried out by adding an amphiphilic molecule such as detergent at a concentration that allows for micelle formation (see CMC in section 1.5.1 Lipidic mesophases). There are three different classes of detergents; ionic, non-ionic and zwitterionic and within each class there are a number of different types available, each with different properties. Therefore a detergent screen is often required to find detergent suitable for the target protein. Detergents self-assembly into micelles with their hydrophobic tails inwards and their hydrophilic heads facing the aqueous solution. The number of detergent molecules in a micelle is referred to as the aggregation number and the length of the tail is direct proportional to the hydrophobicity degree (Lichtenberg, Ahyayauch, Alonso, & Goñi, 2013; Lichtenberg, Robson, & Dennis, 1983). The micelle formation is affected by several factors such as ionic strength and temperature. Ionic detergents are regarded as harsh and an example is sodium dodecyl sulfate (SDS) that is commonly used in biochemical techniques. SDS denatures the proteins making them loose function by interrupting the non-covalent forces maintain the secondary and tertiary structure. Due to their charged head groups, they are highly affected by ionic strength and cannot be removed by ion exchange chromatography. In comparison, non-ionic detergents are more affected by temperature compared to ionic strength and are regarded as mild (Le Maire, Champeil, & Møller, 2000).

2.2.2 Liquid chromatography

Liquid chromatography (LC) is a method that uses the physio-chemical properties of proteins to separate and identify the target protein from the solubilized mix of different proteins. There are different kinds of LC such as immobilized affinity (IMAC), ion exchange (IEC) and size exclusion (SEC) chromatography (Ali, Aboul-Enein, Singh, Singh, & Sharma, 2010) and they all share the properties of one stationary phase and one mobile phase. When purifying proteins for structure determination, the mobile phase is the protein solution while the stationary phase vary with method of LC.

For IMAC the stationary phase is a binding agent that takes advantage of selective and reversible binding. These bindings occur naturally in many interactions, for example between and antigen and an antibody or a protein and its substrate. The mobile phase with the target is then passed onto a column containing a resin with a stationary phase that will retain the target in question. Other sample components can then be eluted by passing on excess amount of weak application buffer onto the column. The target protein is then released from the stationary phase by either non-competitive elution buffer that changes the pH or ionic strength or by excess of competitive elution buffer that compete with the target protein (Rodriguez et al., 2020). Another chromatographic method is IEC that separate molecules by their net charge. A positively charged stationary phase (anion exchange) will bind to the negatively charged protein while

more positively charged proteins will be washed out and vice versa. The protein is then eluted by increasing the salt concentration (Helfferich, 1995). SEC separates molecules by their size by having a matrix with porous gel beads that will pass proteins with small molecular masses but not larger ones. Larger proteins will then migrate faster through the matrix and therefore elute earlier than smaller ones. SEC is also used as a way to validate the integrity of the protein. The elution profile can also give hints about purity, aggregation forms and oligomeric state (Striegel, 2017).

2.2.3 Production and purification of *ba*$_3$-type C*c*O (paper I-III)

Cells of *T. thermophilus* (with a selection marker for Kanamycin) were obtained from another lab and cell growth and protein production optimization proceeded from previously described growth protocols (Chen et al., 2005). Several cell cultivation systems were tested such as fermenters and different sized shaking flasks. Variables such as temperature, rpms and different inoculation sample volumes and time of growth before and after induction were optimized against the limitation of the equipment. In the end, a cell growth protocol was established were cells were first grown over night in 3L baffled flasks at 60 ºC with oxygen to obtain larger amount of cells before transferred to unbaffled Fernbach flasks of 3-5 L filled with 73 % media, at 60 ºC at 110 rpm for 3-4 days, to lower the oxygen levels to induce the *ba*$_3$-type C*c*O expression. During gene expression of *ba*$_3$-type C*c*O, the unbaffled flasks were tested with different sealing methods. If sealed too much cells started to die if and sealed too lightly *ba*$_3$-type C*c*O did not express. Flasks were best capped with aluminum foil and a minimum of three layers of parafilm to keep the oxygen levels low and avoid contamination of other organisms.

Harvested cells were broken with sonication and a purification protocol was developed and extended based on previously described methods (Chen et al., 2005). A mild non-ionic detergent, Triton X-100, was used to solubilize the membrane followed by IMAC using a nickel resin (Ni-NTA) as a stationary phase which binds to the His-tag on the N-terminus of subunit I. The protein was washed and eluted competitively by an elution buffer containing a higher concentration of imidazole. The protein was then immediately subjected to dialysis for removal of the imidazole. For paper III additionally steps were added to increase purity due to a change of buffer from sodium cacodylate trihydrate (SCT) to MES which seems to decrease stability of the protein but lacks the highly toxic features of arsenic. A few different anionic IECs were tested before a DEAE FF anionic IEC (HiPrep^{TM} 16/10, GE Healtcare Life Science) was used to exchange buffers (5 mM Hepes to 20 mM Tris-HCl) and increase purity to crystallization standards. A final SEC (Superdex 200 Increase 10/300 GL, GE Healthcare Life Science) step was sometimes required to remove aggregation if protein had been stored for a longer period of time and the ratio of A(414 nm)/A(280 nm) was below 0.70 which is correlation of absorbance of oxidized heme *b* and total protein concentration. Pure protein was then stored in 4 ºC until crystallization. Purified *ba*$_3$-type C*c*O was then concentrated to a final concentration using an ultrafiltration unit (100 000 MWCO cut off), validated by absorbance spectroscopy and spun down in Eppendorf tubes (1h, 16,9krcf) to remove any precipitated protein. Three methods was mainly used to monitor the process of purification and measure concentration; UV/VIS, SDS-page and Western blotting.

2.2.4 Absorption spectroscopy

Since *ba*$_3$-type C*c*O contain several absorbing species (chromophores), a nondestructive technique such as ultraviolet-visible adsorption spectroscopy (UV/VIS spectroscopy) can be used to quantify and identify different states such as intermediates of the protein. UV/VIS spectroscopy measures the interaction of proteins with electromagnetic radiation in the UV/VIS range (150-400 kJ/mol) by exciting delocalized electrons primarily from aromatic structures such as porphyrins in C*c*Os or aromatic residues such as tryptophan and tyrosine at wavelengths around 280 nm. The strength of the absorbance and wavelength of absorption also depends on the molecular environment of its chromophores, making it ideal for enzymatic kinetics, ligand-binding measurements and conformational transitions. By observing how the absorption spectra shifts in wavelength and strength of the absorbance upon structural change in the environment of the chromophore, protein kinetics can be measured as a function of time, capturing intermediate states of the protein. The activity of the protein can also be determined by measuring change in substrate- and protein concentration as a function of time. The reaction rates can thus be calculated from the absorbance data by Lambert-Beers law. According to this law, there is a linear relationship between the absorbance (A), the molar concentration of the protein (c), the molar adsorption coefficient (ε) and the path length of the light (l):

$$A = \varepsilon * c * l \tag{1.1}$$

Where the molar adsorption coefficient measure how strong an absorber the sample is at a certain wavelength and the length of a pathway depends on the spectrophotometer but usually 1 cm if a cuvette is used (Schmid, 2001).

Ba$_3$-type C*c*O give rise to a multiple set of different UV/VIS-spectra (Figure 6, Table 1) due to their porphyrin-containing hemes that can either be reduced or oxidized but also affected by ligands such as CO. Hemes typically give rise to an intense peak in the blue wavelength region around 400 nm of the visible spectrum, also called a Soret peak that is characterized by a ground state to second state excitement of electrons. The low spin heme *b* give rise to two Soret peaks depending on the state of the protein; 427 (reduced) and 408 nm (oxidixed). Upon reduction the protein also give rise to two absorbance peaks at wavelengths of around 528 and 559 nm, both in the Q-band region corresponding to ground to first state excited transition. Heme *a*$_3$ also contributes to a Soret peak giving rise to a shoulder at 441 nm and a small peak at 611 nm, both in reduced state (Giovannetti, 2012; Hellwig, Soulimane, Buse, & Mantele, 1999). In our spectra we saw a small shift of some peaks compared to the literature likely due to ligands and pH. We measured the oxidized peak at 414 nm compared to 408 nm and 427, 445, 538 and 560 nm for the reduced state.

Table 1. Absorbance peaks of *ba*$_3$-type C*c*O in three different states which can be used to measure concentration as well as a validation method.

Oxidized sample (nm)	Reduced sample (nm)	Reduced and CO-bound (nm)
415	-	-
-	427	427
-	445	
-	530	530
-	560	560

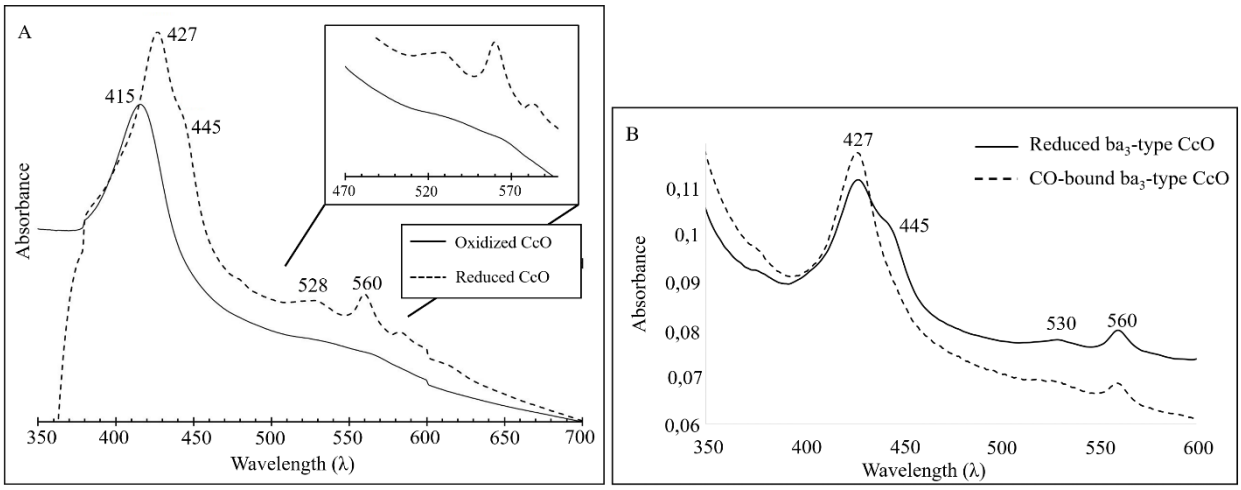

Figure 6. UV/VIS absorbance spectra of *ba*$_3$-type C*c*O crystals. In (A) the difference between oxidized (black line) and reduced (dashed line) crystals are shown. For the reduced spectrum, three clear peaks are seen at 427, 528 and 560 nm with a shoulder at 445 nm. The oxidized spectrum only has one clear peak at 415 nm. In (B) the difference between reduced (black line) and CO bound (dashed) crystals are shown. The CO-bound crystals lack the shoulder at 445nm. Figures from paper III

2.3 Crystallization (paper I-V)

Crystals are formed when protein molecules are organized in an orderly array, requiring a crystallization condition with a high purity and oligomeric homogeneity of the protein sample. For protein molecules to self-organize they need specific interactions that are both highly directional and organized in a way that allows for a three-dimensional lattice formation. The crystallization process then ends when the solution is depleted of protein molecules or contaminated by impurities. Crystallizing membrane proteins is regarded as more challenging compared to soluble proteins due to their surface duality with both hydrophilic and hydrophobic regions and their instability in solution (Krauss, Merlino, Vergara, & Sica, 2013).

2.3.1 *In surfo* crystallization

To accomplish crystallization, there are two major methods: *in meso*- and *in surfo* crystallization (Chayen, 1999; Moraes et al., 2014). The difference between them are that *in meso* crystallization use lipids and *in surfo* methods use aqueous solutions during crystallization. One example of a common *in surfo* method is vapor diffusion. Vapor diffusion aims to supersaturate a protein solution by migration of water molecules from the protein solution to a reservoir solution containing a higher concentration of solutes. This is achieved by adding reservoir solution and a protein solution in a sealed chamber. The details of how the protein solution is added to the chamber determines if it is a sitting drop- or hanging drop vapor diffusion method.

For membrane proteins this method involve being in an environment that is aqueous, most often also ionic due to addition of different salts. To retain stability and functionality in a highly hydrophilic- and ionic system, the membrane proteins need to be imbedded in detergent micelles to cover their hydrophobic parts. Finding a suitable detergent and the right detergent concentration often requires a screening process performed with a validation method such as a temperature screen or chromatography, to find a condition that increase protein stability and promote crystal growth. Depending on the protein concentration and precipitant solution, the route towards crystals may vary (Krauss et al., 2013).

The crystallization process can be visualized with a two-dimensional phase diagram (Figure 7). As the water molecules vaporizes, the protein- and precipitant solution will increase in concentration. The crystallization process will then move towards the nucleation zone. Here the protein molecules can start to arrange themselves into arrays if conditions are right. This process consumes protein molecules from the solution, making the concentration decrease. As a result, the process will shift from the nucleation zone to the metastable zone where crystal growth is possible. However, for most cases the process will continue to the more energy beneficial precipitant zone and the protein sample will precipitate. To find a favorable metastable condition to avoid precipitation, several factors can be varied such as pH, salt, detergent and temperature to mention some (Krauss et al., 2013; Mcpherson & Gavira, 2014; Moraes et al., 2014).

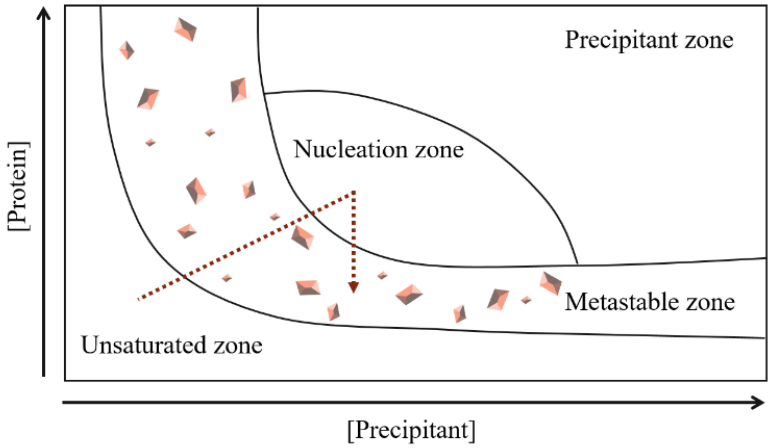

Figure 7. A phase diagram visualizing the crystallization process in a vapor diffusion setup. As the protein and precipitant concentration increases due to evaporation of water, the process moves from lower left to the nucleation zone where the protein molecules starts to order themselves. From there, the process can either move further to the upper right and precipitate or continuing to build the three-dimensional lattice, creating crystals, in the metastable zone.

Since the vapor diffusion method is quite unstable with changing conditions during the equilibrium process upon crystal growth, efforts have been made to control growth and nucleation rates to gain larger crystals such as changing drop size and adding additives. One way to control the crystal growth is to use a method called crystal seeding with the use of nucleants. It is a technique used to create a starting point, a template on which protein molecules can bind and a new crystal can emerge. Seeding can be performed by both using crystals from the same protein or by foreign material such as silicon. The added material allows for crystallization directly from the crystal growth stage in the metastable zone and thus skipping the nucleation process entirely (Figure 7) (Bergfors, 2003; Saridakis & Chayen, 2009).

Another way of obtaining large crystals under controlled circumstances is to use a batch crystallization method. Batch crystallization involve direct mixing of protein sample with a crystallization solution in contrast to diffusion through air as in vapor diffusion crystallization. There are a few different batch crystallization set ups where one involve the use of oils to prevent dehydration of the drop (microbatch) (Chayen et. al., 1990; Dessau & Modis, 2011) and one without oils. The latter method mixes precipitant with protein in a slow manner before transferring the solution to a sealed container such as wells with coverslips for crystal growth. However, these methods require pre-knowledge of crystallization conditions that can be screened around (Rayment, 2002). For example, only 60-80 % of the precipitant concentration is needed in a batch crystallization compared to the amount precipitant needed in a hanging drop set up (Chayen, 1998) which needs to be adjusted for. In addition, a difference of down to 0.5 % of precipitant concentration can have major effects on crystal size and growth in batch crystallization (Rayment, 2002).

2.3.2 Lipidic mesophases

Mixing amphiphilic molecules such as lipids with water under proper conditions will spontaneously create a matter neither solid or liquid, referred to as a mesophase (Landau & Rosenbusch, 1996; Luzzati, Tardieu, & Gulik-Krzywicki, 1968). The driving force of this spontaneous organization of lipids is shielding the hydrophobic core of the bilayer from water by exposing the polar head groups to the surface of the aqueous solution (Lindblom & Rilfors, 1989). At low lipid concentration, the lipids will be dispersed in solution without any ordering. By increasing the lipid concentration, different formations of lipid assemblies will occur. With enough lipids, the amphiphilic molecules will self-assemble into spherical aggregates also referred to as micelles. The concentration, when aggregation occurs, is known as the critical micelle concentration (CMC). The CMC of lipids depends on several factors such as the addition of electrolytes, pH, type of lipid and temperature (Fuguet, Ràfols, Rosés, & Bosch, 2005). At even higher concentrations, the aggregates start to become ordered and disposed regularly in space. At this point the lipid containing solution has become a lyotropic crystalline matter, a mesophase (Lindblom & Rilfors, 1989).

For biologists, one type of mesophase, the lamellar phase, has been well known with its multi-bilayer structure in several biological systems and it was not until the 1960s that another class of phases was discovered; the cubic phase (Ia3d-symmetry) (Luzzati et al., 1968; Spegt & Skoulois, 1966). There are different types of cubic lipidic mesophases and they are formed by a single lipid bilayer. Compared to lamellar phases that exhibit one dimensional periodicity and hexagonal (rod shaped) with two dimensions, cubic phases display a three dimensional space recurrence which make them optically isotropic in contrast with the two former phase groups that are anisotropic. The structure of the cubic bilayer in three dimensions can either be arranged into a micelles arranged in a cubic lattice (discontinuous micellar array) or be continuous and separate two distinct interpenetrating water channels (bicontinuous) (Figure 11) where they follow an infinite periodic minimal surface (IPMS), large cell structures that can be considered as crystals of surfaces or film with cubic symmetry (described in section 2.3.4) (Rummel et al., 1998; Sadoc & Charvolin, 1989). Both cubic systems diffuse water-soluble molecules in the aqueous compartments but only the bicontinuous phase diffuse lipid-soluble substances freely within the bilayer since with the micellar array, diffusion is restricted within the micelles (Rummel et al., 1998). This property of lateral movements within the bicontinuous cubic phase will be important in the matter of protein stability and crystallization later in this thesis.

2.3.3 Monoolein

Monoolein (MO) is a monoacylglycerol (MAG) and was the first lipid to be used *in meso* crystallization and is often regarded as the standard lipid to be used in protein crystallography (Qiu & Caffrey, 2000). MO is also denoted 9.9 MAG due to its carbon structure of a nine carbon neck and nine carbon tail making it 18 carbons long with a double bond between C9 and C10 (Figure 8). MO forms a bilayer of approximately 32 Å in width and a water channel of 40 Å in diameter at 40 ºC (50 Å Ø at RT) in the Pn3m phase (L. V Misquitta et al., 2004). Because of the temperature-dependent size of the water channels, the unit cell of MO range from 112.8 Å (20 ºC) to 84.6 Å (50.1 ºC) with 43.6 % respectively 42.5 % water (w/w) (Jason Briggs, Hesson Chung, & Martin Caffrey, 1996). For ba_3-type C*c*O MO was used as a standard lipid, both for development of a new crystallization method and for crystal production.

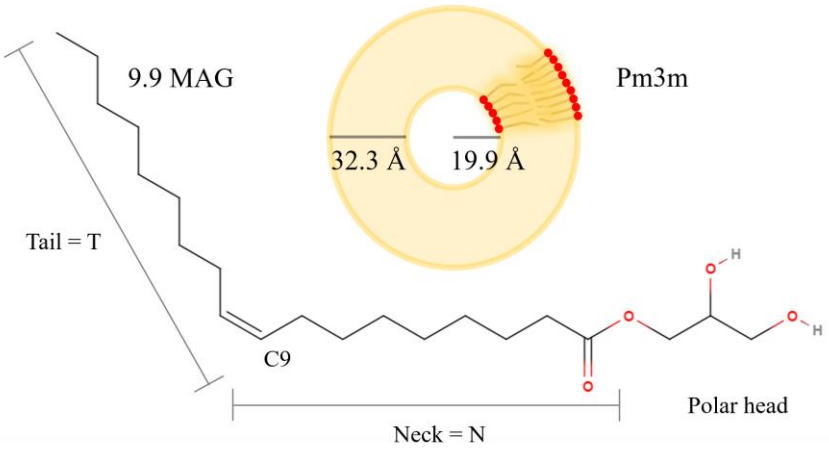

Figure 8. Structure of 9.9 MAG with its two nine carbon elements of neck and tail together with a cross cut of the fully hydrated Pn3m phase that emphasize the thickness of the bilayer and water channel at 40 º C. The length of the acyl chain is one of the factors both affecting the thickness of the bilayer and the diameter of the aqueous channel.

2.3.4 Description and classification of bicontinuous lipidic cubic phases

To describe lipidic bicontinuous cubic phase, a mathematical description of infinite periodic minimal surfaces (IPMS) is used. A minimal surface can be described as a soap film with equal pressure on each side that stretches in three dimensions (Mackay, 1985). The IPMS is located in LCP within the non-intersecting bilayer and extends with it making it run parallel with the two monolayers covering it, separating space into two channels. The bending of the surfaces, the periodic saddles (Figure 9), can be described by two equal principal curvatures with opposite signs at every point, making the net overall curvature of the surfaces zero (Rummel et al., 1998; Sadoc & Charvolin, 1989).

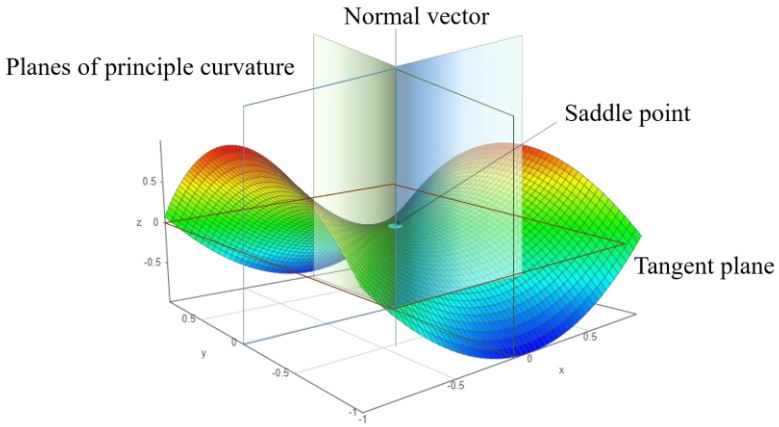

Figure 9. A saddle surface ($z = x^2 - y^2$) with a saddle point in the Euclidean space. The infinite periodic minimal surface that describes the lipidic bicontinuous cubic phase with two principal curvatures has a saddle point that's equal to the equilibrium point.

Even though IPMS is a way of describing bicontinuous cubic phases in a mathematical way and can be used to develop new phases for different applications (Ichikawa, Okafuji, Kato, & Ohno, 2016), classifying them is usually done by using the geometrical space groups obtained by X-ray diffraction. A cubic structure can be either be a primitive lattice that is denoted with P, a body-centered lattice I and face-centered lattice denoted as F accordingly to the Bravais lattices in three dimensions (Lindblom & Rilfors, 1989).

Phases of MO (Figure 10) include the lamellar crystalline phase (L_C), the lamellar mesophase (L_α) and two cubic phases with the space group Pn3m, also denoted as a Q^{224} (diamond lattice, Figure 11) and Ia3d (Q^{230}) to mention a few (Briggs & Caffrey, 1994). For protein crystallization with MO, the standard water/MO ratio is typically 40 % water and 60 % MO to obtain the cubic bicontinuous Pn3m phase at room temperature (Figure 10). Less water will convert the Pn3m-phase into the cubic Ia3d-phase while more water will fully hydrate the Pn3m-phase and bulk water (Y. Misquitta et al., 2004). Hydration levels of less than 20 % water will transform the cubic phases into lamellar phase at the same temperature, first into the L_α and then at about 10 % water (w/w) into the L_c-phase. At temperatures as high as 90 degrees Celsius, the two cubic phases will turn into a hexagonal phase. These boundaries can be seen in temperature phase diagrams over different lipids and are useful during crystallization trials (Figure 10) (Cherezov et al., 2006).

The letter denotation of the space groups represent different symmetry operations, an operation that can be performed in which the appearance of an object is without change. For example the letter m symbolizes a mirror plane symmetry; an operation that by cutting the object in half and placing a mirror in the cross section will reproduce the other half of the object (Giacovazzo, 2014).The different surfaces of the bilayer are also represented with a capital letter. For example, the cubic space group Ia3d or Q^{230}, is described mathematically by the IPMS denoted G for gyroid or gerrymander's walk while the cubic bicontinuous Pn3m (Q^{224}) holds the IPMS letter D for diamond or devil's delight (Rummel et al., 1998).

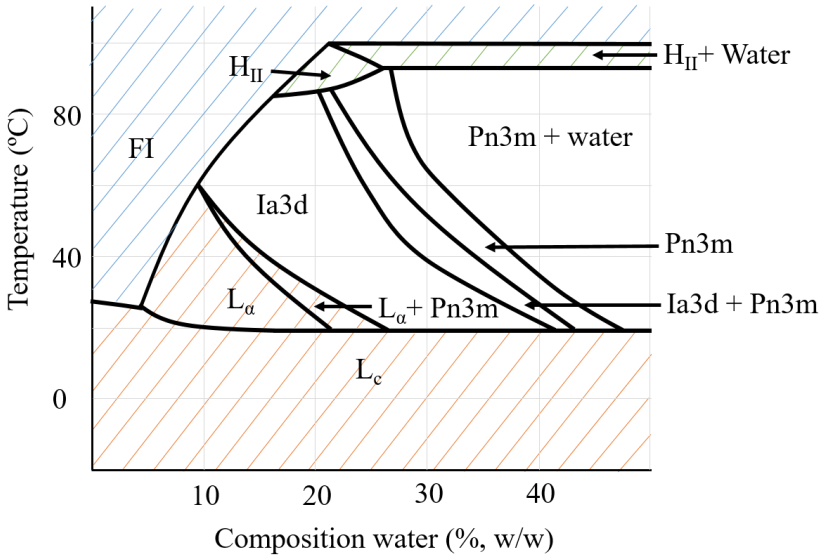

Figure 10. A schematic temperature-composition phase diagram of monoolein in water. Red lines represents a lamellar phase (L_c and L_α), green lines hexagonal phases (H_{II}) and blue lines a fluid isotropic phase (FI). Unmarked area represent cubic phases (Ia3d and Pn3m). Figure remade from Qui and Caffrey, 2000.

2.3.5 LCP as a protein host

There are several ways to grow membrane protein crystals, all have the common challenges of extracting the protein out of their native membrane by detergent solubilization and arranging the protein molecules so that they form crystalline matter. One way of creating crystals is to use LCP that mimic the membrane to increase stability of the protein and support crystal growth in a well ordered manner (Landau & Rosenbusch, 1996).

The lipid bilayer in LCP is regarded as constant in thickness over temperature which presumes that the structural constraint to the incorporation of membrane protein into LCP is the size of the aqueous channels. At room temperature, the water channel is about 50 Å but can be altered by temperature, the length of the acyl chain and location of the double bond in the acyl chain (Rummel et al., 1998). By either lowering the temperature or decreasing the length of the chain, the aqueous channel can be enlarged to accommodate large hydrophilic protein domains (Jason Briggs et al., 1996). The thickness of the bilayer itself can also be altered by changing the structure of the acyl chain which is of interest to adapt the bilayer to the size of the hydrophobic intersection of the membrane protein (Li, Lee, & Caffrey, 2011; Li, Shah, & Caffrey, 2013; Y. Misquitta et al., 2004). The altering of the lipids building up the bilayer is also a way of increasing the range of working temperature during crystallization. 9.9 MAG loose its mesophase properties in temperatures lower than 17 ºC (Qiu & Caffrey, 2000), but by using 7.9 MAG, crystallization of heat sensitive proteins is possible at 4 ºC (Y. Misquitta et al., 2004). Adding additives such as other lipids to the lipidic phase, can impact the lipid structure in several different ways. This includes lowering the degree of curvature allows for more water to be absorbed and thus expands the lattice parameters.

Another way of expanding the lattice parameters is to transform the cubic phase into an hexagonal or lamellar one (Cherezov, Clogston, Misquitta, Abdel-Gawad, & Caffrey, 2002). Addition of small amphiphilic peptides can both induce swelling or shrinking of the unit cell but also induce phase transformation (Yaghmur, Laggner, Zhang, Rappolt, & Scalas, 2007). These additions can increase or decrease protein stability either by the change of the structure of the lipidic phase or by interacting with the protein or lipids directly (Liu et al., 2010). One example is the addition of cholesterol which has shown increased stability of membrane proteins and improvement of crystal shape and size in LCP as for the human β2 adrenergic receptor (Hanson et al., 2008; W. Liu et al., 2010).

Figure 11. Model of cubic Pn3m (diamond)-mesophase during the event of crystallization. *Ba*$_3$-C*c*O situated in the bilayer of the bicontinuous phase (micelle-like in 2D, channel-like in 3D) diffuse and concentrate into a lamellar structure upon addition of precipitant. The rearrangement and spontaneous organization of protein progresses to nucleation. Model is not to scale and is a modified illustration made from Li, Lee, & Caffrey, 2011.

2.3.7 *In meso* crystallization

Proteins reconstituted into LCP are in their native conformation and are unconfined to move laterally within the bilayer. Upon addition of precipitant to the LCP, the cubic bicontinuous phase dehydrates and a phase separation into a lamellar phase occurs (M Caffrey, 2008; Cherezov & Caffrey, 2007; Paas et al., 2003; Qutub et al., 2004). The lateral movement of the protein within the bilayer then enables enrichment of protein in the lamellar phase which induce nucleation and crystallization when protein molecules are free to organize themselves into repeated elements (Figure 11) (Landau & Rosenbusch, 1996; Lindblom & Rilfors, 1989).

Membrane protein crystals are classified by how they are formed. For membrane protein crystals there are mainly two types of crystal lattices; type I and type II. In type I, lipids (detergents) surround the protein molecule in a bilayer-type of way mimicking the natural environment of the protein, the membrane, which increase stability of the protein by allowing for multiple protein-protein and protein-lipid interactions. In comparison, type II crystal packing is mostly due to hydrophilic interactions between the protein molecules since the hydrophobic domains of the protein is shielded by detergent micelles. This reduces the amount

of protein-protein contacts making the crystals less stable and thus more fragile. LCP enables protein packing to be of type I (Figure 12) which means that membrane protein crystals of two-dimensions are arranged in stacks in each geometrical plane making it three-dimensional in space. This arrangement can be derived from the amphiphilic nature of the lipids which enables hydrophobic interactions between protein-protein molecules as well as protein-lipids while polar interactions stabilize the crystal structure in the third dimension. As a result, higher order of protein organization can be achieved due to both hydrophilic and hydrophobic protein-protein and protein-lipid interactions. (Hartmut, 1983; W. Liu et al., 2010). According to previous research, *ba*$_3$-type C*c*O crystallized in LCP is confirmed to be of a type I crystal packing as expected (Tiefenbrunn et al., 2011)

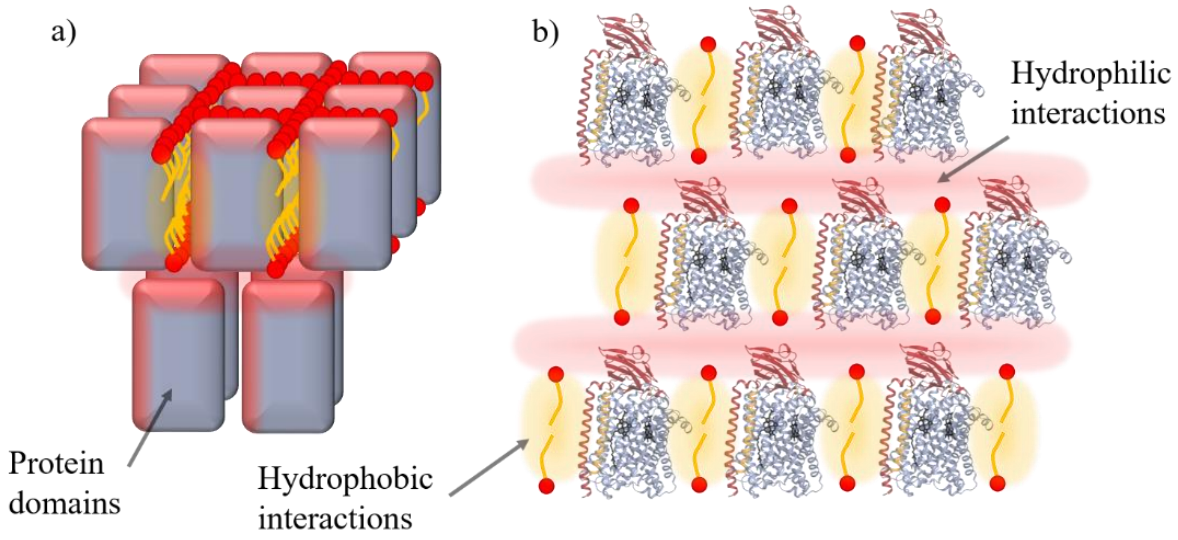

Figure 12. Two representations of type I crystal packing in LCP. In a) the three-dimensional structure is visible and in b) the two-dimensional packing is showcased with hydrophilic and hydrophobic interactions within the crystal packing.

2.3.8 Lipidic sponge phase

The LCP has been a matter of discussion regarding its saddle-shaped bicontinuous bilayer and it has been suggested that the inner small aqueous channels may not allow for lateral migration for membrane proteins with a large hydrophilic domain (Cherezov et al., 2006). This would in turn slow down or even hinder nucleation and crystal growth. The diameter of the water channel also affects crystallization of soluble protein in LCP. Reduced size of the aqueous channels affects soluble protein crystallization negatively (Clogston & Caffrey, 2005). One solution to these arguments is to enlarge the pores and flatten the bilayer. As described before in section 2.3.5, there are a few ways to do this where one is to change the temperature and another is to alter the lipid tails. Another way is to use a solvent or an additive like polyethylene glycol (PEG), dimethyl sulfoxide (DMSO), butanediol and jeffamine among others to create a more liquid and swollen phase also known as lipidic sponge phase (Cherezov et al., 2006; Engström et al., 1998; Evertsson et al., 2002; Imberg et al., 2003; Wadsten et al., 2006). Visually it looks

like a melted cubic phase but with 2-3 times larger water channels (Ridell et al., 2003). The low viscosity makes methods used in vapor diffusion, such as automation and standard protocols directly transferable to be used on lipidic sponge phase (Wadsten et al., 2006). However, even though *in surfo* methods can be directly applicable, the possibility of using the crystallization matrix as an extrusion medium is lost (section 2.5.3). This is due to the application of the viscous phase of LCP that can be used as a way to deliver microcrystals to the X-ray beam in a slow controlled manner (Ishchenko, Cherezov, & Liu, 2016) which is why crystal sample viscosity is often manipulated just before the experiment to make the sample run smoothly. Therefore, considering using lipidic sponge phase instead of LCP needs to be carefully weighted with the choice of experimental set up at the beamline or adjustment of the viscosity needs to be altered of the crystal grown in lipidic sponge phase prior to loading the sample cartridge.

2.4 Crystallography (paper I-V)

2.4.1 X-ray diffraction

In the early 20th century, Lawrence Bragg and his father William discovered that incoming X-rays scattered in a certain angle when they hit a crystal. This resulted in Bragg's law and the start of crystallography (Bragg, 1913):

$$n\lambda = 2dsin\theta \quad (2.1)$$

Where n is a positive integer, λ represent wavelength, d is the space between two lattice planes in the crystal and θ refers to the scattering angle (Figure 13). What it means is that when the incoming X-rays hit the crystal, electrons within the structure will scatter the waves, resulting in constructive interference if the scattered X-rays are in phase, giving rise to a Bragg reflection. According to Bragg, each set of lattice planes are considered as an independent diffractor and will produce a reflection while the intensity of the reflections depends on how much electron density is accommodated in the sets of planes within the unit cell. The more electrons available, the more X-rays can be scattered and the intensity of the scattered beam will be higher. Since the diffraction angle, θ, is inversely related to the distance between the planes, d, large unit cells with large spacing will give small θ which means more reflections within a certain angle from the incoming beam. In other words, the distance OP (Figure 13A) is equal to d^{-1}. This can also be linked to the fact that larger unit cells also contains more atoms and therefore produces more information in a diffraction pattern of the same size (Rhodes, 2006).

The space occupied by Bragg reflections is called reciprocal space and the planes in a unit cell and the directions of them can be drawn through lattice points by three number called Miller's indices denoted h, k and l. Reciprocal lattice points must be arranged in a certain way to satisfy Bragg law in order to produce a reflection. This can be used to predict directions of the diffracted ray by using the Ewald's sphere (Ewald, 1969) (Figure 13A). To fulfill Bragg law and produce a reflection, the reciprocal lattice point must intersect with the Ewald sphere. To sample all of the reciprocal space, all of the reciprocal lattice points needs to be brought into diffracting conditions. This can be done by simply rotating the crystal around one axis which will cause more reciprocal lattice points to satisfy Bragg's law by crossing Ewald's sphere. The minimum degree of rotation depends on the amount of symmetry of the unit cell where high symmetry needs less rotation. (Rhodes, 2006).

.

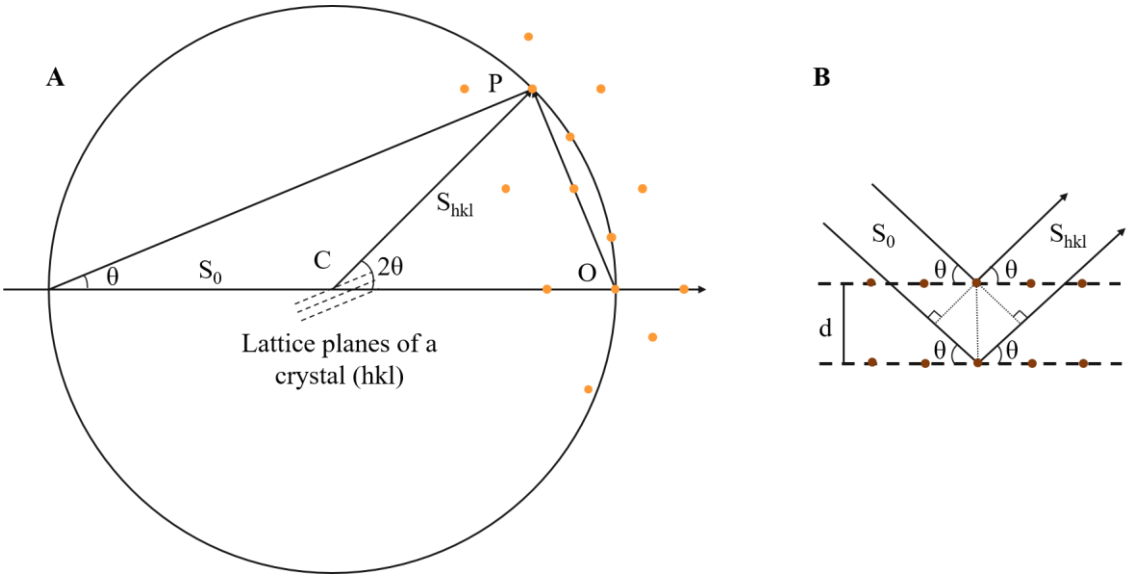

Figure 13. Illustration of Ewald's sphere (A) and geometry used in Bragg's law (B).

2.4.2 Data processing and refinement

When the reciprocal space with its lattice points are sampled at an X-ray facility using a powerful X-ray beam and an X-ray detector, a set of diffraction patterns containing multiple Bragg reflections are generated. By considering each atom instead of planes as a scatterer, diffraction can be summed up to a structure factor (F_{hkl}) of the hkl reflection (2.2), the lattice point in reciprocal space. Each individual atomic component contributing to the structure factor is called the atomic scattering factor $f_{j\theta\lambda}$ or just simply f_j. F_{hkl} represents the scattered wave that consists of an amplitude $|F_{hkl}|$ and a phase ϕ_{hkl}. From the structure factors, electron density (ρ) can be calculated at a certain position (x,y,z) in the unit cell by using Fourier synthesis (2.3).

$$F_{hkl} = |F_{hkl}|e^{i\phi hkl} = \sum_{j=1}^{n} f_j \, e^{2\pi i}(hx_j + ky_j + lz_j) \tag{2.2}$$

$$\rho_{xyz} = \frac{1}{V}\sum_{h}\sum_{k}\sum_{l} F_{hkl,xyz} = \frac{1}{V}\sum_{h}\sum_{k}\sum_{l} |F_{hkl}| \, e^{-2\pi i(hx+ky+lz)+i\phi_{hkl}} \tag{2.3}$$

Where V represents the volume of the unit cell and ϕ denotes the phase (Rhodes, 2006). To be able to calculate the electron density, diffraction data obtained from X-ray facilities such as synchrotrons, are processed through a number of different steps. Firstly, the unit cell parameters need to be determined to require the space group from a few patterns. Space group and unit cell parameters are then used for indexing and integration of the whole data set (Leslie, 2006) using

software such as MOSFLM (Battye et al., 2011). The indexed data then needs to be scaled and merged to create a single file with $|F_{hkl}|$ for all the Bragg peaks which is the final step when processing the experimental data.

To calculate electron density through a Fourier synthesis, both structure factor amplitudes and phases are required. However, since only amplitudes can be obtained from the intensities of the diffraction patterns, phases needs to be retrieved somewhere else. One common approach is to use a method called molecular replacement (MR) to overcome the 'phase problem'. MR borrows theoretical phases from a structurally similar model to the target protein which enables electron density to be calculated. Several rounds of refinement in the reciprocal space are then followed to better fit the experimental data and an initial model is subsequently built (Rhodes, 2006). The process of refining the structure is iterative where the initial model will provide new phases that in turn, after refinement, will provide a new structural model and so on. The work of refinement is validated by the R-factor, also known as R_{work} (Tickle, Laskowski, & Moss, 2000). R_{work} summarizes the structure factor amplitudes $|F_{hkl}|$ in reciprocal space and compares the $|F_{hkl}|$ between the model and experimental data. In other words, it will estimate how well the refined model predicts the observed data:

$$R_{work} = \frac{\sum ||F_{obs}| - |F_{calc}||}{\sum |F_{obs}|} \tag{2.4}$$

R_{work} is given as a value between 0-1 where 0 is ideal, corresponds to a perfect fit of the calculated and experimental model. This is never the case when analyzing data and a R-factor of about ten times the resolution is usually acceptable. There is a balance in how to select data for building the model. By including too much noise and pushing the refinement to fit a particular set of data, a false low R_{work} will be obtained. This is known as an overfitted structure and includes more information than can be justified by the experimental data. Overfitting can be detected by excluding a small subset of the data, about 5 %, before refinement to generate R_{free}. A structural model is then refined against the 95 % of the data and this model is compared to the R_{free}. A valid model has a R_{work} close to the R_{free} and by comparing the two factors during refinement, overfitting can be avoided. Another way of checking the validity of the structure is to keep track of that the chemical constraints are fulfilled, e.g. bond lengths, bond- and torsion angles lie within expected values (Rhodes, 2006). Structure determination from X-ray diffraction data can be performed by software suits such as CCP4 contain a series of crystallographic programmes that provides a whole pipeline from start to end (Potterton et al., 2018; Winn et al., 2011).

2.4.3 Conventional crystallography

Synchrotron sources have been the most influential facilities for macromolecular protein crystallography since the early 1970s (Dauter, Jaskolski, & Wlodawer, 2010) and still provide a powerful X-ray tool to produce structures of protein molecules. Synchrotron radiation occurs when the direction of electrons are changed by bending magnets or undulators in storage rings creating electromagnetic radiation (Elder et al., 1947). In conventional X-ray crystallography that is a common method used at synchrotrons, a single preferably large crystal is mounted onto a goniometer and rotated in the X-ray beam to sample Bragg reflections of the whole reciprocal space. However, the method has a few major disadvantages; first-and second degree radiation damage and the need for large well diffracting crystals (Hartmut, 1983). Radiation damage arises when some of the photons are absorbed by the sample causing free radicals to form (Garman & Weik, 2011; Holton, 2009). For membrane proteins, the need for large well diffracting crystals can be of concern since membrane proteins are notorious to be both more difficult to purify and to crystallize due their localization in native membranes (Bill et al., 2011; Hartmut, 1983) To minimize data loss due to radiation damage, cryogenic temperatures are used by flash-freezing the crystals in liquid nitrogen before the experiment. To obtain higher resolution structures, cryoprotectants can be added for crystal protection during flash freezing (Garman & Weik, 2011; Hunsicker-Wang et al., 2005). To obtain large well diffracting crystals there are also numerous ways of post-crystallization treatments to improve diffraction such as soaking the crystals in different solutions or dehydration of crystals to remove water to increase crystal packing densities (Heras & Martin, 2005).

2.5 Serial crystallography and Microcrystallization (paper I-V)

2.5.1 Serial crystallography

To obtain structures in a more physiological temperature and to avoid using large protein crystals, several small crystals can be used instead at light sources with much higher brilliance. This method is called serial femtosecond crystallography (SFX) and involves a stream of small crystals below 20 μm in size that are illuminated by such a high radiation dose that the crystals vaporize (Chapman, Caleman, & Timneanu, 2014; Chapman et al., 2011; Neutze et al., 2000). Before destruction of the crystal, a diffraction pattern is sampled which means that one crystal in a random orientation is used for one single exposure, so called diffraction before destruction. This can be achieved since the femtosecond pulse is shorter than the time required for the atoms to move approximately an Angstrom. As a result, the data collected consists of massive amount of snapshot diffraction patterns from thousands of crystals differing in shape and size, each containing only partially measured intensities (Chapman et al., 2014, 2011).

To accomplish these ultrashort bunches of extremely bright X-ray pulses, a light source with a peak brilliance of billion times stronger than synchrotron radiation is used, delivering the same amount of energy in 50 fs that a synchrotron typically delivers in 1 s. The high brilliance is produced by accelerating electron pulses to almost the speed of light in a kilometer linear tunnel, LINAC, passing them through a multitude of switched dipole magnets called undulators which

will force the electrons to oscillate and thereby emit electromagnetic radiation (Ayvazyan et al., 2006). The advent of X-ray free electron lasers (XFELs) enables data collection at room temperature with pulse lengths of a few femtoseconds making it also possible for ultra-fast time-resolved (TR) pump-probe experiments (Standfuss, 2019; Standfuss & Spence, 2017).

In recent years, the methods developed for SFX at XFELs have been applied to the new generation of synchrotrons with fast low-noise high-frame rate detectors, high viscosity injectors, sophisticated software suites, microfocused- and submicron beams and improved optics. This enables synchrotrons to close in on XFELs by collecting data at room temperature by serial crystallography on a millisecond time scale which in turn frees beamtime on XFELs and allows for screening of crystals (Standfuss & Spence, 2017). Serial Synchrotron Crystallography (SSX) includes different methods such as fixed target SX or the use of a viscous sample extruder, where the latter method needs microcrystals in grease or in LCP (Coquelle et al., 2015).

2.5.2 Pump-probe experiments

To fully understand protein function, structural information on protein dynamics are of great importance. By combining the SFX technique with time resolved studies (TR-SFX) structural changes upon triggering of the protein can be visualized. This is achieved by continuously exposing microcrystals to a predetermined delayed XFEL pulse after initiating a reaction trigger such as light, temperature, chemicals, substrates or electric field (Figure 14). By taking snapshots at various time-points, intermediates of the reaction can be sampled and analyzed. To cope with the high radiation doses and fast repetition rates, XFEL detectors are built as panels arrange with a hole in its center to allow the high-energy X-rays to pass through them without damaging the detector. Other requirements are fast read-out to match the repetition rates of the XFEL and maximizing the measurable peak signals (Kameshima et al., 2014). When performing pump-probe experiments using a laser for either illumination of light sensitive proteins or as in C*c*Os, knocking out the bound CO from the active site prior to X-ray exposure, there are a few factors of importance. Firstly the wavelength, size and energy of the pump laser needs to be adapted to the requirements of the experiment. The wavelength must trigger the reaction of interest, the size of the laser must be large enough to cover the crystal and the energy level must be balanced so that the occupancy of the protein is high but with the lowest amount of photodegradation.

Besides the importance of pump laser and X-ray probes, timing is also crucial since several factors such as flow rate, distances in the experimental set up and time delay needs to coincide (Sanchez-Gonzalez et al., 2017) When the experimental set up and alignment is ready and sample is running smoothly, collecting enough data in several different time-points during a reaction cycle can result in a ‘molecular movie’ where the structural changes upon protein triggering is visualized over time (Kupitz et al., 2016; Nango et al., 2019). Pump-probe experimental data is processed by looking at the F_{obs}-F_{obs} maps, so called difference maps between two different states of a protein. Often the map of light state (laser on) is compared to dark state (laser off), often referred to as F_{light}-F_{dark} difference density maps. By refining the dark structure optimally, the phases from the dark structure can be used to calculate the

difference electron density maps. However, since the signal is usually much weaker due to lower occupancy, more data needs to be collected, especially for small structural changes that are close to the noise level. To see how much data needs to be collected, the progress is monitored by calculating maps using structures that are not fully refined.

Since the mechanism of proton pumping and the route of ligand binding is still unknown in C*c*Os, one method to explore the mechanism is to use time resolved pump-probe SX to elucidate structural changes when the protein is triggered. To trigger C*c*Os, the ideal ligand is to use the natural ligand oxygen to capture the intermediate states at different time points since oxygen can give insight in both proton pumping and ligand transfer in the ligand channel. However, using oxygen has proven to be difficult due to the requirement of an anaerobic experimental set up and the need to activate as many proteins molecules as possible as fast as possible. If the active state occupancy of the protein population is too low or the diffusion too slow, a smearing effect will emerge making the noise level too high. In our project, we have aimed to use caged oxygen together with LCP as a crystallization and extrusion matrix. The oxygen is then released upon illumination by a laser and diffuse to the active site. Meanwhile, a simpler system is to use CO to track reverse structural changes by CO dissociation as a mimic for how O_2 binds to the active site. By flashing off CO using a laser and then sampling intermediate states of the protein, insight of how the ligand is transferred in the ligand channel can be made. However, since the biological reaction does not take place, the mechanism of how the protons are transferred within the protein will still not be revealed by this method.

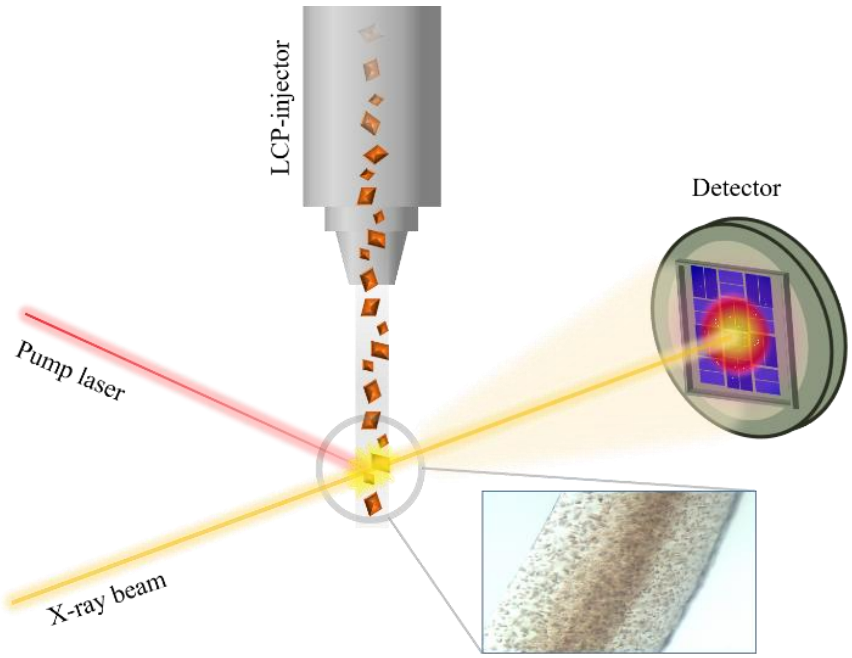

Figure 14. Illustration of the pump-probe SFX experimental setup with a LCP-injector and pump laser. For ba_3-type C*c*O. Crystals are delivered in LCP that acts as both crystallization- and extrusion medium. The thickness and optical density of LCP entails a higher laser power to penetrate the viscous matter.

2.5.3 Sample delivery injectors

SFX and especially TR-SFX demands large volumes of sample compared to conventional crystallography experiments. This is due to several reasons: firstly, crystals are destroyed after a single X-ray pulse which mean that new crystals needs to be delivered to the beam continuously. To collect a data set covering all reflections of the crystal lattice, thousands of diffraction patterns are needed and consequently also a large number of crystals. Secondly, the injector systems are sample demanding and significant volumes are often lost in the sample handling, such as sample preparation, sample mounting and during the run of the experiment. The first injector utilized at XFELs was a gas dynamic virtual nozzle, a liquid jet injector with a flow of 10 μl/min with a 50-100 μm nozzle size. This meant that most of the sample would not be probed by X-rays (DePonte et al., 2008). To provide the experiment with enough crystals up to grams of sample were needed. This pushed for a development of new injectors where sample consumption was less.

Two main injector set ups are used; fixed target- and moving target injectors which includes the gas dynamic virtual nozzle (Zhao et al., 2019). Example of fixed target injectors are single-crystalline silicon chips (Roedig et al., 2015) that consists of a thin membrane of 10-20 μm thickness with a periodic pattern of crystal wells (Lieske et al., 2019). Moving target injectors vary from the liquid jet to tape drives (Roessler et al., 2013), high viscosity injectors (HVE), acoustic droplet injector (ADE) (Roessler et al., 2016) and capillaries (Stellato et al., 2014) among others. The capillary technique delivers sample in a glass capillary by pushing the sample through with an injection pump at a flow rate up to 2.5 μl/min (Monteiro et al., 2019). ADE delivery systems jet droplets containing crystals by acoustic waves with a high hit rate (Roessler et al., 2016). By depositing samples on a Kapton belt with the acoustic injector, not only structural determination is possible but also in situ crystallography, crystallizing directly on the belt without any crystal handling in between the crystallization and experiment (Fuller et al., 2017). High viscosity injectors are a development of the liquid jet injector by using similar nozzles and gas to direct the flow but with slower flow rates down to 0.001-0.3 μl/min due to the more viscous extrusion medium (Zhao et al., 2019). It was first developed to extrude LCP but can also be used by reconstituted crystals in viscous medium such as grease (Sugahara et al., 2014), vaseline (Botha et al., 2015) and agarose (Conrad et al., 2015) which enables crystals grown in surfo to use the injector system. HVEs are not limited to XFELs and can also be used in serial synchrotron crystallography using a microfocused beamline (Nogly et al., 2015). The advantage of using LCP in HVEs is that LCP is used both as a crystallization- and extrusion medium keeping handling of the crystals to a minimum (Weierstall et al., 2014).

2.5.4 Microcrystallization *in surfo*

The development of serial crystallography has also pushed the development to produce thousands of microcrystals each measuring less than 20 μm crystals in size compared the production of a few large ones as was preferable in conventional crystallographic methods (Zhao et al., 2019). There are several ways of obtaining microcrystals. One way is to crush large crystals to make them smaller or to aim for crystallization conditions that favor rapid nucleation and crystal growth. Another way is to promote microcrystal formation by using supersaturated

solutions in vapor diffusion set ups to increase the evaporation of water thus speeding up the crystallization process (Lee et al., 2018). As described before in section 2.3.1, batch crystallization is a way to control nucleation and crystal growth. By changing the crystallization conditions, microcrystal formation can be favored instead of large crystals (Beale et al., 2019; Dods et al., 2017). The aim of batch microcrystallization is to create a large amount of nucleation sites by increasing the precipitant and/or the protein concentration. The large amount of nucleation sites will rapidly drop the protein concentration depleting the protein reservoir and therefore making the crystals smaller since there are not enough protein molecules left for larger crystals. To increase formation of microcrystals further in batch crystallization, seeding crystals can be added to increase the amounts of nucleation sites. In addition, batch crystallization is not only a way for producing large amounts of sample but also a way to decrease the work load for sample preparation at the experimental site (Coe et al., 2015).

2.5.5 Microcrystallization *in meso*

Since the development of new injectors in SX that deliver high viscous extrusion medium to lower the amount of sample used in an SX experiment (Ishchenko et al., 2016; Weierstall et al., 2014), there are mainly two ways of getting protein crystals into a viscous medium. One way is to crystallize proteins *in surfo* and then mix the crystals with grease to get the right consistency (Sugahara et al., 2014). A second way is to use LCP as both a crystallization medium and as an extrusion medium.

LCP was first regarded as difficult to work with due to the time consuming work of mixing and spinning the lipid in tubes to get the right phase and with difficulties monitoring and collecting crystals (Landau & Rosenbusch, 1996). It was not until years later when the method had been developed using syringes that allowed for the LCP suspension to be easily mixed in a couple of minutes that the method gained new popularity (Cheng, Hummel, Qiu, & Caffrey, 1998). Several new PDB structures were then deposited including proteins of the large g-protein coupled receptor (GPCR) family such as the structure of the β2 adrenergic receptor–Gs protein complex that rewarded Brian Kobilka and Robert Lefkowitz with the Nobel Prize of Chemistry in 2012 (Clark, 2013; Ghosh et al., 2015; Kato et al., 2012; Rasmussen et al., 2011).

The method of working with syringes made it easier to both dispense and screen large numbers of crystallization conditions with small volumes of protein. With robot-assisted pipetting of LCP suspension onto commercially available plates in combination with commercial crystals screens, small scale screening can be done quick and effortless. Although optimization of the detergent and detergent concentration might needed for the detergent lipids to be compatible with the lipidic phase. (Ai & Caffrey, 2000; Martin Caffrey, 2015; Cherezov & Caffrey, 2003, 2005; Cherezov, Fersi, & Caffrey, 2001; Gaisford, Schertler, & Edwards, 2011; Ishchenko et al., 2016; Li et al., 2012).

The most commonly used method to screen for microcrystal formation is to use syringes. After a crystallization hit is found by small scale screening, a 100 µl gas tight syringe is filled with 60-70 µl of the precipitant solution that gave a hit and 5 µl of LCP suspension is pushed into the precipitant before the syringe is sealed (Ishchenko et al., 2016; W. Liu, Ishchenko, &

Cherezov, 2014). Conditions are then screened around the small scale hit to optimize the larger scale production of microcrystals. To monitor crystallization growth using magnitudes with good focus, the crystallization process is terminated and a small portion of crystals is taken out, spread on a glass slide with a coverslip and observed in a microscope. Another option is to monitor the crystals directly in the syringe with a microscope with some difficulties finding focus. This is because the thickness and curvature of the glass, the shape of the LCP-string in different depths makes it hard to magnify to a higher extent (Figure 15). With our stereomicroscope (Nikon SMZ18) a magnification of about 15x (1.5) was maximum before focus was lost. Using a polarization filter can aid the monitoring by looking for the shimmering of the microcrystals but still makes it very difficult to evaluate the quality and size of the crystals.

When a large scale hit is found, the same method is then used to produce larger amounts of sample for experiments. To collect crystals from the syringes, previously published methods describe that crystals are collected from the syringe by removing the precipitant solution by slowly pushing the plunger forward and then pooling the 5 µl crystals from different syringes into one syringe (W. Liu et al., 2014). This method needs a large set of gas tight syringes to accommodate the need for large amount of sample. Another way of screening and producing microcrystals in LCP is to use Eppendorf tubes with a metal wire instead of syringes. The metal wire is used to easily collect the crystals (Eriko Nango et al., 2016). However, this method cannot visualize the crystal growth over time directly in the tubes using a microscope.

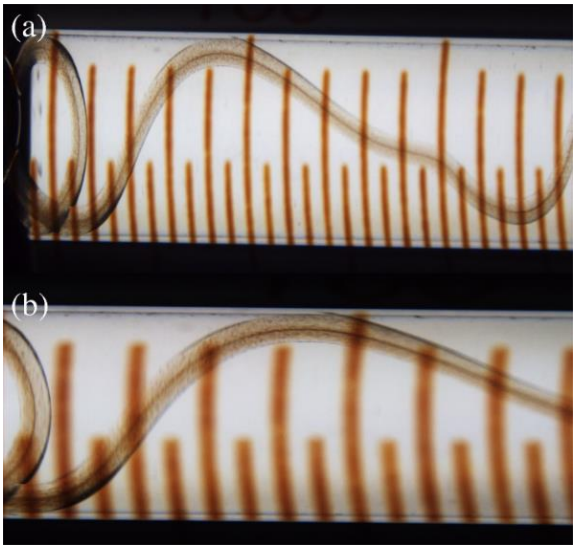

Figure 15. Two different magnifications of a LCP string containing *ba*$_3$-type C*c*O crystals are visualized in a 500 µl Hamilton syringe with precipitation buffer using a stereo microscope. In both of the syringes it is hard to analyze the crystal quality in the means of shape and size, indifferent of the 7.5x magnification (a) and 15x magnification which was maximum magnification before focus was lost (b). This can be explained by the curvature of the syringe itself, the different depths of the LCP-string and the thickness of the LCP making crystals overlap in view in different focus points. Figure from paper I, Acta Cryst. (2019) D75, 937-946.

2.5.6 Serial data collection and processing

Since microcrystals are flowed in a continuous stream, sprayed or spread on sheet in SFX experiments, controlling flow rate of the extruding media and the density of crystals are of great importance. When an X-ray pulse crosses paths with a crystal, a "hit" will be registered if a diffraction pattern has enough Bragg reflections with high enough intensities over a certain defined signal-to-noise (SNR) ratio. An X-ray pulse can also go through the extrusion medium without hitting any crystals, a so called empty shot. On the other hand, an X-ray beam can also hit more than one crystal in the same pulse generating a multi-hit if the density is too high. To find the optimal flow rate during data collection, the hit rate is monitored to view the percentage of hits compared to the number of X-ray pulses. By altering the injection system (nozzle size for example), diluting crystals or adjusting flow rate, the optimal hit rate can be achieved for that particular sample and experimental setup for efficient data collection.

Since random orientated crystals with different shapes and sizes are hit, a full SFX data set contains several thousand diffraction patterns with partial reflections where each reflection will be measured several times. This demands software for fast data reduction and processing such as Cheetah for hit finding (Barty et al., 2014) and Crystfel for indexing, scaling and merging (White et al., 2012). To meet the challenge of crystal to crystal variation, the redundancy of SFX experiments needs to be very high and requires validation methods such as CC½ and R_{split} where R_{split} is a measurement of the consistency within a data set by dividing the data set in half, merging them separately and then comparing the intensity lists of them both. Low R_{split} indicates a good comparison of the two separated half data sets. CC½ (Pearson correlation coefficient) is also way of comparing the two halves of the data set (Kirian et al., 2010; White et al., 2012). After merging, software also applied for conventional crystallography such as CCP4 (Potterton et al., 2018) can be used for MR of SX data.

Chapter 3

3. Result and discussion

3.1 Part I: Well-based crystallization of LCP microcrystals for SX (paper I)

3.1.1 Large scale production of crystals in wells

To produce of up to milliliters of microcrystals for SFX experiments in an efficient way where the crystallization process can be monitored over time, we present method developed from LCP methods for crystal production for serial crystallography (section 3.2.3). The method enables crystals to be screened, optimized and produced in a large scale using glass (or plastic) plates sealed with a transparent adhesive plastic cover, allowing for easily visualization with a stereomicroscope over time without interrupting the crystallization process. Crystals produced in this large scale well based system can be zoomed in at least six times more with better focus (Figure 16) compared to crystals produced in syringes (Figure 15). To crystallize LCP directly in a plate, a short removable needle is connected to the syringe with the LCP suspension and a string of up to 50 µl of LCP suspension is dispensed to a well filled with up to 1 ml of precipitant solution. Crystals can then be produced without the need of syringes filled with precipitant solution. Besides the common screening factors such as buffers, pH and salt etc., screening of crystals in the well based method can also include LCP suspension volume, precipitation volume and gauge size of the removable needle to find optimal large scale microcrystallization conditions.

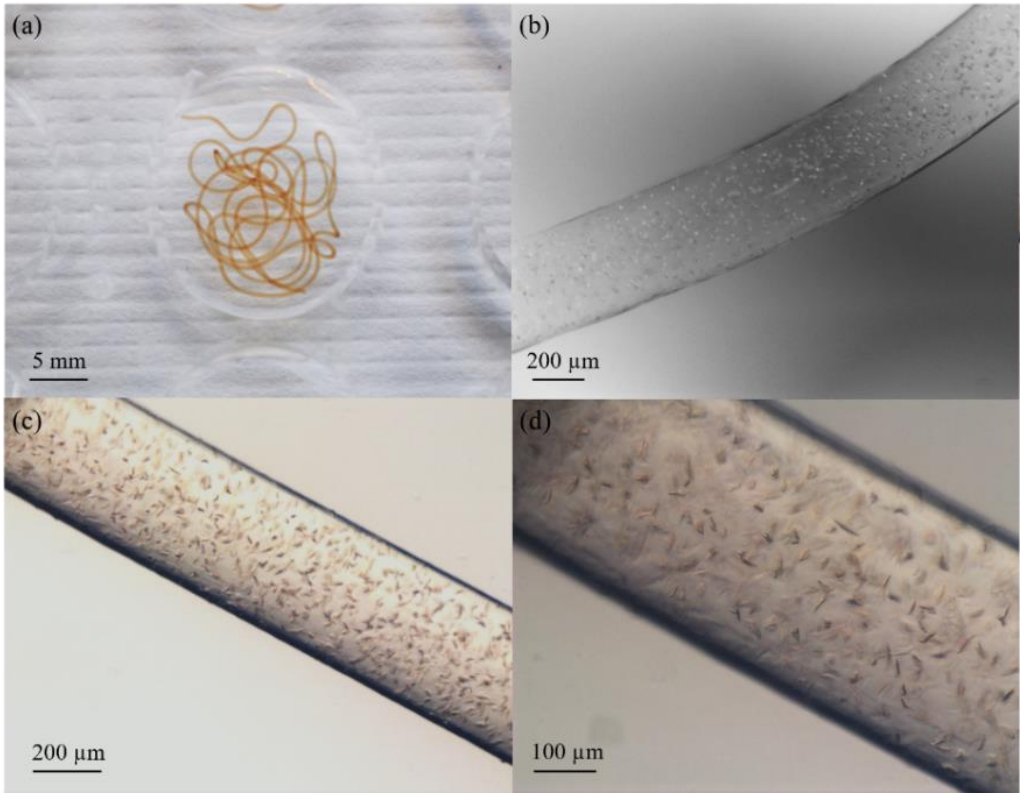

Figure 16. Different zoom of magnitudes of crystal containing LCP-strings in wells. In (a) the string itself can easily be visualized optically by the eye and crystals are easily zoomed in using a stereomicroscope over time without interrupting the crystallization process. In (b) the crystals are viewed with a magnitude of 40x using a polarization filter to view case the shimmering of the crystals while (c) and (d) shows crystals without a polarization filter under 50x and 135x magnification. Figure from paper I, Acta Cryst. (2019) D75, 937-946.

A plunger is then used to collect the formed crystals by pooling the crystal-containing LCP strings into one well. This can then be transferred as a single lump into a 500 µl syringe from the back and the harvested microcrystals are then pressed down into the syringe. Since the method is fast and the LCP is only exposed to air for a few seconds, no visible abnormalities of the phase or crystals were detected and crystals behaved in the same way as crystals produced by the syringe approach for ba_3-type C*c*O. Another way of collecting crystals was tested by using a pipette with a cut off 1000 µl pipette tip. By drawing the well solution containing the crystal-containing LCP string, the crystals could be transferred to the syringe from the back with a few drawbacks. Since the volume of drawn precipitant solution was quite large, it was easy to mechanically press in solution to the LCP-string making it less viscous. The LCP-string also stuck on the sides of the plastic pipette tip resulting in large sample loss, which in the end favored the first collecting procedure. Residues of precipitant solution are then removed by tilting the syringe into a vertical position before pushing the plunger forward (step-by-step in Figure 17). To remove precipitant solution from a sample with low viscosity, the syringe can be stored with the plunger upwards until the precipitant solution has separated and the residual precipitant solution can then be removed.

One of the main advantages of this method is the efficient way of collecting a larger amount of crystals in a short time since several plates can be transferred into the same syringe. A 9-well plate maximized with 50 µl LCP suspension in each well results in 450 µl of crystal containing LCP. In this case the time limiting step is the reconstitution of protein in lipid by mixing besides the production of protein target itself. With an automated LCP mixer (SPT Labtech) even the step of mixing LCP is more or less effortless.

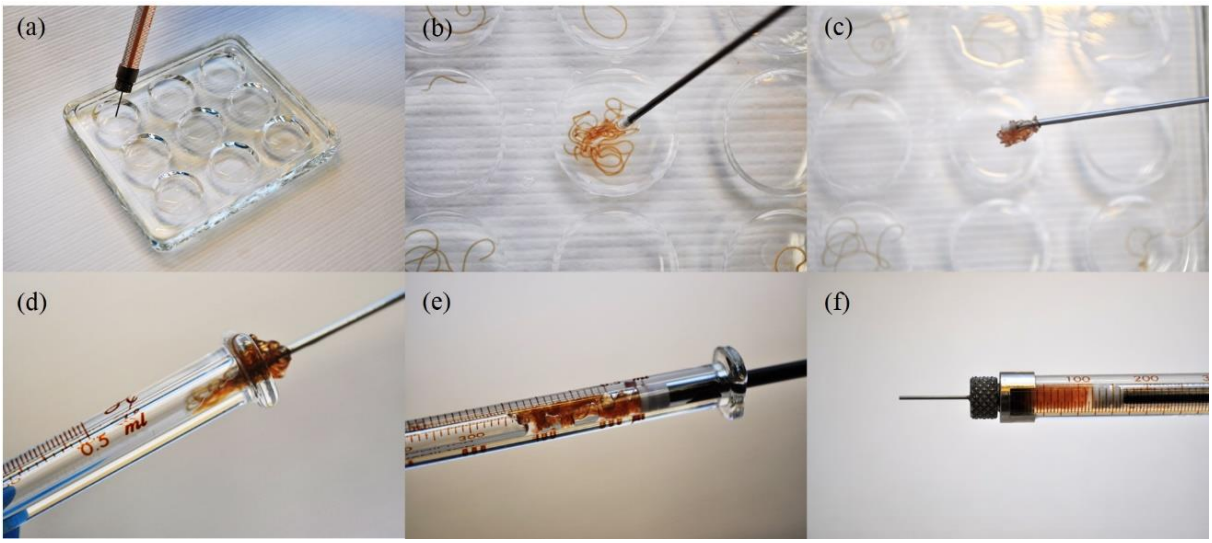

Figure 17. Step-by-step procedure of collecting microcrystals from a well into a syringe. LCP suspension is dispensed in each well of a 9-well glass plate by connecting a short needle to the Hamilton gastight syringe (a). A plunger is then used to pool the crystal-containing LCP (b) and forming a lump that sticks to the tip of the plunger (c). The LCP-lump is then transferred to a new clean syringe from the back (d) before a plunger is inserted and the residual precipitant solution is removed (e). (f) shows a packed Hamilton syringe ready to be sealed and used at an experiment. Figure from paper I, Acta Cryst. (2019) D75, 937-946.

3.1.2 Summary and discussion part I

Producing crystals of membrane proteins for conventional crystallography has been challenging due to the nature of the protein itself being imbedded in a phospholipidic bilayer. When stripped from the membrane and solubilized in detergent, membrane proteins are often prone to aggregate and lose functionality. By substituting the membrane with a synthetic bilayer mimicking the native environment of the target protein, the protein retains its stability and functionality. The different phases and opportunities to add other molecules to change the properties of the LCP, give rise to tremendous variation and advantages when it comes to crystallization by altering the size and shape of the bilayer to fit the target protein. LCP is also aiding crystallization by inducing lamellar organization of the lipids which increase crystal contact and the packing density of the crystal (Tiefenbrunn et al., 2011). The higher order of protein organization results in a more densely packed crystal, probably due to the mediation of the lipids in the cubic phase. This can be seen in the much lower values of B-factors, ranging

from 17-31 Å^2 for one protein system (Tiefenbrunn et al., 2011) compared to structures deriving from *in surfo* methods where B-factors on average exceed 50 Å^2 (Hunsicker-Wang et al., 2005; Soulimane, Buse, et al., 2000). Another aspect to consider regarding LCP crystallization is temperature. Lipidic phases are temperature dependent and the cubic Pn3m phase that is commonly used in crystallization with MO, transforms into a lamellar phase in temperatures below 17 ºC. However, the Pn3m phase can be used in temperatures up to 80 ºC if the water content is lowered. Even though temperatures of up to 80 ºC can be relevant for heat tolerant enzymes as the *ba*$_3$-type C*c*O, collecting data at temperatures such as 37 ºC for structural determination of human proteins have higher biological relevance.

3.2 Part II: Applications of well-based microcrystallization in LCP for serial crystallography (Paper I-V)

3.2.1 Novel structure of *ba*$_3$-type C*c*O at room temperature (Paper II)

To obtain microcrystals from *ba*$_3$-type C*c*O, a crystallization condition from previous research was used as a starting point (Tiefenbrunn et al., 2011). The hit was then screened around protein- and salt concentration, PEG 400 and pH to find the optimal condition for crystal growth. 20 µl LCP with crystals of 5-20 µm were formed in each well with 300 µl 37 % (v/v) PEG 400, 1-1.4 M NaCl and 100 mM sodium cacodylate trihydrate pH 5.3. The plate was then sealed with a ClearVue sheet (Molecular Dimensions) and incubated at 19°C for 2-3 days before crystals could be observed.

15 µl of sample could be collected and transported to BL3 beamline at the Spring-8 Angstrom Compact Free Electron Laser (SACLA) in Japan (Huang & Lindau, 2012). Before the experiment 45 µl of MO was added to the sample to increase viscosity and the sample was run with a 75 µm nozzle connected to a high viscosity injector (Tono, 2017; Weierstall et al., 2014). Diffraction data were collected at 7.6 keV with a repetition rate of 30 Hz and a pulse duration below 10 fs with energy of ~95 µJ/pulse. A flow rate of 0.48 µl/min was used and a hit rate of about 12 % was observed where images with over 20 reflection peaks were identified as a hit. Data reduction and processing was performed by Cheetah (Barty et al., 2014) and then processed using the Crystfel software suite to an indexing rate of 72 % (White et al., 2012). The model was then built using Coot (Emsley, Lohkamp, Scott, & Cowtan, 2010) and refined by REFMAC5 (Murshudov et al., 2011) using the high resolution structure of PDB ID 3S8F for phases to solve the novel structure at room temperature at a resolution of 2.3 Å. Final R_{work} was recovered at 16.2 % and R_{free} slightly higher at 19.8 %. 99.6 % of the side chains were accepted within the Ramachandran regions (PDB ID: 5NDC).

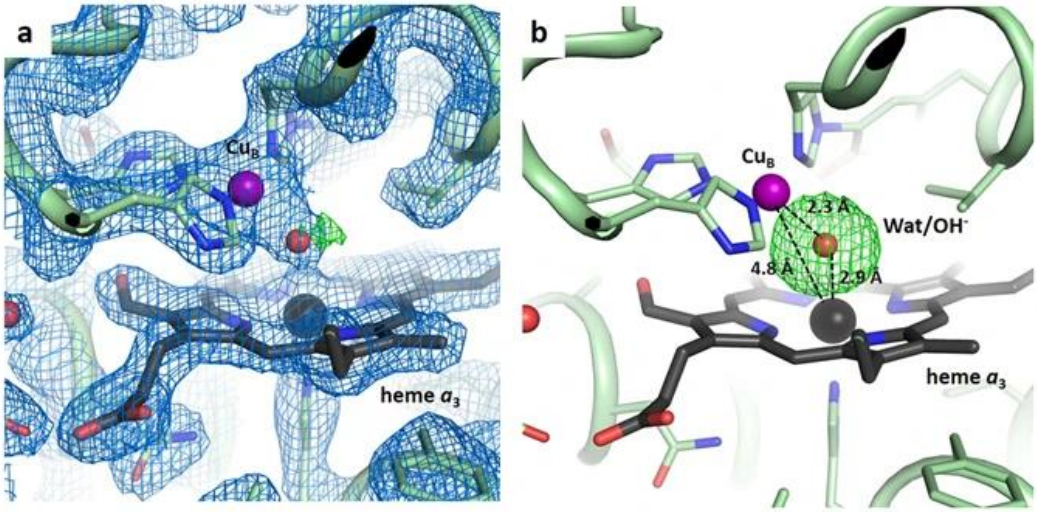

Figure 18. The Cu_B-heme a_3 ligand binding site with a spherical shaped unbiased F_o-F_c omit map indicating a water or hydroxide ion as a ligand where the F_o-F_c difference density in shown in green; σ=4.0 (A) and σ=4.5 (B) and 2 F_o-F_c is shown in blue at σ=1.5 (A). Figure from paper II, Scientific Reports 7, 4518 (2017).

The structure showed high agreement with the cryogenic high resolution structure (PDB ID 3S8F) (Tiefenbrunn et al., 2011) with similar cell unit parameters and C2 as a space group. The proton transfer channel and the water clusters in the expected proton-loading site are conserved when comparing both structures. In contrast, compared to the aa_3-type C*c*Os, the proton pumping site differs from the ba_3-types. Since this site is still under elucidation with suggestions of it being localized near the heme a_3 propionates, the water clusters surrounding them or an aspartic acid residue close by (Ballmoos et al., 2015; Yoshikawa et al., 2016), the comparison of these conserved regions of protein species within the C*c*Os is of high interest. One particular residue is of interest in the discussion of the proton loading site, namely a tryptophan residue (Trp229 in ba_3-type C*c*O). In the A-type C*c*Os, this tryptophan forms a radical during enzymatic turnover (Wiertz et al., 2004) and it has been proposed that this residue is directly involved in proton pumping across the membrane. Since the ba_3-type C*c*O does not form this radical one theory is that it might be related to the number of proton translocated over the membrane since ba_3 transfer approximately half of the protons per oxygen molecule (Kannt et al., 1998; Paulus, Werner, Ludwig, & de Vries, 2015). In addition, the neighboring residues of this tryptophan in B-type C*c*Os differ from the ones in A-types. A magnesium is present in A-type C*c*Os in close proximity with a water cluster in one of the proposed proton-loading sites and not in B-type C*c*Os. Instead a carboxyl group of a glutamic acid residue (Gln126II) is occupying the position in ba_3-type C*c*O (Lu & Gunner, 2014). This gives further arguments to elucidate and compare the proton pumping mechanism between the two groups of C*c*Os since the overall mechanism may be the same but but the details and which structural elements are involved can be different.

Comparing the room temperature structure with cryogenic structures previously deposited in PDB, an interesting feature regarding the ligand was discovered. As the cryogenic structure used for model building has a peroxide modelled in its active site (Tiefenbrunn et al., 2011), we show that a water or a hydroxide ion is situated as a ligand, and this is consistent with what some others also have shown (Hunsicker-Wang et al., 2005; Soulimane, Buse, et al., 2000). This can be seen by the round shape of the unbiased different density omit map which shows a better fit for a water/hydroxide ion than to a peroxide (Figure 18). Uncertainty regarding the species of ligand seems to be attributed as an effect of temperature or induced reduction upon X-ray exposure (B. Liu et al., 2009; Tiefenbrunn et al., 2011).

To validate the water/hydroxide ion as a ligand, a water molecule was modelled into the active site. The absolute intensity of the water molecule was then compared with the peak height of another water molecule in the structure close to the second alcohol of heme a_3 and ser309. Both were found to be very similar (0.99 resp. 0.86 $e^-/Å^3$), supporting the proposal of a water or hydroxide ion as the ligand. To further support the use of a water or hydroxide ion as ligand, the Fo-Fc electron density was compared with cryogenic structures where a water molecule was modelled instead of the peroxide molecule in the active site. As a result, a water built into the model of the cryogenic structure of aa_3-type C*c*O from bovine heart (PDB ID: 3WG7) (Hirata et al., 2014) generated a poor fit to the elongated electron density, similar to the one generated in the cryogenic LCP structure when the same exchange of ligands was conducted (Tiefenbrunn et al., 2011). This supports the difference between our ba_3-type C*c*O structure and published bovine aa_3-type C*c*O structures and strongly indicates that a single oxygen species is more likely to be the ligand in the active site of a *ba3*-type C*c*O structure free of radiation damage instead of a double oxygen species that is the common denominator for most published A-type C*c*O structures (Kaila et al., 2011).

A room temperature structure determined from microcrystals collected at a serial crystallographic experiment, has some advantages over a cryogenic structure. First of all, since the structure derives from crystals only hit one single time, a structure without any radiation damage can be obtained. The room temperature structure of ba_3-type C*c*O was sampled with a X-ray dose of 13mGy in average calculated by RADDOSE-3D (Bury, Brooks-Bartlett, Walsh, & Garman, 2018), a level of energy well below the limit of where radiation damage has been reported for metal cluster using XFEL radiation. Therefore, using microcrystals is particularly important for structures containing metal co-factors such as the HCOs (Nass et al., 2015).

Another advantage of using microcrystals for structural studies are their small size. A smaller sized crystal makes it easier for the pump laser or chemical compound to penetrate and thus triggering a larger population of the protein molecules. This is important when working with pump-probe experiments which are possible now that a high resolution structure can be determined using only 15 µl of microcrystal-containing LCP with a method that easily can produce necessary quantities of sample. For ba_3-type C*c*O this would mean chemical triggering by caged oxygen released by laser or by monitoring CO dissociation over several time points. In addition, working at room temperature makes much more biological sense since its closer to the working temperature of the protein in its native environment. For ba_3-type C*c*O, which is a

heat-tolerant enzyme, this is of even more importance since the protein itself aggregated in much higher grade during freezing compared to storage at 4 ºC implying that the protein structure at higher temperature is of more relevance due to protein stability and thus functionality.

3.2.2 Screening of microcrystal conditions of *ba*$_3$-type C*c*O to find a novel non-toxic crystallization condition (Paper I).

Since the room temperature structure of *ba*$_3$-type C*c*O included working with the arsenic containing salt of cacodylate trihydrate, new crystallization trials were performed to find a new non-toxic crystallization condition. Initial screening was based on previous work using a mosquito robot (Gaisford et al., 2011) for high throughput where sodium cacodylate simply was exchanged by 2-(*N*-morpholino)ethanesulfonic acid (MES) with different pH, PEG400- and NaCl concentration. Several crystallization hits were immediately found and further screened using the well based method by dispensing protein strings of different protein concentration and volume in each MES- containing up to 1 ml precipitant solution. Cacodylate trihydrate-containing plastic plates were used as reference to compare the crystals shape, size and density (Figure 19). Plastic plates were used to minimize handling of the toxic solution and facilitating waste disposal. No visual difference of size and shape could be detected for crystals grown in plastic wells and glass plates. However, the LCP string attaches easily to the plastic sides of the wells making it harder to visualize them. A problem not present in glass wells. Crystals of 20 µl 0.238 mM *ba*$_3$-type C*c*O were obtained in 500 µl precipitant solution containing 100 mM MES pH 5.3, 1.4 M NaCl and 34-37 % (v/v) PEG400 after 2 days of incubation at room temperature.

Samples were brought to BioMAX beamline of MAX IV Laboratory for the first Serial Synchrotron Crystallography (SSX) in Lund (Thunnissen et al., 2013). The crystal-containing LCP were mixed with MO in Hamilton syringes with a LCP:monoolein ratio of 80:15 to get the right viscosity of the sample before loaded into the sample cell and mounted to the HVE (designed and engineered by Bruce Doak, MPI Heidelberg). A nozzle with a diameter of 100 µm was used with an average flow rate of 1.2 µl/min. Data were collected at

room temperature at 100 Hz yielding 215 000 diffraction images that was processed using the software NanoPeakCell (Coquelle et al., 2015) with a hit rate of 4.7 %. CrystFEL (White et al., 2012) was used for indexing with a indexing rate of 65 %. The model was then built using Phaser (Mccoy et al., 2007) and MR with the phases from previous room temperature structure (PDB ID 5NDC). REFMAC5 (Murshudov et al., 2011) was used in refining the structure resulting in R_{work} = 30.4 % and R_{free} = 30.6 % after one round of rigid body refinement giving a structure at a resolution of 3.6 Å. However, as this was the first user SSX experiment at BioMAX, there is the potential for improved results in the future by optimization of both the crystal-injection and data-collection parameters.

The results show that the method of using LCP microcrystals is not only limited to SFX experiments at XFELs but have applications at micro-focused beamlines at synchrotrons as well. Not only can this open up for more time at XFELs since synchrotrons will take over a bit

of the applications, more opportunities will arise for screening experiments and possibilities to test experimental set ups. This will be even more important as the need for more advanced set ups arise with pump-probe experiments, for example with chemical triggering which might need inert chambers or the need for fast mixing.

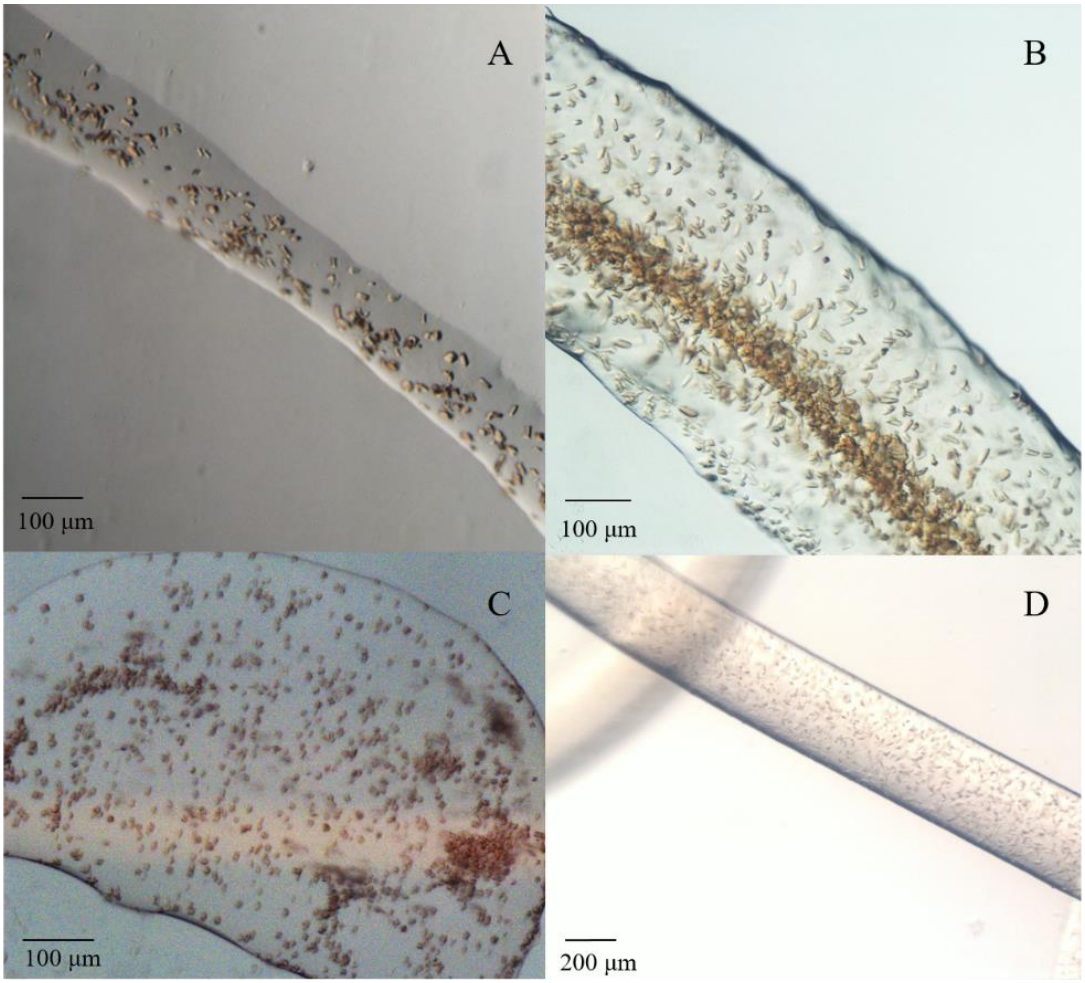

Figure 19. Pictures comparing *ba*$_3$-type C*c*O crystals in two different precipitant buffers. (A) and (C) show crystals in a highly toxic and environmental hazardous solution containing sodium cacodylate trihydrate. In (A) 120x magnification is displayed in an LCP string and (C) 100x magnification where crystals have been spread out on a glass sheet. (B) and (D) show crystals in a non-toxic buffer containing MES instead. (B) and (D) are different LCP batches made at different occasions at 135x and 50c magnitudes respectively. Variation in crystal growth were seen even if protocols were standardizes. Small factors such as different protein batches, a newly opened detergent bottle or small temperature fluctuations in the room are a few of the variables that we could detect made crystals grow differently. Each crystal well had to be evaluated before crystal packing to collect a homogenous sample for measurements.

3.2.3 Development of *ba*$_3$-type C*c*O crystals with bound CO (Paper III)

The next step after obtaining an oxidized structure at room temperature was to develop a protocol for producing reduced CO-bound crystals in larger amounts for serial crystallography. To achieve this several aspects had to be taken in consideration. The most important consideration was to work under oxygen-free conditions and to figure out a way how to validate crystals under inert conditions using optical spectroscopic measurements. These two obstacles were overcome by using an aerobic glove box (Coy Laboratory Product Inc.) and an air tight calciumdifluoride cell in which crystals could be transferred to the glove box and then used in a regular spectrophotometer. As a result, crystallization trials could be performed in an anaerobic environment consisting of 95-97 % nitrogen- and 3-5 % hydrogen gas to supply the platinum catalysts with reactants. Crystal spectra could be achieved for oxidized, reduced and reduced CO-bound crystals (Figure 6).

Prior to CO-binding, the catalytic site was reduced with two electrons using the reductant dithionite. After reduction, the sample was kept in an anaerobic atmosphere to avoid re-oxidation. There are multiple ways of reducing crystals and we developed two different ways where one was slightly more efficient. The first way was to add 1mM sodium dithionite to the wells after crystallization to fully reduce them. To be sure that the atmosphere inside the glove box was kept oxygen free, all buffers and chemicals were purged with nitrogen for a few minutes prior to insertion into the anaerobic chamber. This was accomplished using a septum- and parafilm covered tube made by a cut off 15ml falcon tube of 2-4 cm in length (Figure 20). Crystals reduced by this method could be obtained in two different ways. Either the crystals were produced in an oxygen-free environment from start or they were produced aerobically by crystallizing in normal work space area. To remove oxygen, the oxygen containing crystals were transferred into the glove box and the plates unsealed for oxygen diffusion. The box was purged to empty out excess oxygen and then left for equilibration for 45-60 min with an oxygen catalyst to remove the residual oxygen. Crystals were monitored using a stereo microscope over time and no visual change could be detected regarding size and shape of the LCP-string or the crystals. After the incubation time, reductant was added in the same way as with the anaerobic crystals.

The second way producing reduced crystals was to grow crystals in a reduced condition. Different reduction agents were screened with different concentrations and a condition with sodium dithionite at a concentration of twenty fold excess of the protein concentration was found where crystals grew as expected. Crystals were monitored over time in the anaerobic glove box and crystal samples were taken out for UV/VIS spectra using the CaF_2-cell. They showed that additional reducing agent was needed to a final concentration of 1mM. The simplicity of just adding reducing agent to the already formed crystals made this method the method of choice for crystal production.

The next step was to add CO to the reduced crystals. To add CO under secure circumstances according to safety regulations, the reduced anaerobic crystals had to be removed from the glove box and transferred into an adjacent room with fume hoods, locked storage cabinets and CO-detectors. To move sample around in an aerobic atmosphere without contamination of oxygen, septum capped glass vials of 2 ml were used (Figure 20). Glass vials were used over

plastic tubes to avoid adhering of LCP to the sides of plastic material. To transfer the crystals to the glass vials, 0.5-1 ml of the precipitant solution was pipetted over before the crystals were collected with a plunger. The tubes were then capped with the septum cap and parafilmed before exiting the anaerobic atmosphere. To add CO, the crystal containing vial was purged a few seconds using a syringe needle, creating an overpressure before an outlet was added to keep the inside of the vial oxygen free. To terminate the purging of CO, the same procedure was applied by first taking out the outlet before the CO-inlet was removed to keep the over pressure inside the vial. Crystals were then incubated for up to an hour in CO atmosphere to allow for diffusion. Crystals were evaluated before and after the procedure and no visual abnormalities could be detected of the LCP matrix or the crystals. UV/VIS spectra confirmed the binding of CO and that the crystals still were CO-bound after 60-90 seconds before crystals started to lose their CO upon expose to the inert atmosphere of the glove box. The crystals were then packed into Hamilton syringes and tested for oxygen leakage. Tests showed that sealed syringes could be stored in aerobic atmosphere for at least 5 days without losing their CO. The amount of crystals purged in a tube depended upon the plates. Prior to collection, every plate was evaluated in a stereo microscope to determine which crystals were equal in size, density and shape and would be pooled to make up a sample. For example, 20 µl of protein-containing LCP suspension had been added to each well in a 9-well glass plate and 6 of these was decided during evaluation to be harvested into a pooled sample. This pooled sample would then make up a volume of approximately 120 µl of crystal containing LCP in a tube. To only use one plate per tube was decided on the basis of not letting the crystals be stored in the tube more than necessary during harvesting and to keep the volume of LCP in the tube low for better CO penetration of the lipidic phase. A UV/VIS spectrum confirmed a fully reduced and CO-bound sample by this method.

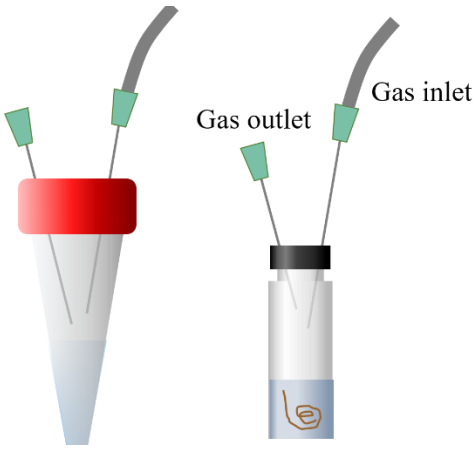

Figure 20. Illustration of a cut off falcon tube with a rubber septum and a glass vial with a gas tight septum used for purging sample, buffers, chemicals etc. with nitrogen- and carbon monoxide gas. For CO this was especially important since purging of CO needed to be done in a separate location due to safety regulations.

Milliliters of reduced CO-bound crystals were then brought to the BL3 beamline at SACLA in Japan (Huang & Lindau, 2012) for data collection. An aerobic glove box was used on site for sample preparation which included homogenization with MO and addition of CO to ensure that as large fraction as possible of the protein population was CO-bound. CO was added through the mixing of extra MO by purging melted MO with CO using the cut off Falcon tubes and septum prior to addition. CO-containing MO was then added in small aliquots of 3 µl until the right consistency was obtained. The sample cartridge was filled up with sample, spun to remove any bubbles and mounted with the HVE (Tono, 2017) with greased outlets on the sample side of the nozzle to prevent oxygen contamination and CO dissociation. The mounted injector was then put in a gas-tight plastic bag containing an oxygen indicator tablet and sealed by heat before taken out of the anaerobic glove box and to the experimental site. The grease seal would then be extruded during the run of the experiment.

Data were collected in anaerobic conditions with helium gas surrounding the sample during extrusion using an X-ray of 7.5KeV and 30 Hz repetition rate <10 fs. With a flow rate of 0.5-1.5 µl/min over 200 000 images were obtained with 41.059 hits. 60.4 % were indexed with the same work flow and software suits as previously described. A structure was solved at 2.0 Å in which binding of the CO molecule in the active site could be confirmed by unbiased difference omit maps.

The aims of binding CO to the *ba*$_3$-type C*c*O was both to gain insight into the structural movement upon CO binding at room temperature, but also to compare *ba*$_3$-type C*c*O with the previous structures obtained at cryogenic temperatures and the model protein *aa*$_3$ of the HCOs. The structure of which has been successfully determined with CO bound (Ishigami et al., 2017). Comparing the reduced CO-bound structure (paper III) with the oxidized structure of *ba*$_3$-typ C*c*O at room temperature (paper II) which had a spherical shape of the unbiased F_o-F_c omit maps (Figure 18), the reduced CO-bound structure showed an elongated electron density corresponding to a CO molecule (Figure 21).

To confirm a CO molecule as the ligand in the active site, a water molecule representing single oxygen species was modelled in the active site and the F_o-F_c electron density maps were refined. As a result, residual density remained elongated after refinement at a contour level of σ= 4.5 which indicated that a water molecule was not a good candidate for the ligand. After a CO molecule was modelled in and the maps refined, no residual density was found at σ=4.5 and only small residual density was remained at a sigma level of 3.5 which indicates a good fit for a CO molecule in the active site as the ligand. CO also fit angle- and distance wise in the active site by binding 1.95 Å from the carbon to the iron and 2.56 Å to the Cu_B with an angle of 141 º relative to the normal of the heme. The binding geometry is similar to the bovine *aa*$_3$-type C*c*O collected at 5 ºC (Shimada et al., 2017) but not similar to the structure obtained at room temperature (Ishigami et al., 2017). To further validate the ligand, UV/VIS spectroscopy was performed on the crystals before the experiment which showed a fully reduced CO-bound spectra (Figure 6).

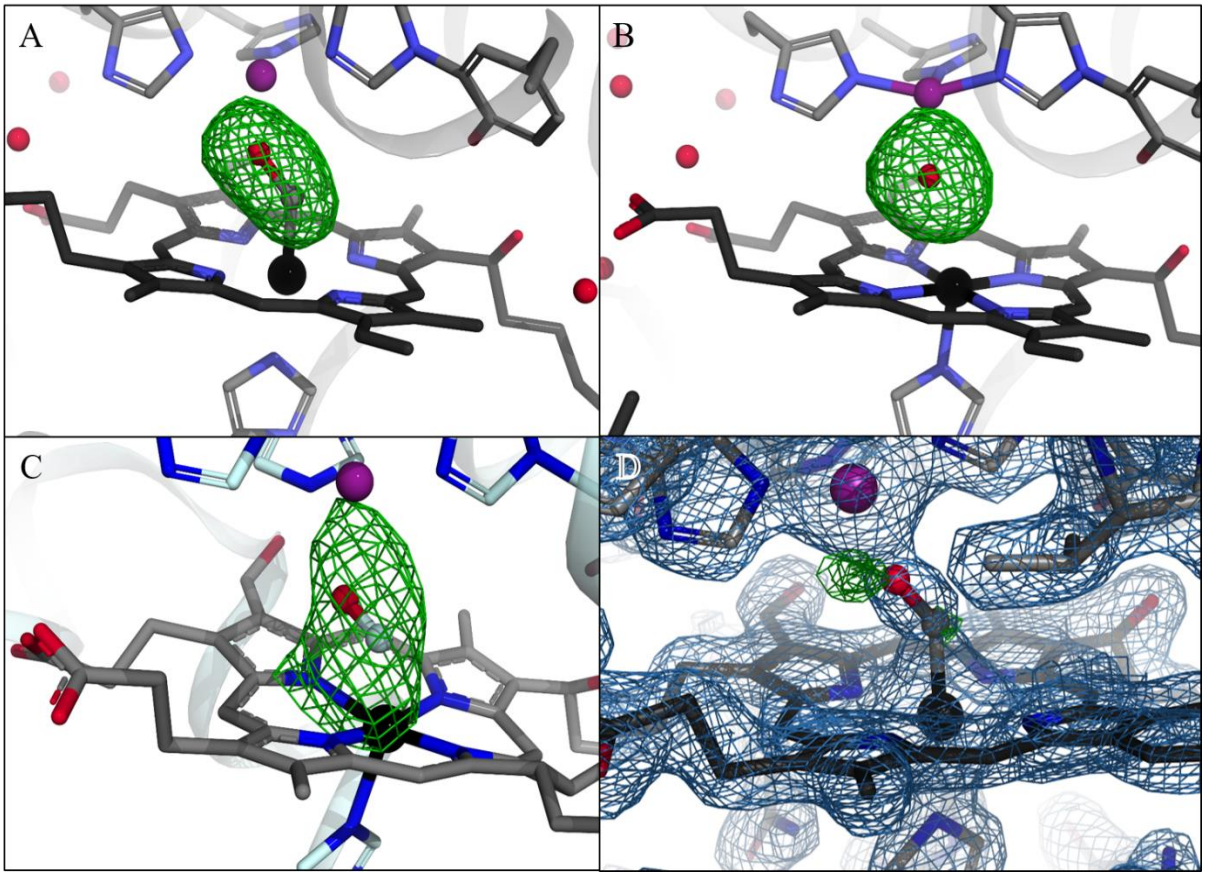

Figure 21. F_o-F_c omit maps of the active site of *ba*$_3$-type C*c*O showing: (A) the reduced-CO bound structure with the F_o-F_c omit map density without the ligand calculated in the active site contoured at 4.5 σ. (B) oxidized structure (PDB ID 5NDC) also calculated without the ligand in the active site at 4.5 σ. (C) A cryogenic structure from synchrotron data (PDB ID 3QJQ) for comparison. (D) $2F_o$-F_c electron density maps of the reduced structure with a CO calculated in the active site. Blue is contoured at σ=2 and represent the $2F_o$-F_c density maps while the omit map is visualized in green at 3.5 σ.

The CO-bound structure showed high agreement with the oxidized SFX structure (PDB ID 5NDC) (paper II) with similar cell unit parameters and C2 as a space group. Conserved structural features such as the proton transfer channel and the water clusters in the expected proton-loading site could be observed in both structures. An interesting difference was found when comparing bovine *aa*$_3$-type C*c*O and the microbial *ba*$_3$-type C*c*O. Upon CO binding of bovine *aa*$_3$-type C*c*O a major structural change is displayed in a region called helix x, especially of two residues (Ser382 and Val 380). This occurs when a ligand bind to the active site and heme a_3 shifts upon change in redox state (Muramoto et al., 2010; Tomitake Tsukihara et al., 2003). No similar movement is found in *ba*$_3$-type C*c*O indicating that the *ba*$_3$-type C*c*O differs from *aa*$_3$-type C*c*O regarding what conformational changes are triggered upon ligand binding to the active site. This gives further evidence that it is of importance to compare structures of the two different species of C*c*Os since the overall mechanism may be the same but the details and which structural elements are involved can be different.

This work has also been performed with a purpose of doing two different types of pump-probe studies. Firstly, dissociating CO from the active site with a 532 nm pump laser pulse to reveal reverse structural movements in the protein. Secondly, by photolysis of caged oxygen, hints about the mechanism of proton pumping and ligand transfer in the ligand channel can be revealed. The CO-bound intermediate states are achievable crystal production wise using the protocols developed with the well-based method to produce the milliliters of CO probed sample needed for the experiments. For oxygen binding, protocols are still under development.

Overall, the method of using wells has proven to be useful in CO-bindning of ba_3-type C*c*O to screen for different reducing agent, the amount of reducing agent required and the approach of how to reduce the sample. The wells also gave an advantage in creating homogenous sample since crystals could be evaluated before pooled together prior to CO-purging.

3.2.4 A combined approach to make microcrystals of Photosynthetic reaction center for SFX studies (Paper I and V)

Production, purification and crystallization of RC in LCP were based on previous conditions (Chiu et al., 2000; Dods et al., 2017; Wöhri et al., 2009) and in addition of some commercial LCP screens. To crystallize RC, crystal contacts need to be aided by adding amphiphilic additives such as diols, triols or heptanetriol which was also confirmed by the commercial screening results. Production of crystals in Hamilton syringes yielded a few large diffracting needle-like crystals which were not optional for serial crystallography. Instead the well-based LCP method was tested with crystal seeds, a method commonly used in vapor diffusion. This method of using crystals from in surfo methods and crushing them by vortexing has previously been described (Dods et al., 2017) but not used together with LCP until now.

Previous attempts of using LCP crystals and adding them as seeds to LCP conditions has been done before (Kolek, Bräuning, & Stewart, 2016) with promising results. However, this method is dependent on there already being a condition in LCP where crystals grow which might not always be the case. The method also shows similar problems with monitoring crystal growth with high focus using a stereo microscope over time without interrupting the crystallization process. An obstacle that is enhanced by the need to harvest the crystals as they are small since the method does not involve crushing of crystals. When using crushed vapor diffusion microcrystals to seed LCP, diffracting microcrystals of RC were obtained (Figure 22) which diffracted to 2.2 Å, unfortunately with a hexagonal space group too large for being indexed. The condition was further screened and an optimized crystallization hit was achieved, producing crystals suitable for SFX and TR-SFX studies using XFEL radiation.

Protein was centrifuged (16 900 rcf, 15 min), concentrated to 0.3 mM and mixed with crystal seeds prior to reconstitution into LCP with the use of MO that already had been mixed with 0.5% (v/v) uiquinone-2 (UQ2), a cofactor that occupy the Q_B pocket. The LCP suspension was then dispensed as 10-15 µl aliquots in 100 µl precipitant solution consisting of 40 mM zinc sulphate, 120 mM 1,2,3-heptanetriol isomer T, 100 mM sodium citrate and pH 6.0. Crystals were obtained after 3 days at room temperature. The amount of crystals and their shape were dependent upon the ratio of MO in contrast to the amount of seeding crystals that had little

effect on crystal growth. An increase of volume of MO during the mixing with protein solution resulted in higher density of smaller crystals (Figure 22). The microcrystals were then collected and stored in syringes before transportation to SACLA (Huang & Lindau, 2012) in Japan where they diffracted to 2.3 Å and ~6000 images could be indexed enough to solve a structure at a resolution of 2.4 Å.

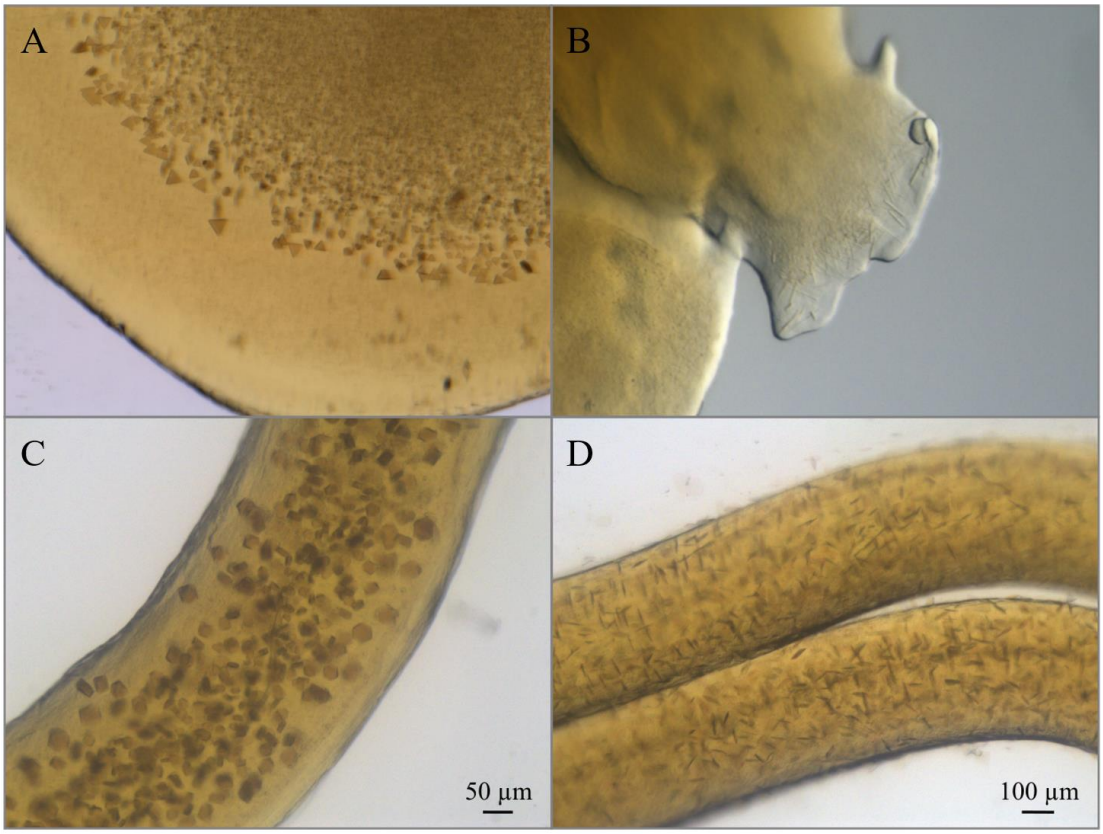

Figure 22. Microcrystals in LCP of RC at different stages during crystallization screening and optimization. (A) shows a crystallization hit early in the screening process. (B) optimization of the condition in Hamilton syringes as previously described (Ishchenko et al., 2016) yielded needle like crystals not enough crystal density for data collection. (C) displays crystal grown using the well-based approach. They diffracted to 2.2 Å but the symmetry of the unit cell was too large for indexing. (D) Optimized crystals obtained from seeded LCP which diffracted and a structure of RC was determined to 2.4 Å resolution.

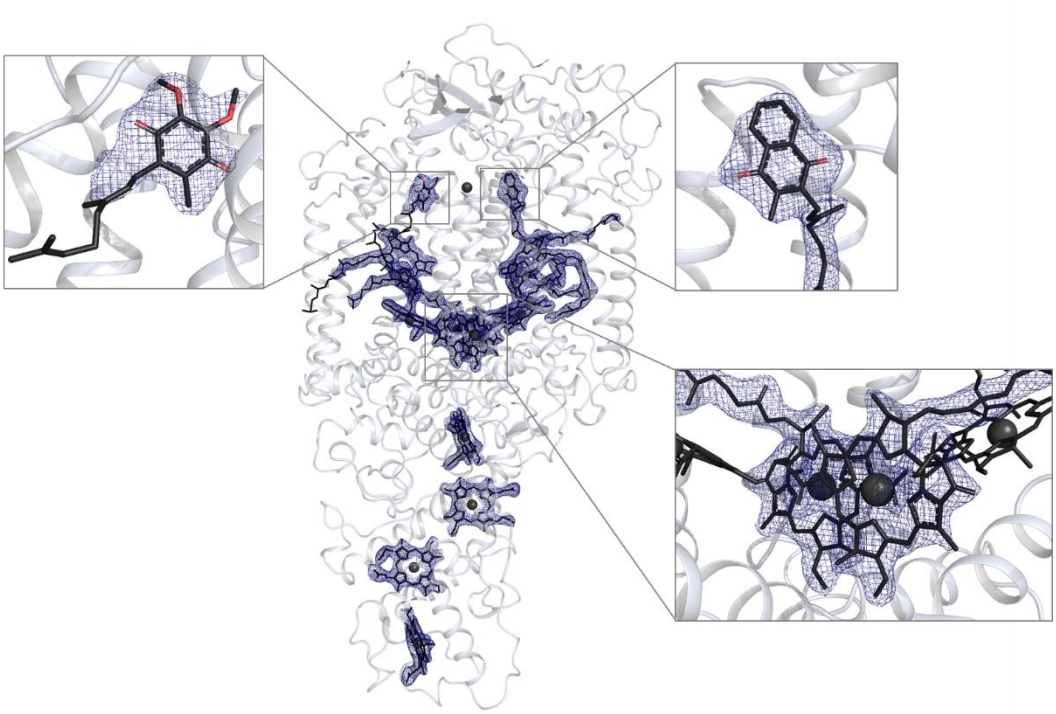

Figure 23. Structure of RC with the co-factors $2F_o$-F_c electron density maps calculated in blue and contoured at 1 σ. The electron density of UQ in Q_B was similar to the density calculated for the other cofactors.

One of the advantages in crystallizing RC in LCP is the possibility to add ubiquinone (UQ) directly to the MO before reconstitution of the protein in the cubic phase since UQ mixes well with the lipids. The occupancy of UQ in the Q_B pockets can be seen in the electron density maps where the electron density is comparable with that of other co-factors in the structure (Figure 23). Ubiquinone can have two different positions in the binding pocket. Either a proximal position or a distal position depending on the position of the adjacent residues for hydrogen bonding possibilities. It was first thought that the distal binding position was the dominant form in RC (Lancaster & Michel, 1997) but more recent research has found that pH affects the distribution between the two binding positions (Koepke et al., 2007) as well as illumination since dark structures is mostly populated with the proximal position (Baxter et al., 2005). Also, as the UQ2 tail is very flexible it is hard to model the UQ in the right position with high certainty. A second ubiquinone binding site feature was also observed in the structure. A hydrophobic pocket could be observed in the structure with a UQ2 molecule with lower occupancy located between two highly conserved residues; phenylalanine and tryptophan. However, this binding pocket is not observed in all structures and its purpose is still under elucidation. Another effect that was seen in the structure that might derive from the data collection at room temperature, is the high flexibility of bound lipids. Several tails of co-factors possess a highly flexible regions causing poor electron density. Other SFX structures sampled at room temperature show the same phenomenon as well as fewer detergent molecules (Dods et al., 2017; Johansson et al., 2013).

The method of combining features of vapour diffusion to enhance LCP crystallization in wells by seeding opens up a new way of crystallizing proteins. It is a unique possibility to add as a screening method if vapour diffusion crystals have been formed for a target protein that show promises to crystallize in LCP to enhance the crystallization growth. The article also highlight a difference in crystal growth comparing LCP crystallization in syringes with wells. Whether or not this is the case for RC needs to be further investigated, but it is not unthinkable since they are two separate crystallization systems with different properties. While the crystallization in syringes offers a completely closed system without an air pocket, the well-based system offer more variety regarding screening factors which affect the crystallization process.

3.2.5 Sensory rhodopsin structure obtained from microcrystals grown in wells (Paper I and V)

SRII was purified according to previous described methods (Hohenfeld, Wegener, & Engelhard, 1999) with following modifications; n-Octyl-β-D-Glucopyranoside (β-OG) was used instead of n-Decyl-β-D-Maltopyranoside as a detergent and a SEC was added after IMAC (Ni-NTA) using a buffer containing 150 mM NaCl, 25 mM Na^+/K^+ phosphate, 0.8 % (w/v) β-OG with a pH of 5.1. SRII, with a protein concentration of 1.6 mM, was reconstituted in LCP and automated screening was performed with a crystallization robot (Gaisford et al., 2011). Hits were found in the crystallization screen of MemGold2 (Molecular Dimensions) and further optimized using the well-based method. Crystals of 10-40 µm were obtained in 38 % (v/v) PEG400, 150 mM $CaCl_2$ and100 mM Glycine at pH 7.5 after 4-12 days in 22 ºC. Crystals were then screened at the BioMAX beamline at MAX IV Laboratory in Lund (Thunnissen et al., 2013) which showed diffraction to approximately 2.7 Å resolution.

Crystals were then further optimized regarding the amount of LCP suspension to precipitant solution and time. As a result, crystals were grown in 10 µl LCP strings dispensed in wells containing 400 µl of precipitant solution (same solution as above) over a time of 1-2 months resulting in 200 µl of crystal containing LCP with crystal sizes of 40-60 µm in size. Crystals were then brought to the beamline PX1 at the Swiss Light Source (SLS) (Weiss, 2001). The crystals were diluted with 20-25 % MO at site and extruded using a HVE injector (Weierstall et al., 2014) and a 75 µm nozzle. The sample was then continuously illuminated by a 2.6 mW laser of 488 nm for 30 min to collect light data before 30 min of dark data was collected. A flow rate of 0.2 µl/min yielded 26382 indexed images for the dark data set and 21518 indexed images for the light data set where crystals diffracted to 2.1 Å and 2.5 Å respectively. Programs used for data processing were CrystFEL (White et al., 2012) and CCP4 (Potterton et al., 2018). The dark state structure was refined in several rounds of refinement using Phenix (Adams et al., 2010) and COOT (Emsley et al., 2010) before being as a model for the difference Fourier electron density maps calculations using Phenix (Pražnikar, Afonine, Gunčar, Adams, & Turk, 2009). The dark state structure showed high agreement with both the light state structure and a cryogenic structure previously determined (Gushchin et al., 2011) regarding unit cell and space group ($C222_1$). Using MR and phases from a 2.1 Å structure (PDB ID 1H68) (A Royant et al., 2001) a room temperature SMX model could be built.

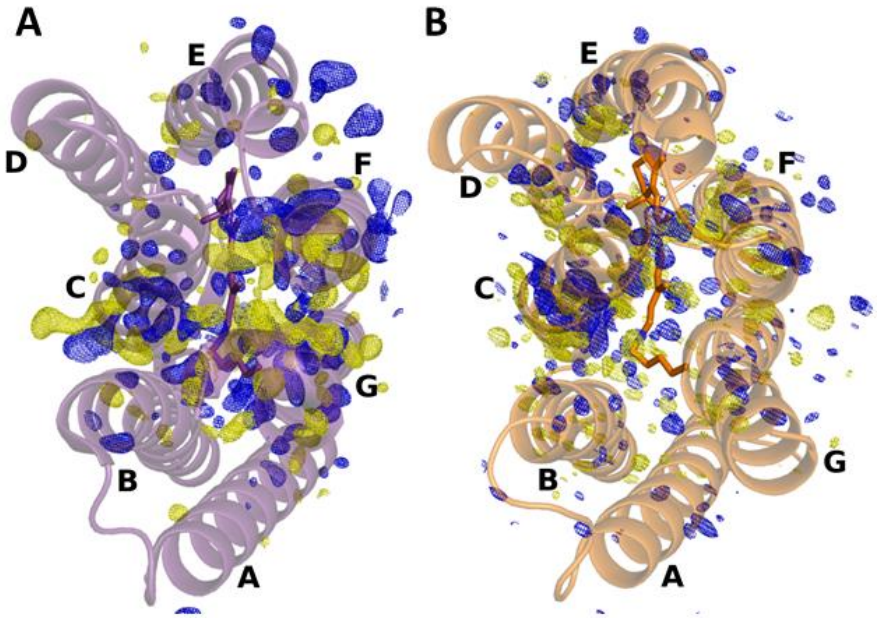

Figure 24. Bacteriorhodopsin (bR) (A) and SRII (B) with difference Fourier electron density maps calculated from continuous illumination of blue light and superimposed upon the dark state. (A) bR maps are calculated from PDB IDs: 6RQP and 6RQO (Weinert et al., 2019). Positive electron density is denoted by blue color and negative electron density by yellow color, both countoured at σ=3. The orange colored stick-representation in the middle of the protein represents the retinal molecule.

Light induced structural changes ins SRII were then compared to light induced structural changes in bacteriorhodopsin (bR), another well-studied light sensitive retinal containing model protein with structural similarities to SRII (Figure 5 and 24). By comparing dark state (laser off) with light state (laser on), structural changes upon illumination could be observed of helix C towards the retinal molecule for both proteins which has been argued to be the rate-limiting step of the Shiff base protonation (Eriko Nango et al., 2016; Antoine Royant et al., 2000). Another similarity is an instant delocalization of a water molecule in the active site of the dark state structure upon light triggering. This water delocalization allows for helix C to move towards helix G which triggers a structural cascade of movements within the protein (Nango et al., 2016; Nogly et al., 2018; Antoine Royant et al., 2000). An outward movement of helix F is also observed in both of the proteins which further gives evidence for similar structural dynamics of the two retinal-containing proteins despite their different functionality. On the other hand there are a few structural differences where the more noticeable one is observed in helix G. In bR helix G unwinds near the retinal on the cytoplasmic side upon illumination driven by the isomerization of the retinal. This movement is thought to aid reprotonation of the Schiff base by defining a site for water binding and thereby creating a water mediated pathway for proton exchange from the cytoplasm (Weinert et al., 2019). In SRII this movement of helix G is negligible which might explain the longer lifetime of the protonated state of the Schiff base. Another difference is a strong difference density in the bR maps that indicate a rotation of an aspartic acid residue (Asp85) in the time as deprotonation of the Schiff base. Upon the rotation, a hydrogen bond is broken with a nearby threonine residue (Thr89) which has been argued to

be important for avoiding protons to back-travel and reprotonate the Schiff base (Eriko Nango et al., 2016). Since SRII does not act as a proton pump there is no need for the protein to have this kind of preventive proton back-travelling mechanism even though SRII takes up and releases protons and have several proton-transferring steps in its photocycle (Sasaki & Spudich, 1999).

By comparing time-resolved diffraction studies of different but structurally similar proteins, subtle but important structural intermediates can be detected for understanding protein function. By comparing bR and SRII, the observations regarding helix G might explain the differences in lifetime of the two photocycles and how they relate to the function of the proteins - bR needs of efficient turnover for proton pumping while SRII needs more time to amplify and transfer the light signal. Using the well-based crystallization method, a new protocol that does not include reconstitution into purple membranes lipids, was developed. Crystallization optimization to increase efficiency of crystal production is crucial for experiments with large sample needs such as serial crystallography. Removing the step of reconstituting the protein into purple membrane is one of those optimization steps that save both time and effort. Crystals produced according to the new protocol based on the well-based LCP approach thus promise for applications in both pump-probe TR-SFX and -SSX.

.

3.2.6 Summary and discussion part II

The development of the well-based approach for production of LCP crystals presents a wide variety of applications that have contributed to the field of serial crystallography. They vary from protocol development (paper I, III, IV and V) to novel structures (paper II) and new crystallization hits (paper I-V). We present three different proteins that have been microcrystallized according to the well-based LCP approach with structures determined at resolutions from 2.0-2.7 Å. Using the well-based approach as a foundation for screening and producing microcrystals in LCP, new applications can dawn such as the combinational method of in surfo seeding in LCP (paper IV) and removal of effort- and time demanding steps such as purifying purple membranes for SRII incorporation prior to crystallization (paper I and V). The method has also been aiding a solution change of a highly toxic crystallization condition to a user- and environmentally friendly condition with MES instead of the arsenic-containing sodium cacodylate trihydrate (paper III). Here plastic plates were used to avoid the risk of solution contact during cleaning of the glass plates and to ease the waste handling. Plastic crystallization plates showed no difference in crystal growth but the LCP adhered to the sides of the plastic wells, a similar problem as we had with the collection of LCP strings for syringe packing using plastic pipette tips.

These results indicate a working method protocol for various purposes. The results also show that crystals might crystallize differently in wells compared to syringes, but this idea needs to be further evaluated before making any firm conclusions. In either case, LCP microcrystallization in wells is a method that has proven to be of great aid for SSX and SFX structural studies and promising results for future time-resolved pump-probe experiments. Overall, this method of producing microcrystals is a good complement to the methods already existing, where monitoring crystals over time with high focus is of importance.

4. Conclusions and future perspectives

Since the method of using LCP with membrane proteins was developed and used to solve several known 'hard-to-crystallize' membrane protein structures, the field of LCP crystallization has expanded enormously. Together with serial crystallography, LCP crystallization opens up a field within life science with endless potential. However, the serial crystallography method requires large volumes of sample, and even more in pump-probe experiments, making membrane protein crystallization demanding. By developing a method of screening and producing crystals in wells rather than in syringes, we present new ways of visualizing the growth of microcrystals in LCP (paper I). The well-based approach offers a way of screening a lot of different crystallization conditions effortless with more screening variables and the opportunity to monitor the crystals over time without interrupting the crystallization process. The method has proven to be useful in many different applications.

In paper II we described the first room temperature structure of ba_3-type C*c*O with a water or hydroxide in the active site compared to peroxide that was previously modelled in structures. The method has also found a way for SRII to be crystallized without using purple membranes resulting in a novel crystallization condition and will be a good foundation for crystal production for pump probe experiments (paper I).

In paper III we found a new crystallization condition with non-toxic properties and developed a protocol for CO-binding of the active site of ba_3-type C*c*O. This work is ongoing with goals to do TR pump-probe studies by triggering structural change by CO dissociation and upon O_2-binding from caged oxygen to reveal the mechanism of proton translocation and the migration of oxygen which is still not fully known. Since we found that crystals can be grown in a reduced condition and CO is shown to dissociate into the lipid phase, a possibility of flushing CO over either in situ produced crystals or crystals transferred to chips could be developed and optimized for fixed target crystallography data collection. This would show that well-based crystallization approach can be used in several different experimental set up strategies

In paper IV the well-based method is combined with techniques from the vapor diffusion method where crushed crystals are mixed with the protein solution before reconstitution into LCP as seeding to aid crystal growth. The combined method showed great results with well diffracting crystals but also drew attention to a difference in crystallizing in syringes compared to wells. A result that needs further investigation.

In paper V a crystallization step could be removed by using LCP instead of purple membranes for SRII and still retain stability and function of the enzyme. Microcrystallization screening resulted in a new crystallization hit that revealed new structural insights. The crystallization protocol developments made for paper V can be used to create enough sample for future time resolved studies.

Altogether, the method of well-based LCP crystallization meet the requirements of producing large volumes of microcrystals for the expanding field of serial crystallography. Overall, this thesis contributes to the continuing development of serial crystallography, which shows great promise for growth, particularly for time resolved studies.

5. Populärvetenskaplig sammanfattning

Varje levande organism är uppbyggd utav celler som hålls ihop av ett cellmembran. Cellmembranet har ofantligt många skilda uppgifter som bland annat skydd från omvärlden, energiproduktion, transport, signalering och organisering av uppgifter. Cellmembranet är så pass viktigt att de flesta processer som sker i kroppen har med cellmembranet att göra vilket gör det föga överraskande att en tredjedel av hela vårt genom kodar för de proteiner som finns där i. Detta i sin tur har medfört att över hälften av alla mediciner som finns tillgängliga på marknaden har dessa proteiner som mål.

En av de mest livsviktiga funktionerna för proteinerna i cellmembranet är att tillverka energi. Detta görs hos människor i cellandningen där vi andas in syre som driver en process där flera proteiner överför protoner, en positivt laddad atom, som skapar en elektrisk potential som cellen sedan kan överföra till kemisk energi. Det är den kemiska energin som används i cellen och kroppen. Trots att det är en sådan livsviktig process så vet vi inte allt om proteinerna i cellandningen ännu. Två av de områden som vi fortfarande behöver mer kunskaper om är hur protonerna transporteras i proteinerna och hur syret som vi andas migrerar inuti proteinet. Detta för att förstå helt hur energin bildas i organismer.

För att ta reda på hur protonpumpningen sker och hur syre förflyttas i proteinet så flyttas proteinmolekylen över från det naturliga cellmembranet till ett syntetiskt tillverkat membran där man kan kontrollera dess egenskaper. Genom att tillsätta salter och andra kemiska substanser kan man sedan få proteinmolekylerna att arrangera sig på ett visst sätt så att de bildar kristaller genom att få det syntetiska membranet att ändra karaktär. Det är dessa kristaller som sedan tas med till stora forskningsstationer, partikelacceleratorer, där röntgenstrålar skjuts på kristallerna. När röntgenstrålen träffar en elektron i en atom som finns i proteinet så ändrar den färdriktning. Genom att ha en detektor kan man mäta den vinkel som färdriktningen ändrades i. Det är denna vinkel vi bland annat kan använda för att genom matematiska beräkningar ta reda på hur proteinerna ser ut på molekylär nivå. En fördel med att använda sig av syntetiska membran är att man kan skapa väldigt små kristaller, mindre än 0,000020 m som man träffar med röntgenstrålen och sedan därefter kasserar. Genom att använda många små kristaller som bara används en gång istället för en stor kristall som man använder fler gånger, så undviker man slitage på kristallen som kan påverka ens data negativt. Detta innebär dock att det krävs tusentals kristaller istället för en vilket kräver en metod för att producera alla dessa.

Den här avhandlingen består av två delar där den första beskriver en metod där man kan odla dessa små kristaller på en glasplatta som gör att man kan övervaka hur kristallerna växer och ser ut utan att behöva stoppa deras tillväxt. På så sätt kan man tillsätta olika kemikalier som påverkar hur kristallerna växer och utvärdera vilket sätt som ger bäst kristaller - d.v.s. de kristaller som ger bäst upplösning så att man ser så många detaljer som möjligt på atomnivå. Det går t.ex. att utskilja enskilda vattenmolekyler och vid riktigt bra upplösning även enskilda väteatomer, den allra minsta atomen i det periodiska systemet.

Den andra delen beskriver sedan hur vi har tagit reda på om huruvida metoden funkar genom att använda den på flera olika proteiner på lite olika sätt. För proteinet som överför protoner över membranet har vi lyckats ta reda på hur proteinet ser ut och även utvecklat vår metod till

att i framtiden kunna göra molekylära filmer genom att få proteinet att röra på sig genom tillsättning av syre eller kolmonoxid och sedan skjuta röntgenstrålar på det vid olika tidpunkter. För ett bakteriellt ljuskänsligt protein har nya kristalliseringsmetoder upptäckts genom att man använder vår metod tillsammans med en annan metod där man tillsätter små kristaller som sedan får växa till sig i plattorna, till skillnad från att låta dem växa från grunden. För det tredje proteinet, ett protein som är involverat i hur uråldriga organismer, arkéer, rör sig, så har vår metod gjort att man kan förenkla kristalliseringen genom att hoppa över vissa steg som annars är viktiga för att proteinet ska arrangera sig till kristaller.

Vad vi kan visa är att vår metod funkar för flera olika applikationer och har enorm potential att kunna utvecklas. Därmed bidrar denna avhandling till utvecklingen av mikrokristallisering o h fältet inom kristallografi. Metoden visar även goda förutsättningar för att användas till tidsupplösta datainsamlingar som kan ge ökad kunskap om proteiners funktion och mekanismer, med mål att kunna utröna hur protoner överförs över membranet och hur syre tar sig till det aktiva sätet i ett av proteinerna i cellandningen.

6. Acknowledgement

First I want to thank **Richard** for once letting me start a PhD with the words; I will have troubles with you, just like I had with.... I think you meant my determined mind and I do not hope I caused too much trouble with it. Then I want to thank **Gisela** for giving me the opportunity to start up the *ba*$_3$ C*c*O project. Of all the projects I've been working on this my favorite all time and I really appreciate that you always took time to talk about everything. And **Martin** for being such a calm and nice examinator for most of my PhD. And **Gergely** who took over from him when Martin retired. Really appreciate it! I also want to thank **Kristina** for being my second co-supervisor but also my chair person during my defense. Always keep on wearing red clothes – it makes the corridor a bit more fancy.

Mike, Elin D, Rajjan, Dods, Emil, Petra E, Rosie, David and Oskar: The lab is not the same since you left. For me Lundberg will always be the time when you were here. Especially **Jennie** who not only was my roomie for a long time but also my supervisor during my Master's thesis and a true ginny pig friend (but I will never get ginny pigs – they poop too much). And **Ida**, you will always be a close friend and I really miss living so close to you. The old days were almost like a Big Bang Theory episode!

And to my lab wife **Petra B** aka T-rex. I do hope you stay in academia because academia needs you. A strong quirky smart woman with tons of hobbies! Every lab needs a dishwashing-cart with speakers on them and you can provide it. **Cecilia S:** you came in to the project with your energy and made it complete. I know you never really felt it like yours but you really took it to another lever with that hard working spirit and fumbling fingers. I could not ask for a better co-parent to this baby. **CW,** I will never forget the day you told me your secret about being pregnant and I told you the same! Together with our pregnancy hormones we made history by changing the whole waste system in the lab.

Dunge, Linnea, Elin C, Wejjan, Tinna, Maja, Majo and Leo: Always so much fun and making the lab sparkle. May the gossip never die. Few people make me laugh so much as you do! **Victor** I hope there will be many more bugs in the system. Always a treat. And **Greger**… I do hope you're having a ball with your defence. I will make my own spex just for you **Florian**, **Amke**, **Bosman, Per and Daniel:** you're the food and party gang of Lundberg. Always bringing food, cakes and arranging barbeques or crayfish parties. I do like food.

Doris, Swaggie, Jonathan, Emil: Good luck with the project! Take good care of her (yes the feet stinking project is a girl!). And to **Owens**: this is not a vacation ;). **Giorgia**: Keep that fire flaming! We Swedes need some heat. **Martin Söderström (LODOR)** your time here was short but you really made an impression. I do hope you use your brain to make greatness and avoid sulfuric acid in the future. Take care old day care friend!

To the unmentioned Westenhoffiens, Kristinians, Neutzians and the gangs below in the dungeon (first floor): Good luck with everything! I will leave the wigs and props to be used for every spex in the future. Especially thanks to Johanna for our gardening talks. I do hope academia recognize the smart strong force you are.

And the lab father, Peter Dahl, who brings calmness to chaotic beamtimes. Nice to have you around!

Last in the lab but not least Bruno and Lars. You are like Kamaji in Spirited away. Without you there would be no steam.

To whoever I might have not mentioned: Sorry but this is harder than you think, especially when you have not been in the lab for a long long time.

Till mina bästisar Maja och Carro för att ni gör livet lite roligare. Och Maia i Holmen (eller bör jag säga Katrineholm?) för alla knäppa konversationer som förgyller livet dagligen.

Till Gun, Bengt och Marthina med familj för att ni är sådana fina familjemedlemmar till Ebba. Tack för att ni alltid ställer upp.

Mamma, pappa, Max och Anton. Vi är en udda konstellation av olika intressen och individer men kärnstark när det väl gäller. Som alltid ställer upp när det blåser storm.

Jonas. Du gav mig det finaste jag har, vår Ebba. Vår fina lilla familj är det bästa jag vet. Älskar dig.

Och till sist det absolut bästa som finns, min dotter Ebba. Allt är för dig. Alltid för dig. Mamma älskar dig.

7. Bibliography

Adams, P. D., Afonine, P. V, Bunkóczi, G., Chen, V. B., Davis, I. W., Echols, N., … Zwart, P. H. (2010). PHENIX : a comprehensive Python-based system for macromolecular structure solution. *Acta Crystallographica Section D*, *66*(2), 213–221.

Ai, X., & Caffrey, M. (2000). Membrane Protein Crystallization in Lipidic Mesophases: Detergent Effects. *Biophysical Journal*, *79*(1), 394–405.

Ali, I., Aboul-Enein, H. Y., Singh, P., Singh, R., & Sharma, B. (2010). Separation of biological proteins by liquid chromatography. *Saudi Pharmaceutical Journal*, *18*(2), 59–73.

Ayvazyan, V., Baboi, N., Bähr, J., Balandin, V., Beutner, B., Brandt, A., … ... (2006). First operation of a free-electron laser generating GW power radiation at 32 nm wavelength. *The European Physical Journal D - Atomic, Molecular, Optical and Plasma Physics*, *37*(2), 297–303.

Ballmoos, C. Von, Gonska, N., Lachmann, P., Gennis, R. B., Ädelroth, P., & Brzezinski, P. (2015). Mutation of a single residue in the *ba3* oxidase specifically impairs protonation of the pump site. *Proceedings of the National Academy of Sciences*, *112*(11), 3397. Retrieved from http://www.pnas.org/content/112/11/3397.abstract

Barber, J. (2017). Photosynthetic water splitting by the Mn4Ca2+OX catalyst of photosystem II: its structure, robustness and mechanism. *Quarterly Reviews of Biophysics*, *50*, e13.

Barty, A., Kirian, R. A., Maia, F. R. N. C., Hantke, M., Yoon, C. H., White, T. A., & Chapman, H. (2014). Cheetah : software for high-throughput reduction and analysis of serial femtosecond X-ray diffraction data. *Journal of Applied Crystallography*, *47*(3), 1118–1131. https://doi.org/10.1107/S1600576714007626

Battye, T. G. G., Kontogiannis, L., Johnson, O., Powell, H. R., & Leslie, A. G. W. (2011). iMOSFLM: a new graphical interface for diffraction-image processing with MOSFLM. *Acta Crystallographica Section D*, *67*(4), 271–281.

Baxter, R. H. G., Seagle, B., Ponomarenko, N., & Norris, J. R. (2005). Cryogenic structure of the photosynthetic reaction center of Blastochloris viridis in the light and dark. *Acta Crystallographica Section D*, *61*(5), 605–612.

Beale, J. H., Bolton, R., Marshall, S. A., Beale, E. V, Carr, S. B., Ebrahim, A., … Owen, R. L. (2019). Successful sample preparation for serial crystallography experiments. *Journal of Applied Crystallography*, *52*(6), 1385–1396.

Bergfors, T. (2003). Seeds to crystals. *Journal of Structural Biology*, *142*(1), 66–76. https://doi.org/https://doi.org/10.1016/S1047-8477(03)00039-X

Bernardino de la Serna, J., Schütz, G. J., Eggeling, C., & Cebecauer, M. (2016). There Is No Simple Model of the Plasma Membrane Organization. *Frontiers in Cell and Developmental Biology*, *4*, 106. https://doi.org/10.3389/fcell.2016.00106

Bill, R. M., Henderson, P. J. F., Iwata, S., Kunji, E. R. S., Michel, H., Neutze, R., … Vogel, H. (2011). Overcoming barriers to membrane protein structure determination. *Nature Biotechnology*, *29*(4), 335–340. https://doi.org/10.1038/nbt.1833

Botha, S., Nass, K., Barends, T. R. M., Kabsch, W., Latz, B., Dworkowski, F., … Doak, R. B. (2015). Room-temperature serial crystallography at synchrotron X-ray sources using

slowly flowing free-standing high-viscosity microstreams. *Acta Crystallographica Section D*, *71*(2), 387–397.

Bragg, W. H. (1913). The Reflection of X-Rays by Crystals. *Nature*, *91*(2280), 477.

Brändén, G., Gennis, R. B., & Brzezinski, P. (2006). Transmembrane proton translocation by cytochrome c oxidase. *Biochimica et Biophysica Acta (BBA) - Bioenergetics*, *1757*(8), 1052–1063. https://doi.org/https://doi.org/10.1016/j.bbabio.2006.05.020

Briggs, J., & Caffrey, M. (1994). The temperature-composition phase diagram and mesophase structure characterization of monopentadecenoin in water. *Biophysical Journal*, *67*(4), 1594–1602.

Bury, C. S., Brooks-Bartlett, J. C., Walsh, S. P., & Garman, E. F. (2018). Estimate your dose: RADDOSE-3D. *Protein Science*, *27*(1), 217–228.

Buse, G., Soulimane, T., Dewor, M., Meyer, H. E., & Blggel, M. (1999). Evidence for a copper-coordinated histidinetyrosine cross-link in the active site of cytochrome oxidase. *Protein Science*, *8*(5), 985–990.

Caffrey, M. (2008). On the mechanism of membrane protein crystallization in lipidic mesophases. *Crystal Growth and Design*, *8*(12), 4244–4254.

Caffrey, Martin. (2015). A comprehensive review of the lipid cubic phase or in meso method for crystallizing membrane and soluble proteins and complexes. *Acta Crystallographica Section F*, *71*(1), 3–18.

Cambi, A., & Lidke, D. (2012). Nanoscale Membrane Organization: Where Biochemistry Meets Advanced Microscopy. *Acs Chemical Biology*, *7*(1), 139–149.

Chapman, H. N., Caleman, C., & Timneanu, N. (2014). Diffraction before destruction. *Philosophical Transactions of the Royal Society of London. Series B, Biological Sciences*, *369*(1647), 20130313. https://doi.org/10.1098/rstb.2013.0313

Chapman, H. N., Fromme, P., Barty, A., White, T. A., Kirian, R. A., Aquila, A., … Spence, J. C. H. (2011). Femtosecond X-ray protein nanocrystallography. *Nature, 2011, Vol. 470, Iss. 7332, Pp. 73-.7*, *470*(7332), 73–77.

Chayen, N E, Shaw Stewart, P. D., Maeder, D. L., & Blow, D. M. (1990). An automated system for micro-batch protein crystallization and screening. *Journal of Applied Crystallography*, *23*(4), 297–302. https://doi.org/10.1107/S0021889890003260

Chayen, Naomi E. (1998). Comparative Studies of Protein Crystallization by Vapour-Diffusion and Microbatch Techniques. *Acta Crystallographica Section D*, *54*(1), 8–15.

Chayen, Naomi E. (1999). Recent advances in methodology for the crystallization of biological macromolecules. *Journal of Crystal Growth*, *198*(I), 649–655.

Chen, Y., Hunsicker-Wang, L., Pacoma, R. L., Luna, E., & Fee, J. A. (2005). A homologous expression system for obtaining engineered cytochrome ba 3 from Thermus thermophilus HB8. *Protein Expression and Purification*, *40*(2), 299–318.

Cheng, A., Hummel, B., Qiu, H., & Caffrey, M. (1998). A simple mechanical mixer for small viscous lipid-containing samples. *Chemistry and Physics of Lipids*, *95*(1), 11–21.

Cherezov, V., & Caffrey, M. (2003). Nano-volume plates with excellent optical properties for fast, inexpensive crystallization screening of membrane proteins. *Journal of Applied*

Crystallography, *36*(6), 1372–1377.

Cherezov, V., & Caffrey, M. (2005). A simple and inexpensive nanoliter-volume dispenser for highly viscous materials used in membrane protein crystallization. *Journal of Applied Crystallography*, *38*(2), 398–400.

Cherezov, V., & Caffrey, M. (2007). Membrane protein crystallization in lipidic mesophases. A mechanism study using X-ray microdiffraction. *Faraday Discussions*, *136*, 195–212.

Cherezov, V., Clogston, J., Misquitta, Y., Abdel-Gawad, W., & Caffrey, M. (2002). Membrane Protein Crystallization In Meso: Lipid Type-Tailoring of the Cubic Phase. *Biophysical Journal*, *83*(6), 3393–3407.

Cherezov, V., Clogston, J., Papiz, M. Z., & Caffrey, M. (2006). Room to Move: Crystallizing Membrane Proteins in Swollen Lipidic Mesophases. *Journal of Molecular Biology*, *357*(5), 1605–1618.

Cherezov, V., Fersi, H., & Caffrey, M. (2001). Crystallization Screens: Compatibility with the Lipidic Cubic Phase for in Meso Crystallization of Membrane Proteins. *Biophysical Journal*, *81*(1), 225–242.

Chiu, M., Nollert, P., Loewen, M. C., Belrhali, H., Pebay-Peyroula, E., Rosenbusch, J. P., & Landau, E. (2000). Crystallization in cubo: general applicability to membrane proteins. *Acta Crystallographica Section D-Biological Crystallography*, *56*, 781–784.

Clark, R. B. (2013). Profile of Brian K. Kobilka and Robert J. Lefkowitz, 2012 Nobel Laureates in Chemistry. *Proceedings of the National Academy of Sciences*, *110*(14).

Clogston, J., & Caffrey, M. (2005). Controlling release from the lipidic cubic phase. Amino acids, peptides, proteins and nucleic acids. *Journal of Controlled Release*, *107*(1), 97–111.

Coe, J., Kupitz, C., Basu, S., Conrad, C. E., Roy-Chowdhury, S., Fromme, R., & Fromme, P. (2015). Crystallization of Photosystem II for Time-Resolved Structural Studies Using an X-ray Free Electron Laser. *Methods in Enzymology*, *557*, 459–482. https://doi.org/10.1016/bs.mie.2015.01.011

Conrad, C. E., Basu, S., James, D., Wang, D., Schaffer, A., Roy-Chowdhury, S., … Fromme, P. (2015). *A novel inert crystal delivery medium for serial femtosecond crystallography.(PHYSICS: FELS)(Report)*. *2*(4), 421.

Coquelle, N., Brewster, A. S., Kapp, U., Shilova, A., Weinhausen, B., Burghammer, M., & Colletier, J.-P. (2015). Raster-scanning serial protein crystallography using micro- and nano-focused synchrotron beams. *Acta Crystallographica Section D*, *71*(5), 1184–1196. https://doi.org/10.1107/S1399004715004514

Dauter, Z., Jaskolski, M., & Wlodawer, A. (2010). Impact of synchrotron radiation on macromolecular crystallography: a personal view. *Journal of Synchrotron Radiation*, *17*(4), 433–444. https://doi.org/10.1107/S0909049510011611

DePonte, D. P., Weierstall, U., Schmidt, K., Warner, J., Starodub, D., Spence, J. C. H., & Doak, R. B. (2008). Gas dynamic virtual nozzle for generation of microscopic droplet streams. *Journal of Physics D: Applied Physics*, *41*(19), 195505. https://doi.org/10.1088/0022-3727/41/19/195505

Dessau, M. A., & Modis, Y. (2011). Protein crystallization for X-ray crystallography. *Journal*

of Visualized Experiments : JoVE, (47), 2285. https://doi.org/10.3791/2285

Dods, R., Båth, P., Arnlund, D., Beyerlein, K. R., Nelson, G., Liang, M., … Neutze, R. (2017). From Macrocrystals to Microcrystals: A Strategy for Membrane Protein Serial Crystallography. *Structure*, *25*(9). https://doi.org/10.1016/j.str.2017.07.002

Dupuy, A. D., & Engelman, D. M. (2008). Protein area occupancy at the center of the red blood cell membrane. *Proceedings of the National Academy of Sciences of the United States of America*, *105*(8), 2848–2852. https://doi.org/10.1073/pnas.0712379105

Eggeling, C., Ringemann, C., Medda, R., Schwarzmann, G., Sandhoff, K., Polyakova, S., … Hell, S. (2009). Direct observation of the nanoscale dynamics of membrane lipids in a living cell. *Nature*, *457*(7233), 1159–1162. Retrieved from http://search.proquest.com/docview/204564364/

Elder, F. R., Gurewitsch, A. M., Langmuir, R. V, & Pollock, H. C. (1947). Radiation from electrons in a synchrotron [8]. *Physical Review*, *71*(11), 829–830.

Emsley, P., Lohkamp, B., Scott, W. G., & Cowtan, K. (2010). Features and development of Coot. *Acta Crystallographica. Section D, Biological Crystallography*, Vol. 66, pp. 486–501. https://doi.org/10.1107/S0907444910007493

Engström, S., Alfons, K., Rasmusson, M., & Ljusberg-Wahren, H. (1998). Solvent-induced sponge (L3) phases in the solvent-monoolein-water system. In B. Lindman & B. W. Ninham (Eds.), *The Colloid Science of Lipids* (pp. 93–98). Darmstadt: Steinkopff.

Evertsson, H., Stilbs, P., Lindblom, G., & Engström, S. (2002). NMR self diffusion measurements of the Monooleoylglycerol/Poly ethylene glycol/water L 3 phase. *Colloids and Surfaces, B, Biointerfaces*, *26*(1–2), 21–29.

Ewald, P. P. (1969). Introduction to the dynamical theory of X-ray diffraction. *Acta Crystallographica Section A*, *25*(1), 103–108. https://doi.org/10.1107/S0567739469000155

Finkelstein, J. M. (2014). Structures of membrane proteins: Challenging protein structures. *Nature*, *511*(S7509), 21. https://doi.org/10.1038/nature13372

Fraenkel, G., & Hopf, H. S. (1940). The physiological action of abnormally high temperatures on poikilothermic animals: Temperature adaptation and the degree of saturation of the phosphatides. *The Biochemical Journal*, *34*(7), 1085.

Fuguet, E., Ràfols, C., Rosés, M., & Bosch, E. (2005). Critical micelle concentration of surfactants in aqueous buffered and unbuffered systems. *Analytica Chimica Acta*, *548*(1), 95–100.

Fujimoto, T., & Parmryd, I. (2017). Interleaflet Coupling, Pinning, and Leaflet Asymmetry-Major Players in Plasma Membrane Nanodomain Formation. *Frontiers in Cell and Developmental Biology*, *4*, 155. https://doi.org/10.3389/fcell.2016.00155

Fuller, F. D., Gul, S., Chatterjee, R., Burgie, E. S., Young, I. D., Lebrette, H., … Yano, J. (2017). Drop-on-demand sample delivery for studying biocatalysts in action at X-ray free-electron lasers. *Nature Methods*, *14*(4), 443–449. https://doi.org/10.1038/nmeth.4195

Funatogawa, C., Li, Y., Chen, Y., Mcdonald, W., Szundi, I., Fee, J. A., … Einarsdóttir, Ó. (2017). Role of the Conserved Valine 236 in Access of Ligands to the Active Site of

Thermus thermophilus ba Cytochrome Oxidase. *Biochemistry*, *56*(1), 107.

Gaisford, W., Schertler, G., & Edwards, P. (2011). mosquito® LCP: Making membrane protein crystallization accessible to the research scientist. *Nature Methods*, *8*(6).

García-Horsman, J. A., Barquera, B., Rumbley, J., Ma, J., & Gennis, R. B. (1994). The superfamily of heme-copper respiratory oxidases. *Journal of Bacteriology*, *176*(18), 5587–5600. https://doi.org/10.1128/jb.176.18.5587-5600.1994

Garman, E. F., & Weik, M. (2011). Macromolecular crystallography radiation damage research: what's new? *Journal of Synchrotron Radiation*, *18*(Pt 3), 313.

Gennis, R. B. (1998). Multiple proton-conducting pathways in cytochrome oxidase and a proposed role for the active-site tyrosine. *BBA - Bioenergetics*, *1365*(1–2), 241–248.

Ghosh, E., Kumari, P., Jaiman, D., & Shukla, A. K. (2015). Methodological advances: the unsung heroes of the GPCR structural revolution. *Nature Reviews Molecular Cell Biology*, *16*(2).

Giacovazzo, C. (2014). *Phasing in crystallography: a modern perspective*. Oxford: Oxford University Press.

Giovannetti, R. (2012). The Use of Spectrophotometry UV-Vis for the Study of Porphyrins. In J. Uddin (Ed.), *Macro To Nano Spectroscopy*. https://doi.org/10.5772/38797

Giuffrè, A., Forte, E., Antonini, G., D'Itri, E., Brunori, M., Soulimane, T., & Buse, G. (1999). Kinetic Properties of *ba3* Oxidase from Thermus thermophilus: Effect of Temperature. *Biochemistry*, *38*(3), 1057–1065. https://doi.org/10.1021/bi9815389

Gushchin, I., Reshetnyak, A., Borshchevskiy, V., Ishchenko, A., Round, E., Grudinin, S., … Gordeliy, V. (2011). Active State of Sensory Rhodopsin II: Structural Determinants for Signal Transfer and Proton Pumping. *Journal of Molecular Biology*, *412*(4), 591–600.

Hanson, M. A., Cherezov, V., Griffith, M. T., Roth, C. B., Jaakola, V.-P., Chien, E. Y. T., … Stevens, R. C. (2008). A Specific Cholesterol Binding Site Is Established by the 2.8 Å Structure of the Human β2-Adrenergic Receptor. *Structure (London)*, *16*(6), 897–905.

Hartmut, M. (1983). Crystallization of membrane proteins. *Trends in Biochemical Sciences*, *8*(2), 56–59.

Helfferich, F. (1995). *Ion exchange*. New York: Dover publications.

Hellwig, P., Soulimane, T., Buse, G., & Mantele, W. (1999). Electrochemical, FTIR, and UV/VIS spectroscopic properties of the ba(3) oxidase from Thermus thermophilus. *Biochemistry*, *38*(30), 9648–9658.

Heras, B., & Martin, J. L. (2005). Post-crystallization treatments for improving diffraction quality of protein crystals. *Acta Crystallographica Section D*, *61*(9), 1173–1180.

Hirata, K., Shinzawa-Itoh, K., Yano, N., Takemura, S., Kato, K., Hatanaka, M., … Ago, H. (2014). Determination of damage-free crystal structure of an X-ray–sensitive protein using an XFEL. *Nature Methods*, *11*(7), 734–736. https://doi.org/10.1038/nmeth.2962

Hohenfeld, I. P., Wegener, A. A., & Engelhard, M. (1999). Purification of histidine tagged bacteriorhodopsin, pharaonis halorhodopsin and pharaonis sensory rhodopsin II functionally expressed in Escherichia coli. *FEBS Letters*, *442*(2–3), 198–202. https://doi.org/10.1016/S0014-5793(98)01659-7

Holton, J. M. (2009). A beginner's guide to radiation damage. *Journal of Synchrotron Radiation*, *16*(Pt 2), 133–142. https://doi.org/10.1107/S0909049509004361

Hosler, J P, Fetter, J., Tecklenburg, M. M., Espe, M., Lerma, C., & Ferguson-Miller, S. (1992). Cytochrome aa3 of Rhodobacter sphaeroides as a model for mitochondrial cytochrome c oxidase. Purification, kinetics, proton pumping, and spectral analysis. *The Journal of Biological Chemistry*, *267*(34), 24264.

Hosler, Jonathan P. (2004). The influence of subunit III of cytochrome c oxidase on the D pathway, the proton exit pathway and mechanism-based inactivation in subunit I. *BBA - Bioenergetics*, *1655*(1–3), 332–339.

Huang, Z., & Lindau, I. (2012). SACLA hard-X-ray compact FEL. *Nature Photonics*, *6*(8), 505–506. https://doi.org/10.1038/nphoton.2012.184

Hunsicker-Wang, L. M., Pacoma, R. L., Chen, Y., Fee, J. A., & Stout, C. D. (2005). A novel cryoprotection scheme for enhancing the diffraction of crystals of recombinant cytochrome ba 3 oxidase from Thermus thermophilus. *Acta Crystallographica Section D*, *61*(3), 340–343.

Ichikawa, T., Okafuji, A., Kato, T., & Ohno, H. (2016). Induction of an Infinite Periodic Minimal Surface by Endowing An Amphiphilic Zwitterion with Halogen-Bond Ability. *ChemistryOpen*, *5*(5), 439–444. https://doi.org/10.1002/open.201600054

Imberg, A., Evertsson, H., Stilbs, P., Kriechbaum, M., & Engstrom, S. (2003). On the self-assembly of monoolein in mixtures of water and a polar aprotic solvent. *Journal Of Physical Chemistry B*, *107*(10), 2311–2318.

Imhoff, J. F. (2007). The Phototrophic Alpha-Proteobacteria. In *The Prokaryotes: Volume 5: Proteobacteria: Alpha and Beta Subclasses* (pp. 41–64). New York, NY: Springer New York.

Ishchenko, A., Cherezov, V., & Liu, W. (2016). Preparation and Delivery of Protein Microcrystals in Lipidic Cubic Phase for Serial Femtosecond Crystallography. *Journal of Visualized Experiments : JoVE*, *2016*(115).

Ishigami, I., Zatsepin, N. A., Hikita, M., Conrad, C. E., Nelson, G., Coe, J. D., … Rousseau, D. L. (2017). Crystal structure of CO-bound cytochrome oxidase determined by serial femtosecond X-ray crystallography at room temperature. *Proceedings of the National Academy of Sciences of the United States of America*, *114*(30), 8011.

Iwata, S., Ostermeier, C., Ludwig, B., & Michel, H. (1995). Structure at 2.8 Å resolution of cytochrome c oxidase from Paracoccus denitrificans. *Nature*, *376*(6542), 660.

Jason Briggs, Hesson Chung, & Martin Caffrey. (1996). The Temperature-Composition Phase Diagram and Mesophase Structure Characterization of the Monoolein/Water System. *J. Phys. II France*, *6*(5), 723–751. https://doi.org/10.1051/jp2:1996208

Johansson, L. C., Arnlund, D., Katona, G., White, T. A., Barty, A., Deponte, D. P., … Neutze, R. (2013). Structure of a photosynthetic reaction centre determined by serial femtosecond crystallography. *Nature Communications*, *4*(Article nr:2911).

Kaila, V. R. I., Oksanen, E., Goldman, A., Bloch, D. A., Verkhovsky, M. I., Sundholm, D., & Wikström, M. (2011). A combined quantum chemical and crystallographic study on the oxidized binuclear center of cytochrome c oxidase. *Biochimica et Biophysica Acta. Bioenergetics*, *1807*(7), 769–778.

Kameshima, T., Ono, S., Kudo, T., Ozaki, K., Kirihara, Y., Kobayashi, K., … Hatsui, T. (2014). Development of an X-ray pixel detector with multi-port charge-coupled device for X-ray free-electron laser experiments. *Review of Scientific Instruments*, *85*(3), 33110. https://doi.org/10.1063/1.4867668

Kannt, A., Soulimane, T., Buse, G., Becker, A., Bamberg, E., & Michel, H. (1998). Electrical current generation and proton pumping catalyzed by the *ba3*-type cytochrome c oxidase from Thermus thermophilus. *FEBS Letters*, *434*(1), 17–22. https://doi.org/https://doi.org/10.1016/S0014-5793(98)00942-9

Kato, H. E., Zhang, F., Yizhar, O., Ramakrishnan, C., Nishizawa, T., Hirata, K., … Nureki, O. (2012). Crystal structure of the channelrhodopsin light-gated cation channel. *Nature*, *482*(7385).

Keightley, J., Zimmermann, B., Mather, M., Springer, P., Pastuszyn, A., Lawrence, D. M., & Fee, J. (1995). MOLECULAR-GENETIC AND PROTEIN CHEMICAL CHARACTERIZATION OF THE CYTOCHROME BA(3) FROM THERMUS-THERMOPHILUS HB8. *Journal Of Biological Chemistry*, *270*(35), 20345–20358.

Kim, Y., Babcock, G. T., Surerus, K. K., Fee, J. A., Dyer, R. B., Woodruff, W. H., & Oertling, W. A. (1998). Cyanide binding and active site structure in heme-copper oxidases: Normal coordinate analysis of iron-cyanide vibrations of a^{2+}_3 CN − complexes of cytochromes ba 3 and aa 3. *Biospectroscopy*, *4*(1), 1–15.

Kirian, R. A., Wang, X., Weierstall, U., Schmidt, K. E., Spence, J. C. H., Hunter, M., … Holton, J. (2010). Femtosecond protein nanocrystallography-data analysis methods. *Optics Express*, *18*(6), 5713.

Klare, J. P., Bordignon, E., Doebber, M., Fitter, J., Kriegsmann, J., Chizhov, I., … Engelhard, M. (2006). Effects of Solubilization on the Structure and Function of the Sensory Rhodopsin II/Transducer Complex. *Journal of Molecular Biology*, *356*(5), 1207–1221.

Koepke, J., Krammer, E.-M., Klingen, A. R., Sebban, P., Ullmann, G. M., & Fritzsch, G. (2007). pH Modulates the Quinone Position in the Photosynthetic Reaction Center from Rhodobacter sphaeroides in the Neutral and Charge Separated States. *Journal of Molecular Biology*, *371*(2), 396–409.

Kolek, S. A., Bräuning, B., & Stewart, P. D. S. (2016). A novel microseeding method for the crystallization of membrane proteins in lipidic cubic phase. *Acta Crystallographica. Section F, Structural Biology Communications*, *72*(Pt 4), 307.

Kracke, F., Vassilev, I., & Krömer, J. O. (2015). Microbial electron transport and energy conservation - the foundation for optimizing bioelectrochemical systems. *Frontiers in Microbiology*, *6*, 575. https://doi.org/10.3389/fmicb.2015.00575

Krauss, I., Merlino, A., Vergara, A., & Sica, F. (2013). An Overview of Biological Macromolecule Crystallization. *International Journal of Molecular Sciences*, *14*(6), 11643–11691. Retrieved from http://search.proquest.com/docview/1526046518/

Kupitz, C., Olmos, J., Holl, M., Tremblay, L., Hunter, M., Aquila, A., … Schmidt, M. (2016). Structural enzymology using X-ray free electron lasers. *Structural Dynamics*, *4*(4). Retrieved from http://search.proquest.com/docview/1951242551/

Lancaster, C. R. D., & Michel, H. (1997). The coupling of light-induced electron transfer and proton uptake as derived from crystal structures of reaction centres from

Rhodopseudomonas viridis modified at the binding site of the secondary quinone, Q B. *Structure (London)*, *5*(10), 1339–1359.

Landau, E. M., & Rosenbusch, J. P. (1996). Lipidic cubic phases: A novel concept for the crystallization of membrane proteins. *Proceedings of the National Academy of Sciences of the United States of America*, *93*(25), 14532–14535.

Le Maire, M., Champeil, P., & Møller, J. V. (2000). Interaction of membrane proteins and lipids with solubilizing detergents. *BBA - Biomembranes*, *1508*(1–2), 86–111.

Lee, D., Kim, J.-M., Seok, J., Lee, J.-H., Jo, J., Mun, J., … Kim, K. (2018). Supersaturation-controlled microcrystallization and visualization analysis for serial femtosecond crystallography. *Sci Rep*, *8*(1), 2541.

Leslie, A. G. W. (2006). The integration of macromolecular diffraction data. *Acta Crystallographica Section D*, *62*(1), 48–57.

Li, D., Boland, C., Walsh, K., & Caffrey, M. (2012). Use of a Robot for High-throughput Crystallization of Membrane Proteins in Lipidic Mesophases. *Journal of Visualized Experiments : JoVE*, (67).

Li, D., Lee, J., & Caffrey, M. (2011). Crystallizing Membrane Proteins in Lipidic Mesophases. A Host Lipid Screen. *Crystal Growth & Design*, *11*(2).

Li, D., Shah, S. T. A., & Caffrey, M. (2013). Host Lipid and Temperature as Important Screening Variables for Crystallizing Integral Membrane Proteins in Lipidic Mesophases. Trials with Diacylglycerol Kinase. *Crystal Growth & Design*, *13*(7), 2846.

Lichtenberg, D., Ahyayauch, H., Alonso, A., & Goñi, F. M. (2013). Detergent solubilization of lipid bilayers: a balance of driving forces. *Trends in Biochemical Sciences*, *38*(2), 85.

Lichtenberg, D., Robson, R. J., & Dennis, E. A. (1983). Solubilization of phospholipids by detergents structural and kinetic aspects. *Biochimica et Biophysica Acta. Reviews on Biomembranes*, *737*(2), 285–304.

Lieske, J., Cerv, M., Kreida, S., Komadina, D., Fischer, J., Barthelmess, M., … Meents, A. (2019). On-chip crystallization for serial crystallography experiments and on-chip ligand-binding studies. *IUCrJ*, *6*(4), 714–728. https://doi.org/10.1107/S2052252519007395

Lillemeier, B. F., Pfeiffer, J. R., Surviladze, Z., Wilson, B. S., & Davis, M. M. (2006). Plasma membrane-associated proteins are clustered into islands attached to the cytoskeleton. *Proceedings of the National Academy of Sciences*, *103*(50), 18992. Retrieved from http://www.pnas.org/content/103/50/18992.abstract

Lindblom, G., & Rilfors, L. (1989). Cubic phases and isotropic structures formed by membrane lipids — possible biological relevance. *Biochimica et Biophysica Acta. Reviews on Biomembranes*, *988*(2), 221–256.

Lingwood, D., & Simons, K. (2010). Lipid Rafts As a Membrane-Organizing Principle. *Science*, *327*(5961), 46–50.

Liu, B., Chen, Y., Doukov, T., Soltis, S. M., Stout, C. D., & Fee, J. A. (2009). Combined Microspectrophotometric and Crystallographic Examination of Chemically Reduced and X-ray Radiation-Reduced Forms of Cytochrome *ba3* Oxidase from Thermus thermophilus: Structure of the Reduced Form of the Enzyme. *Biochemistry*, *48*(5), 820–

826. https://doi.org/10.1021/bi801759a

Liu, W., Hanson, M. A., Stevens, R. C., & Cherezov, V. (2010). LCP-Tm: An Assay to Measure and Understand Stability of Membrane Proteins in a Membrane Environment. *Biophysical Journal*, *98*(8), 1539–1548.

Liu, W., Ishchenko, A., & Cherezov, V. (2014). Preparation of microcrystals in lipidic cubic phase for serial femtosecond crystallography. *Nature Protocols*, *9*(9).

Lozier, R. H., Bogomolni, R. A., & Stoeckenius, W. (1975). Bacteriorhodopsin: a light-driven proton pump in Halobacterium Halobium. *Biophysical Journal*, *15*(9), 955–962.

Lu, J., & Gunner, M. R. (2014). Characterizing the proton loading site in cytochrome c oxidase. *Proceedings of the National Academy of Sciences*, *111*(34), 12414. Retrieved from http://www.pnas.org/content/111/34/12414.abstract

Lubben, M., & Morand, K. (1994). NOVEL PRENYLATED HEMES AS COFACTORS OF CYTOCHROME OXIDASES - ARCHAEA HAVE MODIFIED HEME-A AND HEME-O. *Journal Of Biological Chemistry*, *269*(34), 21473–21479.

Luby-Phelps, K., Mujumdar, S., Mujumdar, R. B., Ernst, L. A., Galbraith, W., & Waggoner, A. S. (1993). A novel fluorescence ratiometric method confirms the low solvent viscosity of the cytoplasm. *Biophysical Journal*, *65*(1), 236–242.

Luzzati, V., Tardieu, A., & Gulik-Krzywicki, T. (1968). Polymorphism of Lipids. *Nature*, *217*(5133), 1028.

Mackay, A. L. (1985). Periodic minimal surfaces. *Nature*, *314*(6012), 604–606. https://doi.org/10.1038/314604a0

Macmillan, F., Kannt, A., Behr, J., Prisner, T., & Michel, H. (1999). Direct evidence for a tyrosine radical in the reaction of cytochrome c oxidase with hydrogen peroxide. *Biochemistry*, *38*(29), 9179.

Mccoy, A. J., Grosse-Kunstleve, R. W., Adams, P. D., Winn, M. D., Storoni, L. C., & Read, R. J. (2007). Phaser crystallographic software. *Journal of Applied Crystallography*, *40*(4), 658–674.

Mcpherson, A., & Gavira, J. A. (2014). Introduction to protein crystallization. *Acta Crystallographica Section F Structural Biology Communications*, *70*(1), 2–20.

Misquitta, L. V, Misquitta, Y., Cherezov, V., Slattery, O., Mohan, J. M., Hart, D., … Caffrey, M. (2004). Membrane Protein Crystallization in Lipidic Mesophases with Tailored Bilayers. *Structure (London)*, *12*(12), 2113–2124.

Misquitta, Y., Cherezov, V., Havas, F., Patterson, S., Mohan, J. M., Wells, A. J., … Caffrey, M. (2004). Rational design of lipid for membrane protein crystallization. *Journal of Structural Biology*, *148*(2), 169–175.

Monteiro, D. C. F., Vakili, M., Harich, J., Sztucki, M., Meier, S. M., Horrell, S., … Trebbin, M. (2019). A microfluidic flow-focusing device for low sample consumption serial synchrotron crystallography experiments in liquid flow. *Journal of Synchrotron Radiation*, *26*(2), 406–412.

Moraes, I., Evans, G., Sanchez-Weatherby, J., Newstead, S., & Stewart, P. (2014). Membrane protein structure determination The next generation. *Biochimica Et Biophysica Acta-Biomembranes*, *1838*(1), 78–87.

Muramoto, K., Ohta, K., Shinzawa-Itoh, K., Kanda, K., Taniguchi, M., Nabekura, H., … Yoshikawa, S. (2010). Bovine cytochrome c oxidase structures enable O2 reduction with minimization of reactive oxygens and provide a proton-pumping gate. *Proceedings of the National Academy of Sciences*, *107*(17), 7740. Retrieved from http://www.pnas.org/content/107/17/7740.abstract

Murshudov, G. N., Skubák, P., Lebedev, A. A., Pannu, N. S., Steiner, R. A., Nicholls, R. A., … Vagin, A. A. (2011). REFMAC5 for the refinement of macromolecular crystal structures. *Acta Crystallographica Section D*, *67*(4), 355–367. https://doi.org/10.1107/S0907444911001314

Nango, E, Kubo, M., Tono, K., & Iwata, S. (2019). Pump-probe time-resolved serial femtosecond crystallography at SACLA: Current status and data collection strategies. *Applied Sciences (Switzerland)*, *9*(24).

Nango, Eriko, Royant, A., Kubo, M., Nakane, T., Wickstrand, C., Kimura, T., … Iwata, S. (2016). A three-dimensional movie of structural changes in bacteriorhodopsin. *Science (New York, N.Y.)*, *354*(6319).

Nass, K., Foucar, L., Barends, T. R. M., Hartmann, E., Botha, S., Shoeman, R. L., … Schlichting, I. (2015). Indications of radiation damage in ferredoxin microcrystals using high-intensity X-FEL beams. *Journal of Synchrotron Radiation*, *22*(2), 225–238.

Neutze, R., Wouts, R., Spoel, D. Van Der, Weckert, E., & Hajdu, J. (2000). Potential for biomolecular imaging with femtosecond X-ray pulses. *Nature*, *406*(6797), 752.

Nicholls, D. G. (2013). *Bioenergetics 4* (Fourth edi).

Nogly, P., James, D., Wang, D. J., White, T. A., Zatsepin, N., Shilova, A., … Weierstall, U. (2015). Lipidic cubic phase serial millisecond crystallography using synchrotron radiation. *Iucrj, 2015, Vol. 2, Pp. 168-.176 Part: 2*, *2*, 168--176 Part: 2.

Nogly, P., Weinert, T., James, D., Carbajo, S., Ozerov, D., Furrer, A., … Standfuss, J. (2018). Retinal isomerization in bacteriorhodopsin captured by a femtosecond x-ray laser. *Science, 2018, Vol. 361, Iss. 6398, Pp. 145-.+*, *361*(6398), 145--+.

Nowicka, B., & Kruk, J. (2016). Powered by light: Phototrophy and photosynthesis in prokaryotes and its evolution. *Microbiological Research*, *186–187*, 99–118.

Oliveira, A. S. F., Damas, J., Baptista, A., & Soares, C. M. (2014). Exploring O-2 Diffusion in A-Type Cytochrome c Oxidases: Molecular Dynamics Simulations Uncover Two Alternative Channels towards the Binuclear Site. *Plos Computational Biology*, *10*(12).

Oshima, T., & Imahori, K. (1974). Description of Thermus thermophilus (Yoshida and Oshima) comb. nov., a Nonsporulating Thermophilic Bacterium from a Japanese Thermal Spa. *International Journal of Systematic and Evolutionary Microbiology*, *24*(1), 102–112. https://doi.org/https://doi.org/10.1099/00207713-24-1-102

Overington, J. P., Al-Lazikani, B., & Hopkins, A. L. (2006). How many drug targets are there? *Nature Reviews Drug Discovery*, *5*(12), 993. https://doi.org/10.1038/nrd2199

Paas, Y., Cartaud, J., Recouvreur, M., Grailhe, R., Dufresne, V., Pebay-Peyroula, E., … Changeux, J.-P. (2003). Electron microscopic evidence for nucleation and growth of 3D acetylcholine receptor microcrystals in structured lipid{\textendash}detergent matrices. *Proceedings of the National Academy of Sciences*, *100*(20), 11309–11314. https://doi.org/10.1073/pnas.1834451100

Paulus, A., Werner, C., Ludwig, B., & de Vries, S. (2015). The cytochrome *ba3* oxidase from Thermus thermophilus does not generate a tryptophan radical during turnover: Implications for the mechanism of proton pumping. *Biochimica et Biophysica Acta. Bioenergetics*, *1847*(10), 1093–1100.

Pebay-Peyroula, E., Rummel, G., Rosenbusch, J. P., & Landau, E. M. (1997). X-ray structure of bacteriorhodopsin at 2.5 angstroms from microcrystals grown in lipidic cubic phases. *Science (New York, N.Y.)*, *277*(5332).

Pereira, M. M., Gomes, C. M., & Teixeira, M. (2002). Plasticity of proton pathways in haem–copper oxygen reductases. *FEBS Letters*, *522*(1–3), 14–18.

Pereira, M. M., Santana, M., & Teixeira, M. (2001). A novel scenario for the evolution of haem–copper oxygen reductases. *BBA - Bioenergetics*, *1505*(2–3), 185–208.

Potterton, L., Agirre, J., Ballard, C., Cowtan, K., Dodson, E., Evans, P., … Wojdyr, M. (2018). CCP4i2: the new graphical user interface to the CCP4 program suite. *Acta Crystallographica. Section D : Biological Crystallography*, *74*(2), 68–84. Retrieved from http://search.proquest.com/docview/2022047897/

Pražnikar, J., Afonine, P. V, Gunčar, G., Adams, P. D., & Turk, D. (2009). Averaged kick maps: less noise, more signal{$…$}and probably less bias. *Acta Crystallographica Section D*, *65*(9), 921–931. https://doi.org/10.1107/S0907444909021933

Qin, L., Hiser, C., Mulichak, A., Garavito, R. M., & Ferguson-Miller, S. (2006). Identification of conserved lipid/detergent-binding sites in a high-resolution structure of the membrane protein cytochrome c oxidase. *Proceedings of the National Academy of Sciences*, *103*(44), 16117. Retrieved from http://www.pnas.org/content/103/44/16117.abstract

Qiu, H., & Caffrey, M. (2000). The phase diagram of the monoolein/water system: metastability and equilibrium aspects. *Biomaterials*, *21*(3), 223–234.

Qutub, Y., Reviakine, I., Maxwell, C., Navarro, J., Landau, E. M., & Vekilov, P. G. (2004). Crystallization of Transmembrane Proteins in cubo: Mechanisms of Crystal Growth and Defect Formation. *Journal of Molecular Biology*, *343*(5), 1243–1254. https://doi.org/https://doi.org/10.1016/j.jmb.2004.09.022

Radzi Noor, M., & Soulimane, T. (2012). Bioenergetics at extreme temperature: Thermus thermophilus *ba3*- and caa3-type cytochrome c oxidases. *Biochimica et Biophysica Acta (BBA) - Bioenergetics*, *1817*(4), 638–649. https://doi.org/https://doi.org/10.1016/j.bbabio.2011.08.004

Ramírez-Arcos, S., Fernández-Herrero, L. A., & Berenguer, J. (1998). A thermophilic nitrate reductase is responsible for the strain specific anaerobic growth of Thermus thermophilus HB8. *BBA - Gene Structure and Expression*, *1396*(2), 215–227.

Ramsay, R. (2019). Electron carriers and energy conservation in mitochondrial respiration. *ChemTexts*, *5*(2), 1–14.

Rask-Andersen, M., Almén, M. S., & Schiöth, H. B. (2011). Trends in the exploitation of novel drug targets. *Nature Reviews Drug Discovery*, *10*(8), 579.

Rasmussen, S. G. F., Devree, B. T., Zou, Y., Kruse, A. C., Chung, K. Y., Kobilka, T. S., … Kobilka, B. K. (2011). Crystal structure of the β2 adrenergic receptor-Gs protein complex. *Nature*, *477*(7366).

Rayment, I. (2002). Small-Scale Batch Crystallization of Proteins Revisited: An Underutilized Way to Grow Large Protein Crystals. *Structure*, *10*(2), 147–151. https://doi.org/https://doi.org/10.1016/S0969-2126(02)00711-6

Razvi, A., & Scholtz, J. M. (2006). Lessons in stability from thermophilic proteins. *Protein Science*, *15*(7), 1569–1578.

Rhodes, G. (2006). *Crystallography Made Crystal Clear : A Guide for Users of Macromolecular Models*. Retrieved from http://ebookcentral.proquest.com/lib/gu/detail.action?docID=269943

Ridell, A., Ekelund, K., Evertsson, H., & Engström, S. (2003). On the water content of the solvent/monoolein/water sponge (L3) phase. *Colloids And Surfaces A*, *228*(1–3), 17–24.

Rodriguez, E. L., Poddar, S., Iftekhar, S., Suh, K., Woolfork, A. G., Ovbude, S., … Hage, D. S. (2020). Affinity chromatography: A review of trends and developments over the past 50 years. *Journal of Chromatography. B, Analytical Technologies in the Biomedical and Life Sciences*, *1157*.

Roedig, P., Vartiainen, I., Duman, R., Panneerselvam, S., Stübe, N., Lorbeer, O., … Meents, A. (2015). A micro-patterned silicon chip as sample holder for macromolecular crystallography experiments with minimal background scattering. *Scientific Reports*, *5*(1), 10451.

Roessler, C. G., Agarwal, R., Allaire, M., Alonso-Mori, R., Andi, B., Bachega, J. F. R., … Zouni, A. (2016). Acoustic Injectors for Drop-On-Demand Serial Femtosecond Crystallography. *Structure*, *24*(4), 631–640. https://doi.org/https://doi.org/10.1016/j.str.2016.02.007

Roessler, C. G., Kuczewski, A., Stearns, R., Ellson, R., Olechno, J., Orville, A. M., … Heroux, A. (2013). Acoustic methods for high-throughput protein crystal mounting at next-generation macromolecular crystallographic beamlines. *Journal of Synchrotron Radiation*, *20*(5), 805.

Royant, A, Nollert, P., Edman, K., Neutze, R., Landau, E. M., Pebay-Peyroula, E., & Navarro, J. (2001). X-ray structure of sensory rhodopsin II at 2.1-A resolution. *Proceedings of the National Academy of Sciences of the United States of America*, *98*(18), 10131–10136. https://doi.org/10.1073/pnas.181203898

Royant, Antoine, Edman, K., Ursby, T., Pebay-Peyroula, E., Landau, E. M., & Neutze, R. (2000). Helix deformation is coupled to vectorial proton transport in the photocycle of bacteriorhodopsin. *Nature*, *406*(6796), 645.

Rummel, G., Hardmeyer, A., Widmer, C., Chiu, M., Nollert, P., Locher, K., … Rosenbusch, J. P. (1998). Lipidic cubic phases: New matrices for the three-dimensional crystallization of membrane proteins. *Journal Of Structural Biology*, *121*(2), 82–91.

Sadoc, J.-F., & Charvolin, J. (1989). Infinite periodic minimal surfaces and their crystallography in the hyperbolic plane. *Acta Crystallographica Section A*, *45*. https://doi.org/10.1107/S0108767388008438

Saiki, K., Mogi, T., & Anraku, Y. (1992). Heme O biosynthesis in Escherichia coli: The cyoe gene in the cytochrome BO operon encodes a protoheme IX farnesyltransferase. *Biochemical and Biophysical Research Communications*, *189*(3), 1491–1497.

Sanchez-Gonzalez, A., Johnson, A. S., Fitzpatrick, A., Hutchison, C. D. M., Fare, C., Cordon-

Preciado, V., … van Thor, J. J. (2017). Coincidence timing of femtosecond optical pulses in an X-ray free electron laser. *Journal of Applied Physics*, *122*(20).

Saridakis, E., & Chayen, N. E. (2009). Towards a 'universal' nucleant for protein crystallization. *Trends in Biotechnology*, *27*(2), 99–106. https://doi.org/https://doi.org/10.1016/j.tibtech.2008.10.008

Sasaki, J., & Spudich, J. L. (1999). Proton Circulation During the Photocycle of Sensory Rhodopsin II. *Biophysical Journal*, *77*(4), 2145–2152.

Schmid, F.-X. (2001). Biological Macromolecules: UV-visible Spectrophotometry. In *eLS*. https://doi.org/10.1038/npg.els.0003142

Schmidt-Rohr, K. (2020). Oxygen Is the High-Energy Molecule Powering Complex Multicellular Life: Fundamental Corrections to Traditional Bioenergetics. *ACS Omega*, *5*(5), 2221–2233. https://doi.org/10.1021/acsomega.9b03352

Seddon, A. M., Curnow, P., & Booth, P. J. (2004). Membrane proteins, lipids and detergents: not just a soap opera. *Biochimica et Biophysica Acta. Biomembranes*, *1666*(1–2), 105–117.

Sharma, A. K., Spudich, J. L., & Doolittle, W. F. (2006). Microbial rhodopsins: functional versatility and genetic mobility. *Trends in Microbiology (Regular Ed.)*, *14*(11), 463–469.

Shimada, A., Kubo, M., Baba, S., Yamashita, K., Hirata, K., Ueno, G., … Tsukihara, T. (2017). A nanosecond time-resolved XFEL analysis of structural changes associated with CO release from cytochrome c oxidase. *Science Advances*, *3*(7).

Singer, S. J., & Nicolson, G. L. (1972). The Fluid Mosaic Model of the Structure of Cell Membranes. *Science*, *175*(4023), 720–731.

Soulimane, T., Buse, G., Bourenkov, G. P., Bartunik, H. D., Huber, R., & Than, M. E. (2000). Structure and mechanism of the aberrant ba 3 -cytochrome c oxidase from Thermus thermophilus. *EMBO Journal*, *19*(8), 1766–1776.

Soulimane, T., Than, M. E., Dewor, M., Huber, R., & Buse, G. (2000). Primary structure of a novel subunit in ba 3 -cytochrome oxidase from Thermus thermophilus. *Protein Science*, *9*(11), 2068–2073.

Soulimane, T., von Walter, M., Hof, P., Than, M. E., Huber, R., & Buse, G. (1997). Cytochrome-c552fromThermus thermophilus:A Functional and Crystallographic Investigation. *Biochemical and Biophysical Research Communications*, *237*(3), 572–576. https://doi.org/https://doi.org/10.1006/bbrc.1997.7041

Spegt, P. A., & Skoulois, A. E. (1966). Structure des savons de strontium en fonction de la température. *Acta Crystallographica*, *21*(6), 892–897. https://doi.org/10.1107/S0365110X66004158

Standfuss, J. (2019). Membrane protein dynamics studied by X-ray lasers – or why only time will tell. *Current Opinion in Structural Biology*, *57*, 63–71. https://doi.org/https://doi.org/10.1016/j.sbi.2019.02.001

Standfuss, J., & Spence, J. (2017). Serial crystallography at synchrotrons and X-ray lasers. *IUCrJ*, *4*(Pt 2), 100–101. https://doi.org/10.1107/S2052252517001877

Stellato, F., Oberthur, D., Liang, M., Bean, R., Gati, C., Yefanov, O., … Chapman, H. N. (2014). Room-temperature macromolecular serial crystallography using synchrotron

radiation.(research letter)(Report). *International Union of Crystallography Journal*, *1*(4), 204.

Striegel, A. M. (2017). Size-exclusion chromatography. In *Liquid Chromatography: Fundamentals and Instrumentation: Second Edition* (Vol. 1, pp. 245–273). Elsevier.

Sugahara, M., Mizohata, E., Nango, E., Suzuki, M., Tanaka, T., Masuda, T., … Iwata, S. (2014). Grease matrix as a versatile carrier of proteins for serial crystallography. *Nature Methods*, *12*, 61–63. https://doi.org/10.1038/nmeth.3172

Surerus, K. K., Oertling, W. A., Fan, C., Gurbiel, R. J., Einarsdóttir, O., Antholine, W. E., … Fee, J. A. (1992). Reaction of cyanide with cytochrome *ba3* from Thermus thermophilus: spectroscopic characterization of the Fe(II)a3-CN.Cu(II)B-CN complex suggests four 14N atoms are coordinated to CuB. *Proceedings of the National Academy of Sciences*, *89*(8), 3195–3199. https://doi.org/10.1073/pnas.89.8.3195

Svensson-Ek, M., Abramson, J., Larsson, G., Törnroth, S., Brzezinski, P., & Iwata, S. (2002). The X-ray Crystal Structures of Wild-type and EQ(I-286) Mutant Cytochrome c Oxidases from Rhodobacter sphaeroides. *Journal of Molecular Biology*, *321*(2), 329–339. https://doi.org/https://doi.org/10.1016/S0022-2836(02)00619-8

Thompson, M. J., & Eisenberg, D. (1999). Transproteomic evidence of a loop-deletion mechanism for enhancing protein thermostability. *Journal of Molecular Biology*, *290*(2), 595–604.

Thunnissen, M. M. G. M., Sondhauss, P., Wallén, E., Theodor, K., Logan, D. T., Labrador, A., … Ursby, T. (2013). Biomax: the future macromolecular crystallography beamline at max iv. *Journal of Physics: Conference Series*, *425*(7), 72012.

Tickle, I. J., Laskowski, R. A., & Moss, D. S. (2000). Rfree and the rfree ratio. II. Calculation Of the expected values and variances of cross-validation statistics in macromolecular least-squares refinement. *Acta Crystallographica. Section D, Biological Crystallography*, *56*, Pt 4/.

Tiefenbrunn, T., Liu, W., Chen, Y., Katritch, V., Stout, C. D., Fee, J. A., … Mayer, C. (2011). High Resolution Structure of the *ba3* Cytochrome *c* Oxidase from Thermus thermophilus in a Lipidic Environment. *PLoS ONE*, *6*(7).

Tono, K. (2017). Fluid sample injectors for X-ray free electron laser atÂ SACLA. *High Power Laser Science and Engineering*, *5*, <xocs:firstpage xmlns:xocs=""/>. https://doi.org/10.1017/hpl.2017.6

Tsukihara, T, Aoyama, H., Yamashita, E., Tomizaki, T., Yamaguchi, H., Shinzawa-Itoh, K., … Yoshikawa, S. (1996). The whole structure of the 13-subunit oxidized cytochrome *c* oxidase at 2.8 A. *Science (New York, N.Y.)*, *272*(5265), 1136.

Tsukihara, Tomitake, Shimokata, K., Katayama, Y., Shimada, H., Muramoto, K., Aoyama, H., … Yoshikawa, S. (2003). The low-spin heme of cytochrome *c* oxidase as the driving element of the proton-pumping process. *Proceedings of the National Academy of Sciences of the United States of America*, *100*(26), 15304. Retrieved from http://www.pnas.org/content/100/26/15304.abstract

Uzman, A. (2001). *Molecular Cell Biology (4th edition): Harvey Lodish, Arnold Berk, S. Lawrence Zipursky, Paul Matsudaira, David Baltimore and James Darnell; Freeman & Co., New York, NY, 2000, 1084 pp., list price $102.25, ISBN 0-7167-3136-3*.

van Meer, G., & de Kroon, A. I. P. M. (2011). Lipid map of the mammalian cell. *Journal of Cell Science*, *124*(1), 5.

van Zanten, T. S., Cambi, A., & Garcia-Parajo, M. F. (2010). A nanometer scale optical view on the compartmentalization of cell membranes. *BBA - Biomembranes*, *1798*(4), 777–787.

Wadsten, P., Wöhri, A. B., Snijder, A., Katona, G., Gardiner, A. T., Cogdell, R. J., … Engström, S. (2006). Lipidic Sponge Phase Crystallization of Membrane Proteins. *Journal of Molecular Biology*, *364*(1), 44–53.

Weierstall, U., James, D., Wang, C., White, T. A., Wang, D., Liu, W., … Cherezov, V. (2014). Lipidic cubic phase injector facilitates membrane protein serial femtosecond crystallography. *Nature Communications*, *5*.

Weinert, T., Skopintsev, P., James, D., Dworkowski, F., Panepucci, E., Kekilli, D., … Standfuss, J. (2019). Proton uptake mechanism in bacteriorhodopsin captured by serial synchrotron crystallography. *Science (New York, N.Y.)*, *365*(6448), 61.

Weiss, G. (2001). Swiss source shows small is powerful. *Science*, *294*(5542), 494. Retrieved from http://search.proquest.com/docview/213584335/

White, T. A., Kirian, R. A., Martin, A. V, Aquila, A., Nass, K., Barty, A., & Chapman, H. N. (2012). CrystFEL: a software suite for snapshot serial crystallography. *Journal of Applied Crystallography*, *45*(2), 335–341. https://doi.org/10.1107/S0021889812002312

Wiertz, F. G. M., Richter, O.-M. H., Cherepanov, A. V, Macmillan, F., Ludwig, B., & de Vries, S. (2004). An oxo-ferryl tryptophan radical catalytic intermediate in cytochrome *c* and quinol oxidases trapped by microsecond freeze-hyperquenching (MHQ). *FEBS Letters*, *575*(1–3), 127–130.

Wikström, M., Krab, K., & Sharma, V. (2018). Oxygen Activation and Energy Conservation by Cytochrome *c* Oxidase. *Chemical Reviews*, Vol. 118, pp. 2469–2490.

Wilhelm, E., Battino, R., & Wilcock, R. J. (1977). Low-pressure solubility of gases in liquid water. *Chemical Reviews*, *77*(2), 219–262. https://doi.org/10.1021/cr60306a003

Winn, M. D., Ballard, C. C., Cowtan, K. D., Dodson, E. J., Emsley, P., Evans, P. R., … Wilson, K. S. (2011). Overview of the CCP4 suite and current developments. *Acta Crystallographica Section D*, *67*(4), 235–242.

Wöhri, A., Wahlgren, W. Y., Malmerberg, E., Johansson, L. C., Neutze, R., & Katona, G. (2009). Lipidic sponge phase crystal structure of a photosynthetic reaction center reveals lipids on the protein surface. *Biochemistry, 2009, Vol. 48, Iss. 41, Pp. 9831-.8*, *48*(41), 9831–9838.

Yaghmur, A., Laggner, P., Zhang, S., Rappolt, M., & Scalas, E. (2007). Tuning Curvature and Stability of Monoolein Bilayers by Designer Lipid-Like Peptide Surfactants. *PLoS ONE*, *2*(5).

Yang, N. J., & Hinner, M. J. (2015). Getting across the cell membrane: an overview for small molecules, peptides, and proteins. *Methods in Molecular Biology (Clifton, N.J.)*, *1266*, 29–53. https://doi.org/10.1007/978-1-4939-2272-7_3

Yoshikawa, S., Muramoto, K., Shinzawa-Itoh, K., Aoyama, H., Tsukihara, T., Shimokata, K., … Shimada, H. (2006). Proton pumping mechanism of bovine heart cytochrome *c*

oxidase. *Biochimica et Biophysica Acta (BBA) - Bioenergetics*, *1757*(9), 1110–1116. https://doi.org/https://doi.org/10.1016/j.bbabio.2006.06.004

Yoshikawa, S., & Shimada, A. (2015). Reaction Mechanism of Cytochrome *c* Oxidase. *Chemical Reviews*, *115*(4), 1936–1989. https://doi.org/10.1021/cr500266a

Yoshikawa, S., Yano, N., Muramoto, K., Shimada, A., Baba, J., Mochizuki, M., … Tsukihara, T. (2016). The Mg2 +-containing water cluster of mammalian cytochrome *c* oxidase collects four pumping proton equivalents in each catalytic cycle. *Biochimica et Biophysica Acta. Bioenergetics*, *1857*, e20--e20.

Yu, M. A., Egawa, T., Shinzawa-Itoh, K., Yoshikawa, S., Yeh, S.-R., Rousseau, D. L., & Gerfen, G. J. (2011). Radical formation in cytochrome *c* oxidase. *Biochimica et Biophysica Acta*, *1807*(10), 1295–1304. https://doi.org/10.1016/j.bbabio.2011.06.012

Zhao, F.-Z., Zhang, B., Yan, E.-K., Sun, B., Wang, Z.-J., He, J.-H., & Yin, D.-C. (2019). A guide to sample delivery systems for serial crystallography. *The FEBS Journal*, *286*(22), 4402–4417. https://doi.org/10.1111/febs.15099

Zorova, L. D., Popkov, V. A., Plotnikov, E. Y., Silachev, D. N., Pevzner, I. B., Jankauskas, S. S., … Zorov, D. B. (2018). Mitochondrial membrane potential. *Analytical Biochemistry*, *552*, 50–59. https://doi.org/10.1016/j.ab.2017.07.009